Self-Replicating Amphiphilic β-Sheet Peptides

Thesis submitted in partial fulfillment

of the requirements for the degree of

“DOCTOR OF PHILOSOPHY”

by

Boris Rubinov

Submitted to the Senate of Ben-Gurion University

of the Negev

January 2014

Beer-Sheva

Self-Replicating Amphiphilic β-Sheet Peptides

Thesis submitted in partial fulfillment

of the requirements for the degree of

"DOCTOR OF PHILOSOPHY"

by

Boris Rubinov

Submitted to the Senate of Ben-Gurion University

of the Negev

Approved by the advisor_____

Approved by the Dean of the Kreitman School of Advanced Graduate Studies_____

January 2014

Beer-Sheva

This work was carried out under the supervision of

Prof. Gonen Ashkenasy

In the Chemistry Department

Faculty of Natural Science

Research-Student's Affidavit when Submitting the Doctoral Thesis for Judgment

I Boris Rubinov, whose signature appears below, hereby declare that:

√ I have written this Thesis by myself, except for the help and guidance offered by my Thesis Advisors.

√ The scientific materials included in this Thesis are products of my own research, culled from the period during which I was a research student.

___ This Thesis incorporates research materials produced in cooperation with others, excluding the technical help commonly received during experimental work. Therefore, I am attaching another affidavit stating the contributions made by myself and the other participants in this research, which has been approved by them and submitted with their approval.

Date: _____ Student's name: Boris Rubinov Signature: _____

Acknowledgments

I would like to thank my supervisor Prof. Gonen Ashkenasy, whose expertise, understanding, and dedication added considerably to my experience. Additional thanks to Dr. Nathaniel Wagner for fruitful discussions and help with the theoretical models. In addition, I want to thank Prof. Hanna Rapaport and her group members, whose advises and work methodology helped me a lot during the first two years of this research.

The cryo-TEM studies were performed with help of Prof. Oren Regev and his group members, especially Dr. Einat Roth to whom I address my thanks.

The AFM studies were performed by collaboration with Prof. Nurit Ashkenasy and her group members, especially Maayan Matmor to whom I address my thanks.

Very special thanks to Dr. Riky Cohen-Luria for her huge support and help during the writing process of this thesis and during the work in the lab.

Additional thanks to all the other members of Prof. Gonen Ashkenasy group for being such good friends and for helping with any concern I had.

I would like to give my deepest appreciation to my parents, who brought me up with their love and encouraged me to pursue advanced degrees.

Finally, I would like to give my heartfelt appreciation to my wife, who has accompanied me with her love, unlimited patience, understanding, helping and encouragement. Without her support, I would never be able to accomplish this work. So, I want to dedicate this thesis to my wife.

Table of Contents

1 Introduction 1

1.1 Synthetic β-Sheet Peptides 2

1.1.1 Peptides Secondary Structures 2

1.1.2 Possible Implications of β-Sheet Peptides to Origin of Life 4

1.1.3 Design of Synthetic β-Sheet Peptides 6

1.1.4 Structural Hierarchy of Synthetic β-Sheet Peptides 7

1.2 Self-Synthesizing Materials 10

1.2.1 Self-Assembly Process 10

1.2.2 Minimal Self-Replication Systems 11

1.2.3 Amyloid Peptides 14

1.2.4 Replication by β-Sheet Peptides 15

2 Objectives 18

2.1 Structural Hierarchy and Characterizations 18

2.2 Replication of β-Sheet Forming Peptides 18

2.3 Replication System Mechanism 19

2.4 Regio- and Stereo-selective Ligation by β-Sheet Peptides 19

3 Results and Discussions 20

3.1 Design and Structural Characterizations of β-Sheet Forming Peptides 21

3.1.1 Peptide Design 21

3.1.2 Peptide Synthesis – SPPS 23

3.1.3 Peptide Structural Characterization 24

3.1.4 Conclusions 33

3.2 Analyzing the Self-assembly Pathway of Peptide 1. 34

3.2.1 The Solubility of Peptide 1 in Neutral Aqueous Solution 34

3.2.2 Time Dependent CD Spectroscopy of Peptide 1 34
3.2.3 Time Dependent ThT Fluorescence of Peptide 1 36
3.2.4 Kinetic Studies by Cryo-TEM 37
3.2.5 Analysis of the Fibrillar Structures 39
3.2.6 Conclusions 40
3.3 Kinetic Studies of Replication System 1 42
3.3.1 Kinetics of Template Free Reaction 44
3.3.2 Template Assisted Reactions 45
3.3.3 Reaction Order of Ligation 49
3.3.4 Conclusions 52
3.4 Replication System Full Mechanism 53
3.4.1 Two Parallel Processes 53
3.4.2 Kinetic Model 54
3.4.3 Simulation of Kinetic Model 55
3.4.4 Conclusions 56
3.5 Regio and Stereo-selective Ligation by β-Sheet Peptides 57
3.5.1 Stability of the Electrophiles 59
3.5.2 Kinetic Studies of Replication System 2 60
3.5.3 Investigation of the β-sheet assisted glutamic ligation mechanism 64
3.5.4 Conclusions 67
4 Summary and Conclusions 69
5 Materials and Methods 71
5.1 Peptide Synthesis 71
5.1.1 Fmoc Method 71
5.1.2 t-Boc Method 72

5.1.3 Purification and Analysis 73
5.2 Structural Characterizations 74
5.2.1 Sonication of Peptides Samples 74
5.2.2 CD Analysis 74
5.2.3 ThT Assays 75
5.2.4 Cryo-TEM Imaging 75
5.2.5 AFM Imaging 75
5.2.6 Surface-Pressure Measurements 76
5.2.7 GIXD Experiments 76
5.2.8 Dynamic Light Scattering 77
5.3 Kinetic Replication Experiments 78
5.3.1 Template Free Reactions 78
5.3.2 Template Assisted Reactions 78
6 Publications 80
7 References 81

List of figures

Figure 1: Schematic presentations of protein secondary structures 2
Figure 2: Stick representation of an anti-parallel and a parallel β-sheet 3
Figure 3: Proposed route for chain elongation of racemic antiparallel β-sheets 5
Figure 4: Schematic diagrams of β-sheet assemblies at the air-water interface 7
Figure 5: Different hierarchical structures that can be formed from β-sheet peptides 8
Figure 6: Hierarchical fiber formation, self-assembled from ten-residue peptides 9
Figure 7: Minimal self-replication system described by auto-catalytic cycle 11
Figure 8: Known synthetic minimal self-replication systems 12
Figure 9: Kinetic profiles of self-replication systems 13
Figure 10: Summary of kinetic steps in the formation of fibrils from amyloids 15
Figure 11: Schematic representation of self-replicating peptides employing the NCL .. 16
Figure 12: Dynamic self-assembly of anti-parallel β-sheets peptides 16
Figure 13: Peptide replication 17
Figure 14: Schematic representation of the proposed formation of fibers 17
Figure 15: Characterization of peptide 1 obtained by Fmoc SPPS. 23
Figure 16: Characterization of the electrophilic fragment E1 obtained by t-Boc SPPS. 24
Figure 17: Surface pressure-area isotherms of peptides 1 and 2 on deionized water. 25
Figure 18: GIXD patterns showing Bragg peaks and molecular model of peptide 1 26
Figure 19: CD spectra obtained in water and buffer of peptides 1, 2 and 1^{gg} 27
Figure 20: ThT fluorescence spectra of peptides 1 and 2 28
Figure 21: Dynamic light scattering experiments of peptide 1 29
Figure 22: Cryo-TEM images of peptis 1 and 2 in water and buffer 30
Figure 23: AFM topography images of 1 and 2 31
Figure 24: MD simulation for each conformer of peptides 1 and 2 32
Figure 25: Precipitation experiments 35
Figure 26: CD spectra obtained 1 min and 120 min after sonication 35
Figure 27: CD ellipticity at 216 nm as a function of self-assembly time for peptide 1 .. 36
Figure 28: ThT fluorescence over time for peptide 1 37
Figure 29: Cryo-TEM images of peptide 1 38

Figure 30: Detailed characterization of the fibril structures formed by peptide 1 39
Figure 31: Representative set of HPLC chromatograms..... 43
Figure 32: Production over time of 1 in the template free reactions..... 44
Figure 33: Production over time of 1 in template assisted reactions 45
Figure 34: Production over time of 1 in template assisted reactions 46
Figure 35: Investigation of replication system..... 47
Figure 36: Cross-catalytic formation of peptide 1 by three other templates..... 48
Figure 37: Production of 1 over time in the presence of various concentrations of E1.. 49
Figure 38: Log-log plot of various concentrations of E1..... 50
Figure 39: Log-log plot of various concentrations of 1 without equilibration..... 51
Figure 40: Log-log plot of various concentrations of 1 with equilibration..... 51
Figure 41: Rate of formation of F_1..... 55
Figure 42: Distribution of products in stability experiments of electrophiles 59
Figure 43: Representative HPLC chromatogram of the four products of peptide 2. 61
Figure 44: Template free reactions with 4 electrophiles..... 61
Figure 45: Template free reaction with racemic mixture of electrophiles..... 62
Figure 46: Products in template assisted reactions 63
Figure 47: CD spectra of the four isomers of peptides 2 65
Figure 48: AFM topography image of 2-γ-D fibrils 66
Figure 49: Balls and sticks representation of the four isomers of peptides 2 67

List of schemes

Scheme 1: Schematic representation of the two processes as described in this thesis ... 20
Scheme 2: Stick representation of peptide 1 and peptide 2 22
Scheme 3: General synthesis of the electrophiles via t-Boc chemistry. 23
Scheme 4: Native Chemical Ligation. 42
Scheme 5: Stick representation of replication system 1. 43
Scheme 6: Schematic representation of the two processes that take place in parallel.... 53
Scheme 7: A kinetic model used to describe the processes shown in this research..... 54
Scheme 8: Stick representation of replication system 2. 57

Scheme 9: Proposed mechanism for formation of structural and diastereo isomers 58
Scheme 10: Proposed network mechanism of β-sheet assisted glutamic acid ligation .. 67
Scheme 11: Solid phase peptide synthesis (SPPS). 71

List of tables

Table 1: Sequences of the peptides used in section 3.3 22
Table 2: Sequences of the peptides used in section 3.5 58

Abstract

Peptides and proteins are capable of converting, under various conditions, from their natural soluble forms (α-helix rich) into ordered insoluble β-sheet rich fibrillar assemblies. These fibrillar assemblies, also known as amyloid plaques, are thought to be responsible for several systemic and neurodegenerative diseases, called "amyloidosis", such as Alzheimer's, Parkinson's and others. Self-assembly processes of such peptides have been intensively investigated during the past decade, with a special focus on amphiphilic sequences, which are organized in alternating sequences comprising both hydrophobic and hydrophilic amino acids (see, for example, Figure 1). This structure gives rise to two distinct surfaces, one being hydrophobic and the other hydrophilic. In aqueous solutions, the hydrophobic side shields itself from water, driving the self-assembly of the peptides in a process comparable to the spontaneous folding of proteins observed in nature. The actual self-assembly process is based on the spontaneous diffusion and specific interactions among molecules governed by non-covalent interactions, including electrostatic, hydrophobic, van der Waals, hydrogen bonding and aromatic π-stacking. Although these interactions are individually weak, they can generate highly stable assemblies when numerous.

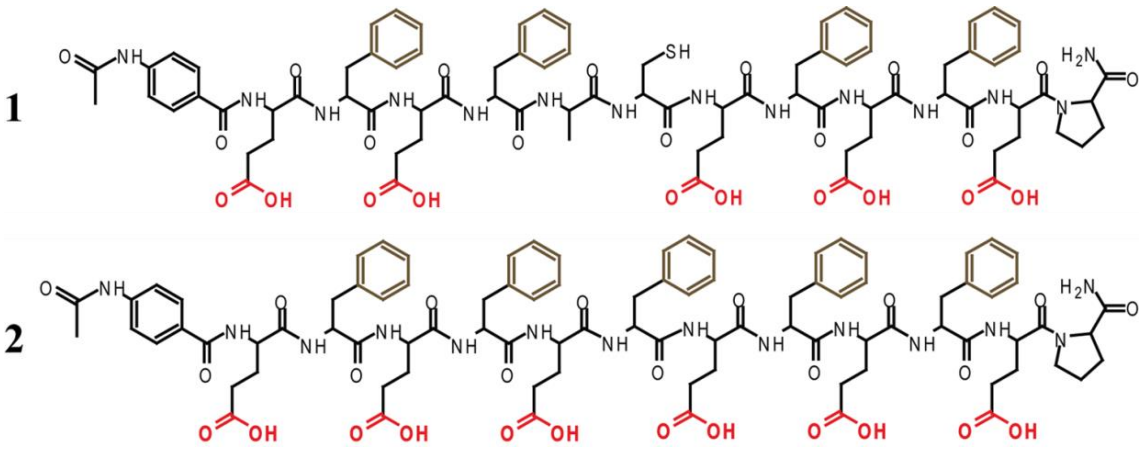

Figure 1: Stick representation of amphiphilic peptides used in this thesis composed of sequences of alternating hydrophobic aromatic phenyl alanines (brown) and hydrophilic charged glutamic acids (red).

An additional line of research has invested much effort in the study of non-enzymatic molecular replication systems. There, the design of replicating peptides has

centered mainly on α-helix forming sequences that self-assemble into coiled-coil tertiary structures. However, it has been postulated that shorter peptides with simpler sequences may serve as templates for self-replication, provided they are able to arrange themselves into unique and well defined structures. In this thesis, I present a study on rather simple peptides (Figure 1), close analogs of the synthetic amphiphilic Glu-(Phe-Glu)$_n$- peptides that form a variety of soluble β-sheet structures in water. Several of these structures have been found to significantly accelerate peptide ligation and self-replication.

I first describe the design and structural characterization of new β-sheet forming peptides, based on alternating sequences of hydrophobic and hydrophilic amino acids. I then present the research conducted, revealing the dynamic self-assembly process these peptides undergo in order to form supramolecular structures. By employing native chemical ligation, we have managed to probe which of these supramolecular structures are able to act as catalysts for the self-replication process and thereby enhance the ligation reaction. Finally, by combining the two parallel processes, namely the self-assembly and the self-replication, we propose a full system mechanism together with a kinetic model. In addition, I present a recent investigation of cysteine-free ligation, occurring only between the activated C-terminal amino acid and the primary amine of N-terminal amino acid, with a reaction that mimics the peptide bond condensation that occurs in nature. This process proceeds in a stereo- and regio-selective ligation reaction by β-sheet forming peptides.

It had been shown previously that peptides composed of alternating sequences of hydrophilic and hydrophobic amino acids have a high tendency to fold into stable β-sheet based structures. In addition, several researchers have promoted the protein first hypothesis, in which β-sheet based short peptides have acted as catalysts in various processes occurring in the origin of molecular evolution, among them self-replication. Towards this aim, we designed and synthesized rather simple peptides (**1** and **2** in Figure 1) in order to examine their self-replication properties. Using a battery of analytical tools, both at the air/water interface and in aqueous solutions, we characterized the different supramolecular structures formed by these peptides. A structural comparison

conducted between the β-sheet forming peptides **1** and **2** reveals highly organized supramolecular structures of peptide **2**, both qualitatively and quantitatively.

Several groups have proposed mechanisms for the self-assembly processes that amphiphilic β-sheet peptides undergo, revealing the structural hierarchy of supramolecular structures these peptides form. In this thesis, I describe the investigation of structural hierarchy in the self-assembly of peptide **1**, namely the dynamic process during which monomers of peptide **1** form β-pleated sheets via formation of a hydrogen bonds net, followed by re-organization into fibrillar structures, and then the formation of hollow nano-tubular structures during the last stage.

Next, I describe the results of the replication experiments, where we designed electrophilic (**E1**) and nucleophilic (**N1**) fragments that reacted through native chemical ligation to form peptide **1**. We followed the template-free ligation reactions, as well as reactions in which various amounts of peptide **1** had been seeded as a template, in order to examine the auto-catalytic properties of peptide **1**. We managed to show an increase in rate of up to 60-fold for the ligation reactions that were initiated with a seeded template, as compared to the template-free reaction. The influence of different forms of supramolecular structures of peptide **1** on the ligation was also investigated, by examining reactions where the ligation was initiated at various stages of the self-assembly process. The experimental results showed an increased ligation rate for the case of initiation by transient fibrillar structures, suggesting that the rate of ligation depends both on the initial template concentration and on the existing supramolecular structure formed by peptide **1**. By summarizing the two parallel processes, namely, the self-assembly and the self-replication, we proposed a full system mechanism (Figure 2) and kinetic model, which we proceeded to simulate and experimentally validate.

The last part of this work presents an additional replication system, where we have examined the capability of peptide **2** to act as a catalyst for its own formation. In this system, we sought to mimic an additional process occurring in nature, namely the non-enzymatic formation of peptide (amide) bonds from activated acid and primary amine only. For this purpose, we designed new electrophilic fragments that possess a thioester C-terminal glutamic acid, and new nucleophilic fragments with a free N-

terminal phenyl alanine. The newly designed electrophilic fragment showed dynamic epimerization and isomerization of the C-terminal activated glutamic acid, resulting in four ligation products upon reactions with the nucleophilic fragment. Interestingly, the glutamic acid-based ligation presented here proceeded efficiently as well as regio- and stereo-selectively, as evidenced by the selective amplification of two out of the four products.

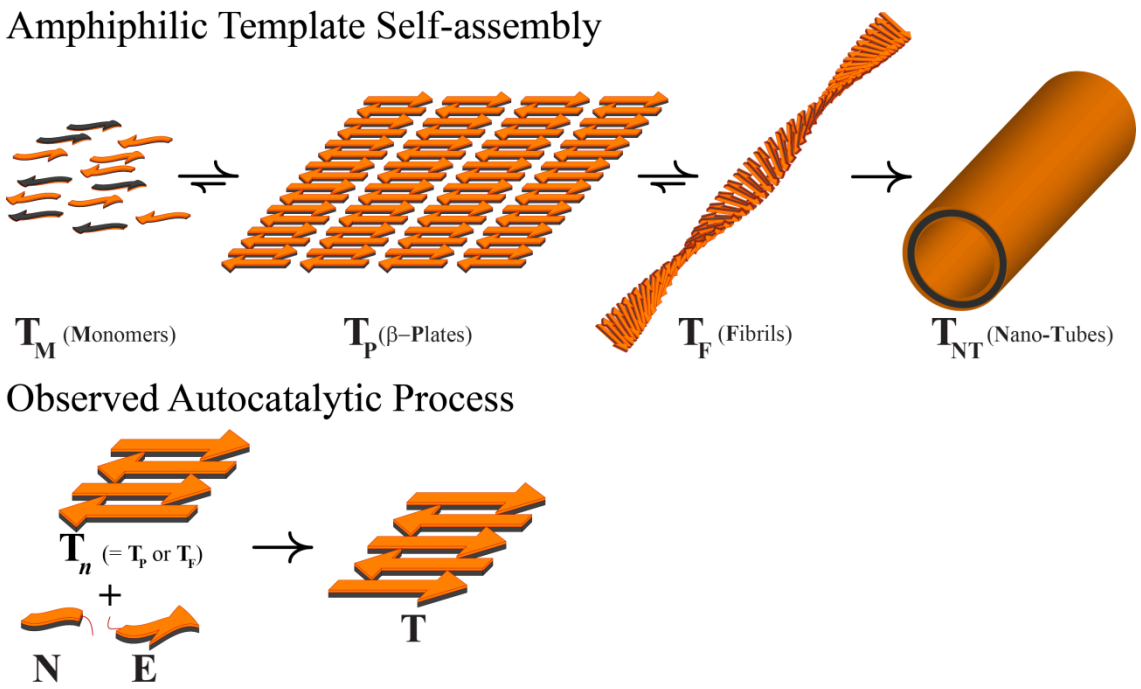

Figure 2: Schematic presentation of the two processes that take place in parallel during β-sheet peptides replication. (Top) Dynamic self-assembly process in which template monomers (T_M) self-assemble to anti-parallel β-pleated sheets (T_P), fibers (T_F), and finally nanotubes (T_{NT}). (Bottom) Autocatalytic reaction in which the β-sheet structure (generally depicted as T_n) serves as a template for registered association of E and N, which then react to form a new copy of T and the larger aggregate (T_{n+1}), available to serve again as a template.

This study allows for the expansion of the repertoire of replicating molecules. Of additional significance is the fact that the β-sheet replication was achieved using short peptides that possess alternating sequences of aromatic and charged amino acids. These systems demonstrate a stepwise mechanism that may have played a role in the origin of life, by which short peptides undergo self-assembly to form defined templates, which in turn become efficient replicators. Furthermore, the finding that β-sheet assisted peptide

ligation is stereo- and regio-selective may have implications on the possible role of β-sheet peptides in the origin of homo-chirality.

Keywords

Amphiphilic peptides, β-Sheet, Fibrils, Native chemical ligation, Self-replication, Auto-catalysis, Origin of Life

1 Introduction

Amphiphilic peptides that self-assemble through formation of β-sheet secondary structures are materials of a great interest in various fields such as nanotechnology, biochemistry and medicine, due to their chemical/physical properties and biological functionalities. They can be easily engineered to form a variety of stable nanostructures such as fibers, rods, tubes, nano-vesicles, globules and so on.[1-12] Since peptides in general are fragments of proteins, they can serve as simple models to study the process of protein aggregation through molecular self-assembly. A better understanding of protein aggregation might be crucial for understanding the onset of conformational diseases such as Alzheimer's and prion diseases and discovering inhibitors and treatments for their prevention or alleviation. Other fields of research, which may benefit from the ability to control the assembly of amphiphilic molecules to large structures, focus on developing "self-synthesizing materials".[13-15] These molecular assemblies can promote their own formation, upon request, by accelerating the synthesis of building blocks and/or assembly of the supramolecular structures via self-replication processes. Self-replicating molecules able to act auto-catalytically for their own synthesis.[16] Such molecules act as a template that non-covalently binds the precursors in a way that the reactive groups come in close proximity. On one hand, self-replication systems can be used to further investigate some basic chemical principles, such as molecular recognition and auto-catalysis, while on the other hand, they can shed light on plausible scenarios that may have led to the origin of life on earth. Of special interest are the self-replicating properties of proteins and peptides. It was shown that oligo-peptides containing only alternating amphiphilic sequences can spontaneously assemble to form relatively ordered macroscopic structures, independent of an external assembly mechanism or instruction code. Brack and Orgel suggested that alternating peptides with a tendency to form β-sheet structures may be able to form "membrane like aggregates" which may have been important in the origin of life.[17]

The following introduction sections provide a literature review describing the background for studying dynamic self-assembly processes of amphiphilic β-sheet

peptides that possess self-replicative characteristics. Accordingly, the introduction covers general β-sheet peptide properties and their possible implications to the origin of life theories, the design of synthetic β-sheet peptides and the structural hierarchy they form. In the area of self-synthesizing materials, the next sections will present general aspects of self-assembly processes, review on minimal self-replication systems, properties of amyloidal proteins that fold to β-sheet secondary structures, and recent works describing their propagation/replication properties.

1.1 Synthetic β-Sheet Peptides

1.1.1 Peptides Secondary Structures

The first elements of secondary structure, the α-helix and the β-sheet, were suggested in 1951 by Linus Pauling and coworkers.[18, 19] In native proteins the most common form of regular secondary structure is the α-helix. The α-helix is a right-handed coiled or spiral conformation (Figure 1a), in which every backbone N-H group donates a hydrogen bond to the backbone C=O group of the amino acid four residues earlier. This secondary structure is also sometimes called a classic Pauling-Corey-Branson α-helix. Among the common α-helix (i+4→i hydrogen bonding), other types of helices can be found in natural proteins, such as 3_{10} helix (i+3→i) and the π-helix (i+5→i).

The β-sheet (also termed β-pleated sheet) is the second form of regular secondary structure in proteins consisting of β-strands connected laterally by H-bonds, forming a generally twisted, pleated sheet. A β-strand is a stretch of amino acids whose peptide backbones are almost fully extended (Figure 1b).

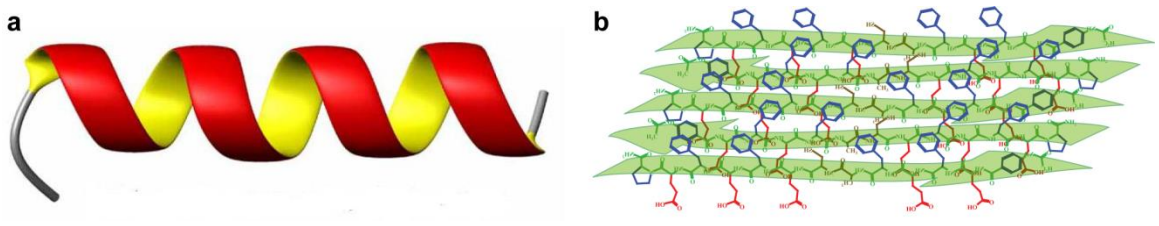

Figure 1: Schematic presentations of protein secondary structures. a) α-helix. b) β-sheet relevant to our study (see text).

β-sheets are important to the structure and biological activity of many peptides and proteins. Silk, for example, is composed predominantly of β-sheets, and most other proteins contain β-sheets as key structural elements. The deposition of an insoluble polypeptide with a β-sheet structure in the brain plays a key role in the progression of Alzheimer's disease. Conformational changes involving the conversion of α-helix into β-sheets is involved in scrappy and other prion diseases also called amyloidal diseases.

In a β-pleated sheet, the majority of β-strands are arranged adjacent to other strands and form an extensive hydrogen bonds network in which the N-H groups in the backbone of one strand establish hydrogen bonds with the C=O groups in the backbone of the adjacent strands.[20] The side chains point outwards from the folds of the pleats, roughly perpendicularly to the plane of the sheet; successive residues point outwards on alternating faces of the sheet. Adjacent β-strands in a β-sheet are aligned so that their C^{α} atoms are adjacent and their side chains point in the same direction (Figure 1b). The "pleated" appearance of β-strands arises from tetrahedral chemical bonding at the C^{α} atom. The "sideways" distance between adjacent C^{α} atoms in hydrogen-bonded β-strands is roughly 5 Å. However, β-strands are rarely perfectly extended; rather, they exhibit a slight twist due to the chirality of their component amino acids (Figure 2). The energetically preferred dihedral angles (φ, ψ) = (–135°, 135°) diverge from the fully extended conformation (φ, ψ) = (–180°, 180°). The twist is often associated with alternating fluctuations in the dihedral angles to prevent the individual β-strands in a larger sheet from splaying apart.

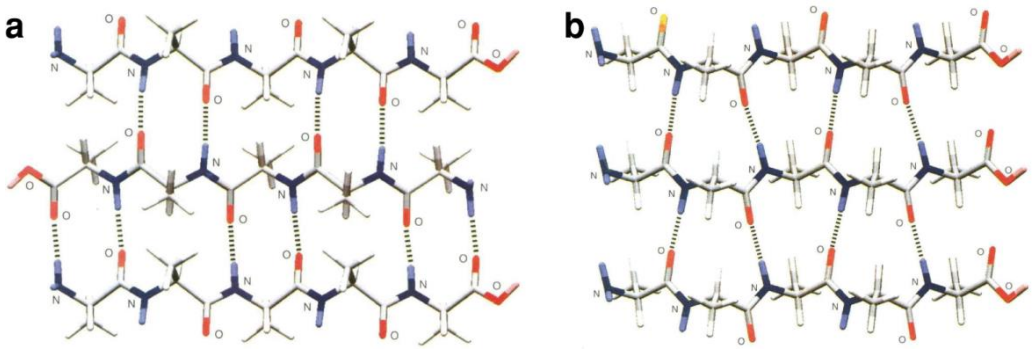

Figure 2: Stick representation of a) an anti-parallel β-sheet; b) a parallel β-sheet.[21]

Adjacent β-strands can form hydrogen bonds in anti-parallel, parallel, or mixed arrangements (Figure 2). In an anti-parallel arrangement, the successive β-strands alternate directions so that the N-terminus of one strand is adjacent to the C-terminus of the next. This is the arrangement that produces the strongest inter-strand stability because it allows the inter-strand hydrogen bonds between carbonyls and amines to be planar, which is their preferred orientation. The peptide backbone dihedral angles (φ, ψ) are about (–140°, 135°) in anti-parallel sheets. In a parallel arrangement, all of the N-termini of successive strands are oriented in the same direction; this orientation is slightly less stable because it introduces non-planarity in the inter-strand hydrogen bonding pattern. The dihedral angles (φ, ψ) are about (–120°, 115°) in the parallel sheets.

1.1.2 Possible Implications of β-Sheet Peptides to Origin of Life Scenarios

Since the pioneering experiment of Stanley Miller, in which he managed to synthesize most of the natural amino acids by imitating the possible conditions in the primitive Earth's atmosphere [22], a successful synthesis of polypeptides from amino acids in prebiotic conditions also has been reported.[17, 23-25] Although the concept of a primordial RNA world has produced great interest, given the informational and autocatalytic properties of ribonucleotides [26-28], the peptide/protein-first hypothesis has remained an alternative.[25, 29, 30] A recent review by Maury,[31] promotes the idea that in the prebiotic peptide/protein world, β-sheet polypeptide aggregates were the first replicating and information-processing molecules that evolved. By pointing out the basis for the β-sheet conformational peptide/protein-first hypothesis, the author concluded that protein-based β-sheet molecular structures possessed the necessary and sufficient characteristics for making a bio-molecular evolution possible under the prevailing conditions.

An important research line on the origin of life is the origin of homo-chirality of biomolecules. In the late 1980's Brack and coworkers examined the properties of

polypeptides with L and D residues that adopted β-sheet secondary structure in aqueous solution.[32-34] They found that while peptides that fold to α-helix secondary structure can accommodate residues of both chirality distributed in the same chain, the amino acids of opposite chirality progressively reduced the formation of β-sheet structures as they were progressively introduced into the chains, and that the peptide itself consisted of β-sheet portions highly enriched in one enantiomer, with the remaining enantiomerically less pure chains in a random folding. Furthermore, oligomerization of racemic NCA-amino acids (NCA = N-carboxyanhydride), showed that racemic NCA−Trp condensation gave chains with preferential homo-chiral sequences: the homo-chiral blocks become increasingly over-represented with increasing oligomer length if compared with the statistical distributions.[35, 36] In addition, NCA-amino acid condensation followed by peptide self-assembly in water and analysis of the results by MALDI-TOF mass spectrometry gave rise to several observations: (i) formation of racemic beta sheet peptides containing isotactic strands of alternating chirality (Figure 3); (ii) increase in isotactic peptides, relative to their statistical binomial probability, with increasing peptide length; (iii) transition of the distribution of diastereoisomers, with increasing peptide length, from a more random distribution to one favoring the more chiral peptides.[37-43]

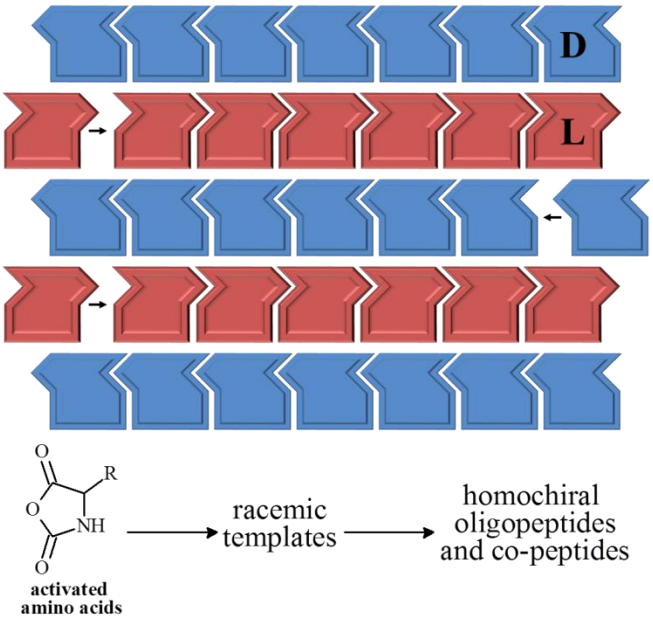

Figure 3: Proposed route for chain elongation via formation of racemic antiparallel β-sheets comprising alternating oligo-D and oligo-L chains.[41]

Recently, in our group we simulated using Matlab™ experimental results of amino acids condensation to form β-sheet peptides, showing how a simple model, consisting of only polymerization of amino acids and reversible β-sheet formation, can explain a wide range of experimental work.[44]

1.1.3 Design of Synthetic β-Sheet Peptides

Early works on the design of synthetic β-sheet peptides showed that there is a basic motif present in most β-sheets which is alternating sequences of hydrophobic and hydrophilic amino acids.[17, 32-34] As a consequence of this alternating pattern, when assembled into a sheet, this gives rise to a hydrophobic and hydrophilic face. This drives two sheets to come together in order to bury the hydrophobic face from the surrounding water, by formation of fibrous structures.[2, 5, 6, 9, 45-49] Well-defined assemblies of β-sheet structures have been achieved also at the air‑water interface. Several works [50-53] have investigated a family of amphiphilic peptides comprised of alternating hydrophobic and hydrophilic moieties with the generic sequence X-Y-(Z-Y)$_n$-X, where the N- and C-terminal residues (X = Pro) bear charged ammonium and carboxylate groups, respectively, and Y and Z are alternating hydrophilic and hydrophobic amino acids. Variations in the amino acid sequence and the number of dyads (*n*) participating in the hydrogen-bond formation were expected to tune the intermolecular interactions. The peptides Pro-Glu-(Phe-Glu)$_n$-Pro (*n* = 4, 5 or 7) formed secondary structures composed of two-dimensional self-assembled β-sheet monolayers at the air‑water interface, as confirmed by in situ grazing-incidence X-ray diffraction (GIXD) investigations.[50] The alternating hydrophobic phenylalanine and the hydrophilic glutamic acid residues caused the peptide chains to orient as β-pleated sheets parallel to the water surface.

The flexibility of the peptide backbone and the repetitive nature of the amino acid sequence may induce dislocation defects (Figure 4a) that limit long-range order to one-dimension (1D), in the direction normal to the peptide backbone. Noteworthy, the two-dimensional (2D) registry of the self-assembled architectures was induced by

placement of proline residues at the peptide termini. Without Pro, only 1D order was achieved, demonstrating the importance of a careful design of the peptide sequence for the successful self-assembling process. Pro was thus chosen to prevent the formation of disordered β-sheets along the a direction (Figure 4b), on the basis of three characteristic features: (i) the tertiary amide, which cannot participate as a donor in the hydrogen bond array; (ii) the restricted dihedral angle (φ) of Pro (ca. -60°) that is significantly different from that of β-sheet peptides (φ ca. -120 to -150°), therefore making inclusion of Pro in the interior of a β-sheet ribbon sterically unfavorable; and finally, (iii) the cyclic Pro side chain, which determines geometric constraints, minimizing disorder at the ribbon edge. In addition, attractive electrostatic interactions between the chain termini were expected to juxtapose the β-sheet ribbons along the b direction (Figure 4b), facilitating the formation of a two-dimensional order.

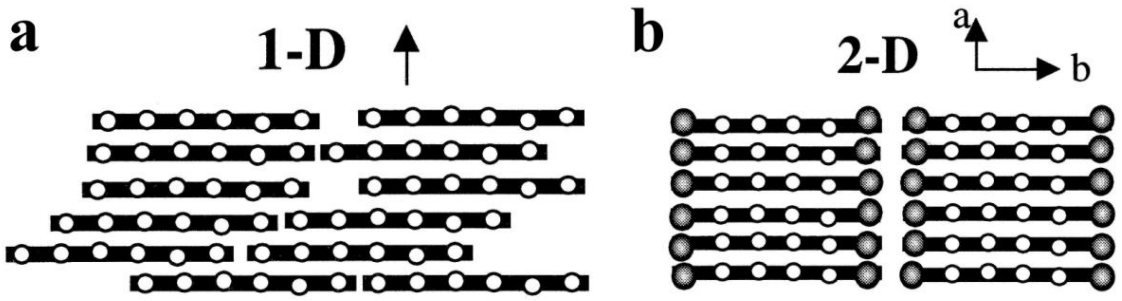

Figure 4: Schematic diagrams of β-sheet assemblies at the air-water interface, represented by peptide backbones (black rods) and hydrophobic amino acids (white dots). A view from above of a β-sheet in (a) one-dimensional order and (b) two-dimensional order induced by proline residues (grey balls) at the termini.[50, 53]

1.1.4 Structural Hierarchy of Synthetic β-Sheet Peptides

The main challenge of designing a self-assembling fibrous system is to control the assembly to form uniform reproducible structures. Several models of β-sheet forming peptide self-assembly mechanisms were described.[54-56] One of the proposed mechanisms showed that β-sheet based fibers can form a series of hierarchical structures in a concentration and time dependent manner. These structures range from the basic peptide structure (Figure 5) as a monomer which assembles into a tape, two of which can bury hydrophobic residues by forming a ribbon. Ribbons can further assemble by lying face to face to form fibrils and additionally side by side to form fibers.

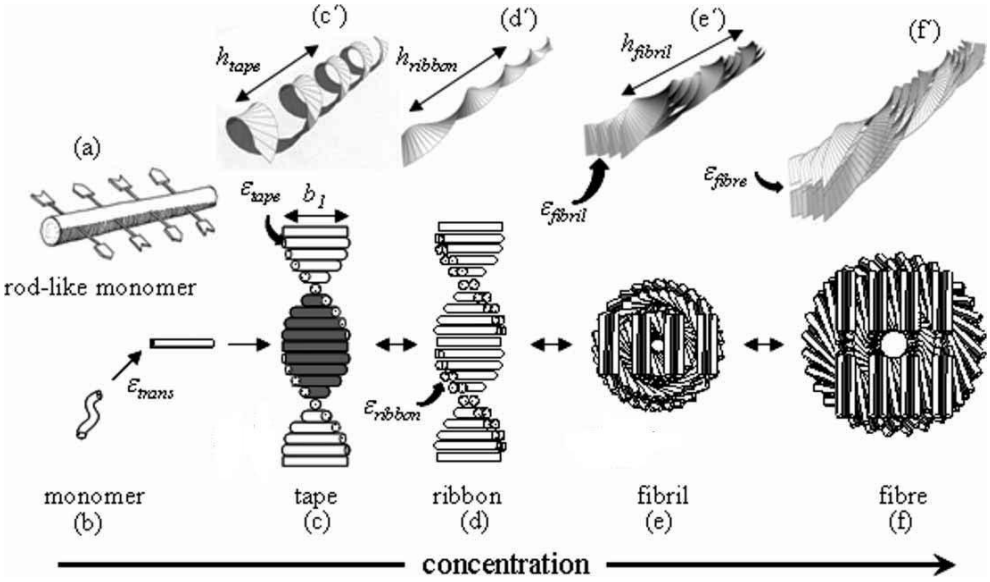

Figure 5: Different hierarchical structures that can be formed from β-sheet peptides (a; b), which were classed as tapes (c and c`), ribbons (d and d`), fibrils (e and e`) and fibers (f and f`), all of which vary in the number of sheets that pack together to form the final structure.[54]

Other researchers probed the self-assembly process of peptides having a general sequence of Pro-Lys-X_1-Lys-X_2-X_2-Glu-X_1-Glu-Pro (X_1 and X_2 hydrophobic residues selected from Phe, Ile, Val, or Tyr), using microscopic tools.[55] They found that the designed peptides self-assembled in a hierarchical manner (Figure 6): peptide β-sheets assembled to form protofibrils, which associated into higher ordered fibrillar assemblies. The measured protofibril width was found to be almost equivalent with the striations width in the assembled fibers. This coincidence implies that protofibrils like those reported were initially formed from the peptide monomers. The protofibrils aligned side-by-side to make up a ribbon, and then the ribbons helically coiled to form straight fibers. The straight fibers exist as a ‘‘single’’ fiber, and intertwisting or bundling can be suppressed.

The designer self-assembling peptide RADA16 forms nano-fiber matrices which have shown great promise for regenerative medicine and three-dimensional cell culture. Molecular sliding diffusion was proposed as a mechanism for dynamic reassembly of RADA16 peptides from β-pleated sheets to fibrillar structures.[46] When the peptides form stable antiparallel β-pleated sheets in water, they create a net of hydrogen bonds along the peptide backbones. The β-sheets have two distinctive sides, one hydrophobic

and the other hydrophilic charged. The hydrophobic residues form overlap packed hydrophobic interactions in water, similar to interactions found in silk fibroin from silkworm and spiders, in a bilayer manner. When the fragments of bilayers first meet, the hydrophobic sides may not fit perfectly but have gaps. However, the nonspecific hydrophobic interactions permit the bilayer to slide diffusively along the forming fiber in either direction, which minimized the exposure of hydrophobic residues and eventually filled the gaps.

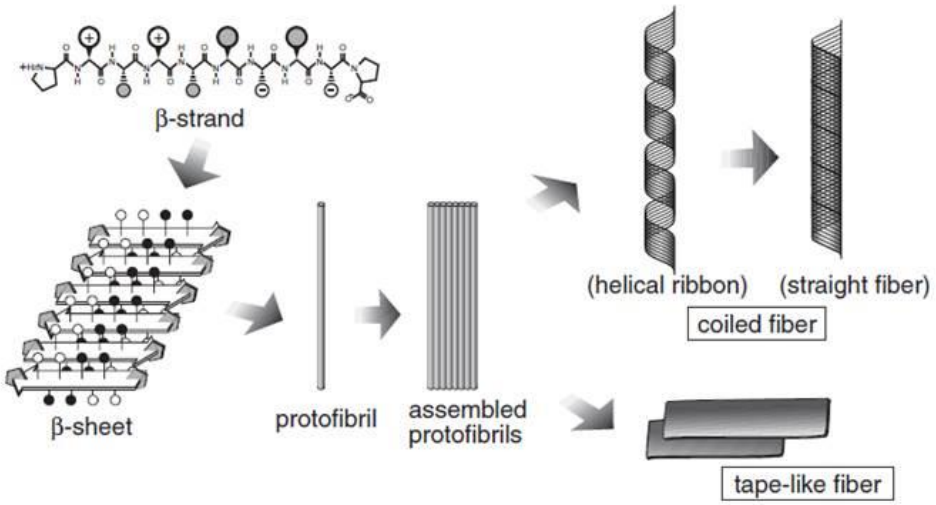

Figure 6: Hierarchical fiber formation, self-assembled from ten-residue peptides ($PKX_1KX_2X_2EX_1EP$). [55]

1.2 Self-Synthesizing Materials

An emerging new direction of research focuses on developing self-synthesizing materials. These supramolecular structures can promote their own formation by accelerating the synthesis of building blocks and/or an entire assembly.

1.2.1 Self-Assembly Process

Self-assembly is a spontaneous organization process of molecules under near thermodynamic equilibrium conditions into structurally well-defined and stable arrangements through non-covalent interactions.[57] Such interactions typically include hydrogen bonding, electrostatic attraction, hydrophobic forces and van der Waals interactions.[58] In engineering for example, self-assembly has emerged as a novel approach to design and fabricate supramolecules with novel functionalities from single and simple molecules. One major achievement has been the evolution of microelectronics toward molecular-scale electronic devices and machines through the development of nanowires, nano-arrays and molecular chips.[59] This has allowed modern-day electronic devices to be scaled down considerably and achieve higher operational efficiency. In both nature and engineering, the control of the self-assembly process is crucial. The failure to exert control over protein assembly is most exemplified by the *in vivo* formation of protein insoluble aggregates, which are associated with numerous conformational diseases such as Alzheimer's and prion diseases.

There are two main types of self-assembly: static and dynamic. Static self-assembly involves systems that are at global or local equilibrium and do not dissipate energy, such as molecular crystals and most folded globular proteins. In static self-assembly, formation of the ordered structure may require energy (for example in the form of stirring), but once it is formed, it is stable. In dynamic self-assembly, on other hand, the interactions responsible for the formation of structures or patterns between components only occur if the system is dissipating energy, processes that occur in biological cells for example.

Through probing various protein motifs found in nature, scientists have been able to elucidate the molecular interactions that govern peptide self-assembly. Peptide self-assembly is highly specific—the intermolecular interactions such as hydrogen bonding, ionic, electrostatic, hydrophobic, and van der Waals interactions are mediated by molecular recognition. The understanding of molecular and structural biology has inspired the design and synthesis of increasingly complex self-assembled biomaterials for biomedicine and bio-nanotechnology. By engineering the amino acid sequence, the secondary structure of peptides can be manipulated to optimize the interactions between adjacent peptides.[4, 5, 46, 49, 53]

1.2.2 Minimal Self-Replication Systems

Self-replication systems are relatively new; research on molecules which are able to self-replicate began in the late 1980's.[60-62] A minimal self-replication system is composed of a template molecule and precursors that can react chemically to form the template molecule. Such a system can be described by an auto-catalytic cycle (Figure 7), in which the ternary complex A·B·T is formed reversibly from the template T and the precursors A and B. The close proximity of the reactive ends facilitates the formation of a covalent bond between the two precursors. Reversible dissociation of the duplex T·T gives two template molecules, each of which can begin a new replication cycle.

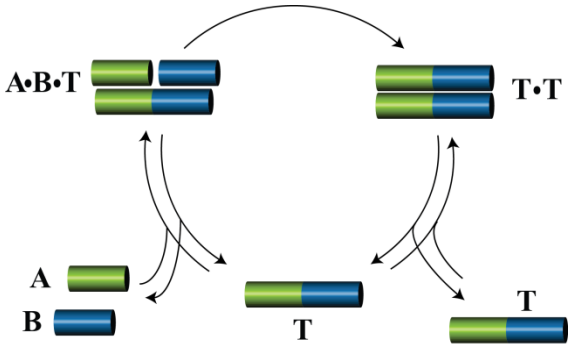

Figure 7: Minimal self-replication system described by auto-catalytic cycle.[63]

Early studies demonstrated a few species of molecules which can form self-replication systems. Orgel and coworkers investigated the template-directed synthesis of

oligo-nucleotides from activated mono-nucleotides.[16] Further investigation of the system showed the influence of the initial seeded template on the self-replicating process (Figure 8a). The results showed increase in the reaction rate as a function of the increase in the initial template seeded. Then,[64, 65] the research was expanded to self-complementary RNA molecules which formed a self-replication system (Figure 8b).

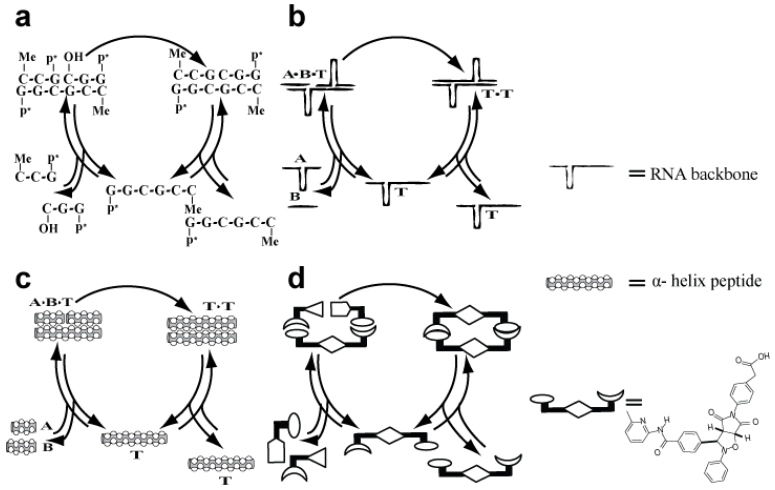

Figure 8: Known synthetic minimal self-replication systems: a) ds-DNA. b) RNA. c) Peptides. d) Organic molecules. [63]

Self-replication process using peptides has also been investigated (Figure 8c). The motivation for these studies was the fact that experiments emulating prebiotic conditions have often been found to yield short peptides as products.[25] Peptides have the ability to self-assemble, and have a route to information transfer through self-replication; therefore they have a huge potential role in the molecular origins of life. Compared with nucleotide-based biopolymers, peptides and proteins are much more diverse in their ability to form defined structures and are capable of self-assembly through a variety of motifs. The initial self-replicating peptides were based on the coiled-coil of the GCN4 transcription factor. By modifying the sequences, researchers have managed to control the self-replication process and even expand the replication system to a molecular network.[66-70] In parallel, the repertoire of self-replicating molecules had been expanded to abiotic/organic molecules (Figure 8d). In this system, a Diels-Adler reaction was catalyzed by the reaction product, which assembled with the reactant by H-bonds. [71-73]

The kinetics of minimal self-replication systems can be described by a simple set of chemical equations (Equation 1): in the first step an association of the precursors and the template takes place to form the ternary complex. Following the conjugation reaction (ligation), the template-product complex T·T must dissociate to provide two free copies of T, which can re-enter the next cycle of replication.

$$A + B + T \underset{k_2}{\overset{k_1}{\rightleftharpoons}} A \bullet B \bullet T$$

$$A \bullet B \bullet T \xrightarrow{k_3} T \bullet T$$

$$T \bullet T \underset{k_5}{\overset{k_4}{\rightleftharpoons}} T + T$$

Equation 1: Chemical equations describing a minimal self-replicating system. A and B refer to precursors of T.

Analysis of several minimal self-replication systems revealed a linear relationship between the initial rate of product formation and only the square root of the initial template concentration. It was found that the kinetic behavior of such systems can be described using two distinct profiles: fast dissociation of T·T results in an exponential behavior, while a slow T·T dissociation presents a parabolic behavior (Figure 9).

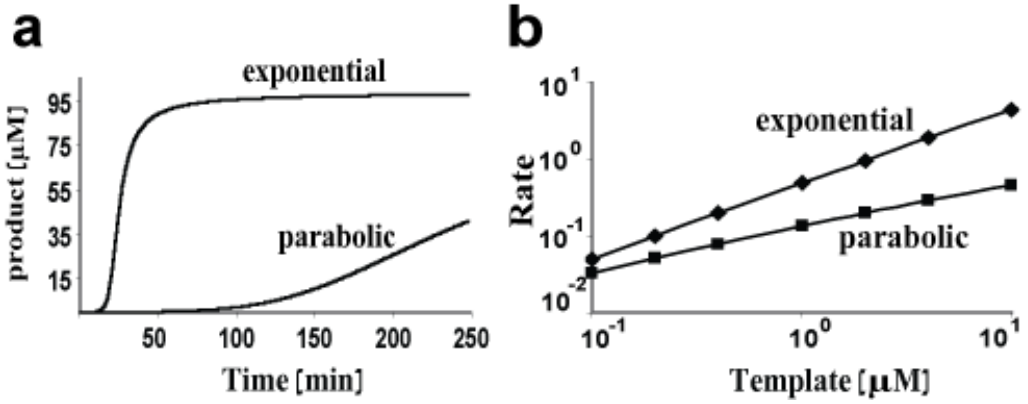

Figure 9: a) Kinetic profiles of parabolic and exponential growth of self-replicating molecules. b) A log-log plot of initial rates of product formation as a function of different concentrations of seeded T. As in the analysis of the experimental results, the slopes in this plot reveal *p* values close to 0.5 and 1 for parabolic and exponential growth, respectively.[63]

In the first case, the efficient dissociation of complex T·T allows auto-catalytic amplification (exponential growth). In the second case, the rate-limiting slow dissociation of the T-T complex results in a significant product inhibition (parabolic growth). By showing the data in a log-log plot, in which the y-axis is the log of initial rate and the x-axis is the log of initial template concentration, it is possible to get a curve for each type, where the slope is the reaction order *p*, which equals to 0.5, for parabolic and to 1, for exponential process.

1.2.3 Propagation of Amyloid Peptides

Amyloids are filamentous proteins composed of aggregated peptide β-sheets formed from parallel or anti-parallel alignments of peptide β-strands. Amyloid-forming proteins have recently attracted a great deal of attention because of their association with over 30 diseases, notably neurodegenerative conditions like Alzheimer's, Huntington's, Parkinson's, Creutzfeldt-Jacob and prion disorders, but also systemic diseases such as amyotrophic lateral sclerosis (Lou Gehrig's disease) and type II diabetes. The highly ordered β-sheet structure of amyloid-β (Aβ) peptides, which is primarily composed of 40- to 42-residues, is distinguished by some unique characteristics. These are self-propagation, protease-resistance and, in some instances, transmissibility.[74-76] *In vitro* structural studies of Aβ using synthetic peptides have demonstrated the spontaneous assembly into amyloid-like fibers. The fibrils are of varying lengths, unbranched, and have a characteristic β-sheet conformation and proto-filament organization.[56, 77-81] From experimental and computational studies of amyloidogenesis, several pathways for fibril formation and elongation have emerged.[82-85] One possible pathway is self-assembly of large unstructured peptide monomers to form nuclei. When the nucleus reaches a critical size, it grows to form full-length fibrils by the addition of monomers to the existing fibril ends. In another pathway, there is first the formation of peptide protofibrils of intermediate length. Such protofibrils then associate to form full-length fibrils. Once full-length fibrils are formed, the amyloid peptide may add directly to existing fibrils or protofibrils (Figure 10).

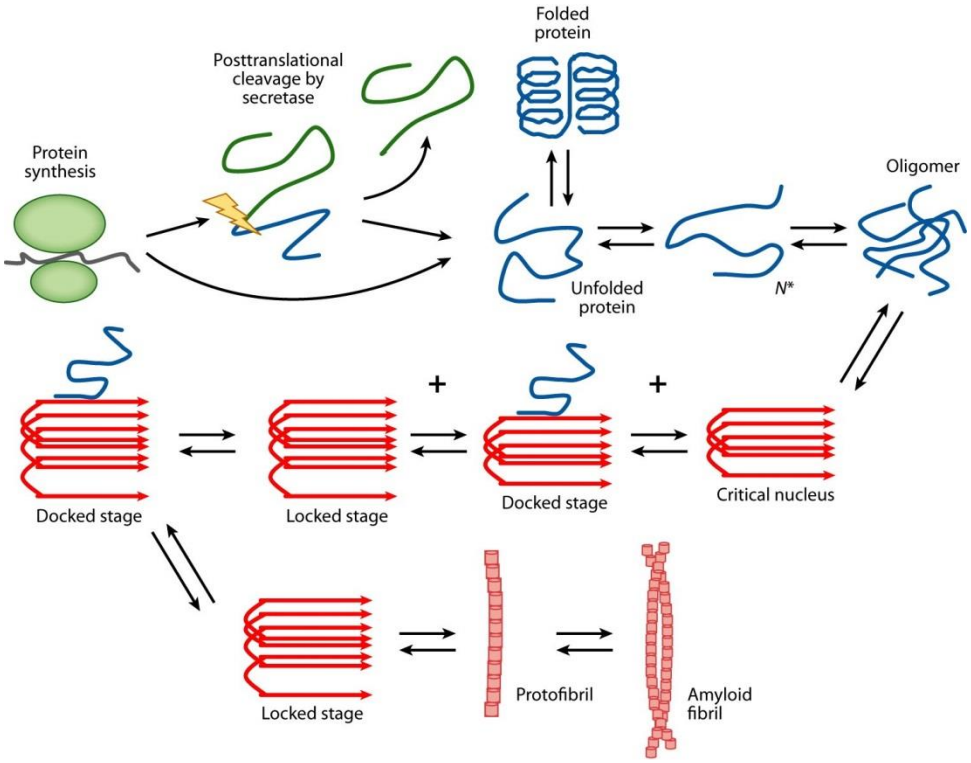

Figure 10: Summary of kinetic steps in the formation of aggregation-prone states and fibrils from amyloid peptides (see text above).[84]

1.2.4 Replication by β-Sheet Peptides

It has been claimed [17, 86] and demonstrated that native amyloid fibrils can replicate, although with moderate efficiency. Based on previous studies, peptide sequences that can assemble into amyloid-like fibrils and thus act as a template for self-assembly and self-replication processes have been designed. The design is based on recognition ability of amyloidal peptides, due to the fact that the amyloid fibril recognizes polypeptide chains possessing the identical chemical structure, namely electrophilic and nucleophilic fragments that react through native chemical ligation.[87] The recognized peptides are assembled on the fibril, in which the conformation of the newly assembled peptide is converted to the amyloid form (Figure 11). The fibril thus extends its own length, but maintains the active sites for the next cycle of reactions.

Although the authors hadn't succeeded in showing significant amplification of the replication process, in reactions that were initially seeded with pre-organized fibrillar structure of the template molecule, compared to the template free reaction, this work

presents the first demonstration of applicability of amyloid-like fibrillar structures as a macromolecular construct possessing molecular recognition and catalytic abilities.

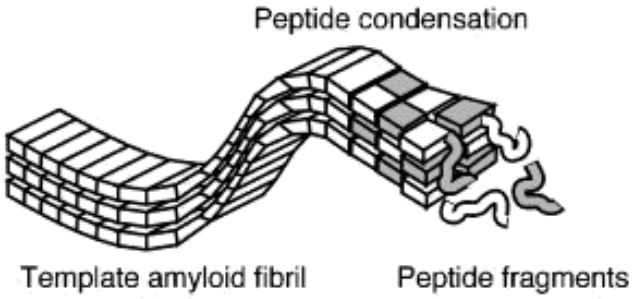

Figure 11: Schematic representation of self-replicating peptides employing the native chemical ligation reaction. [88]

Recently, as described in this thesis, using variety of analytical tools, we followed and analyzed the self-assembly pathway of short amphiphilic peptides into various forms of soluble β-sheet structures in aqueous solutions (Figure 12) and their consequent activity as auto-catalysts for the synthesis of monomeric peptides from simpler building blocks.[89-91]

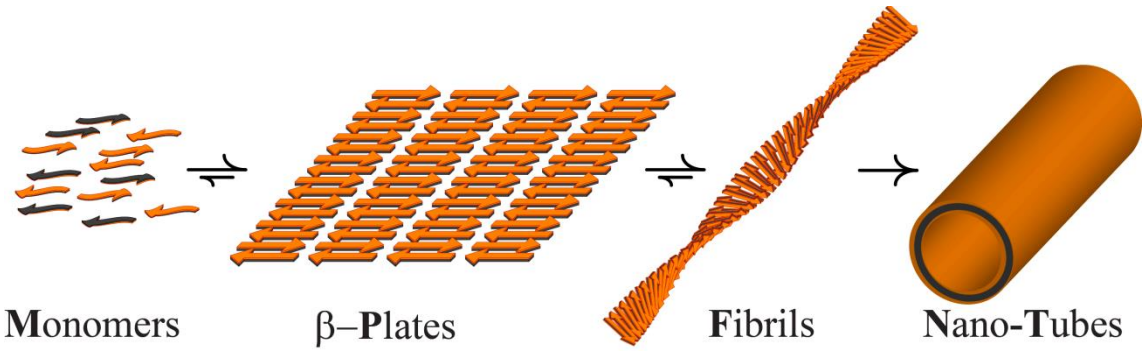

Figure 12: Schematic representation of the dynamic self-assembly of monomers to anti-parallel β-pleated sheets, fibrils, and finally nano-tubes.

A detailed kinetic analysis of both the self-assembly and self-replication processes allowed us to suggest a replication model. In our model, the edges of a preformed anti-parallel β-sheet assembly (T_n) serve for registered association of the two peptide fragments E and N (Figure 13). Due to their close proximity, E and N react immediately to form the full length native chemical ligation thioester intermediate,

which rearranges to form a new molecule of T, and the larger aggregate T_{n+1}, readily available for further enhancing the replication reaction.

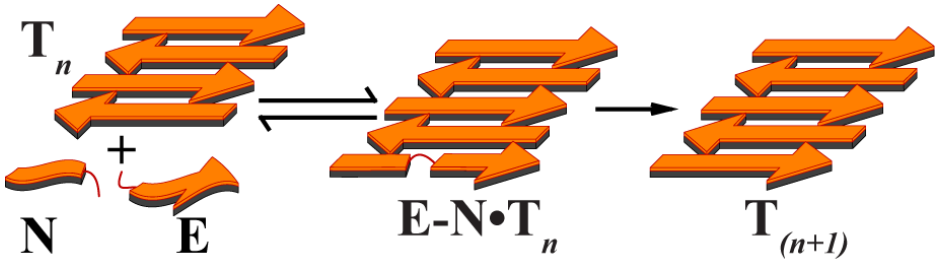

Figure 13: Peptide replication. The arrows represent β-strands which form an anti-parallel 2-D β-sheet assembly and acts as a template for registered association of electrophilic and nucleophilic fragments.[90]

An additional utility of β-sheet peptides in replication systems is shown in Figure 14.[92] The researchers reported on two self-replicating peptide-derived macro-cycles that emerge from a small dynamic combinatorial library (a group of molecules reversibly assembled from building blocks, giving a distribution of inter-converting library members often under thermodynamic control) and competing for a common feedstock (Figure 14). Replication is driven by nanostructure formation, resulting from the assembly of the peptides into fibers held together by β-sheets. Which of the two replicators becomes dominant is influenced by whether the sample is shaken or stirred. Their results established that mechanical forces can act as a selection pressure in the competition between replicators and can determine the outcome of a covalent synthesis.

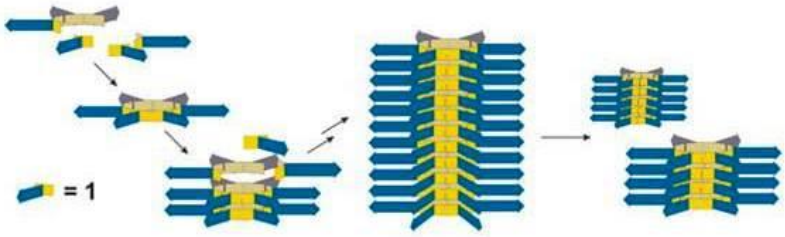

Figure 14: Schematic representation of the proposed formation of fibers. The benzenedithiol core of building block is shown in yellow and the peptide chain in blue. Stacks of hexamer are held together by the assembly of the peptide chains into elongated cross β-sheets. The stacks grow from their ends, which increase in number through stack fragmentation, enabling exponential growth.[92]

2 Objectives

This work aims to design and investigate a new class of self-replicating peptides, based on folding into β-sheet secondary structures. Careful design of sequences led to peptides that self-assemble to fibrillar structures with high solubility and structural organization in aqueous solutions. Towards these aims, a family of synthetic amphiphilic β-sheet peptides were designed, synthesized and characterized. As envisioned, these water soluble β-sheet supramolecular structures induced peptide replication and therefore fibril reproduction.

2.1 Characterizations of Peptide Self-Assembly and Supramolecular Structural Hierarchy

Using guide-lines from previous studies, we designed peptides that self-assemble to 2D β-sheet structures in aqueous solutions. By using a battery of analytical techniques (Langmuir through, GIXD, CD spectroscopy, ThT fluorescence, cryo-TEM imaging, and AFM) we characterized the peptides in aqueous solutions and at the air/water interface. By employing these tools, the kinetics of the self-assembly processes were followed. These analyses revealed the structural hierarchy in supramolecular structures that these peptides form.

2.2 Analysis of β-Sheet Forming Peptides Replication

By insertion of an Ala-Cys dyad in the middle of the β-strand monomer, a self-replication system formed, in which the β-sheet structures functioned as a template for ligation between two short peptide fragments. I examined the ligation reaction between the short fragments in the absence of template or in the presence of initially seeded template, finding that the β-sheet forming peptide can act as a catalyst for its own formation. In addition, I examined which of the different supramolecular structures are suitable for catalyzing the ligation reaction.

2.3 Discover the Replication System Mechanism

By combining all kinetic data, both from self-replication and self-assembly processes, we proposed a possible replication mechanism of β-sheet forming peptides. The proposed mechanism was then simulated, to find a kinetic model using basic chemical equations, and the results correlated well with the experimental results.

2.4 Studying Regio- and Stereo-selective Ligation by β-Sheet Peptides

The repertoire of replicating β-sheet peptides was expanded to a set of peptides that ligate through glutamic acid residue. For this system, the electrophilic thioester fragment was synthesized with a C-terminal glutamic acid. The proximity of the γ-carboxyl of the glutamic acid to the thioester made it more reactive and thus caused the formation of a glutaric anhydride intermediate, which in turn increased the acidity of the α-proton, so L and D stereoisomers formed. Therefore, the ligation reaction yielded four isomers. The nucleophilic fragment, on the other hand, buries only the primary amine of phenylalanine amino acid. The ligation reaction was examined with or without the addition of β-sheet forming peptide in order to probe template effect on stereo- and regio-selectivity in product formation. Finally, we proposed a β-sheet assisted glutamic acid ligation mechanism based on the experimental results.

3 Results and Discussions

The following chapter describes the experiments in which I managed to show regio and stereo template assisted β-sheet polymerization by using rather simple peptides. This chapter covers the design and synthesis of β-sheet forming peptides **1** and **2** (3.1, p. 21). The new synthesized peptides were characterized using variety of analytical tools, both at the air/water interface and in aqueous solutions, revealing their assembly to β-sheet structures. Then, the self-assembly pathway of peptide **1** in solution was investigated by different tools revealing the structural hierarchy peptide **1** forms (3.2, p. 34). By employing native chemical ligation, the self-replication properties of peptide **1** were investigated in experiments where various concentrations of peptide **1** were initially seeded. The influence of different supramolecular structures formed by peptide **1** on the self-replication process was examined as well (3.3, p. 42). Based on all the data obtained from the self-assembly kinetics experiments and the replication kinetics experiments, we proposed a full system mechanism which consists of these two processes (Scheme 1) and the kinetic model simulated using Matlab™ (3.4, p. 53).

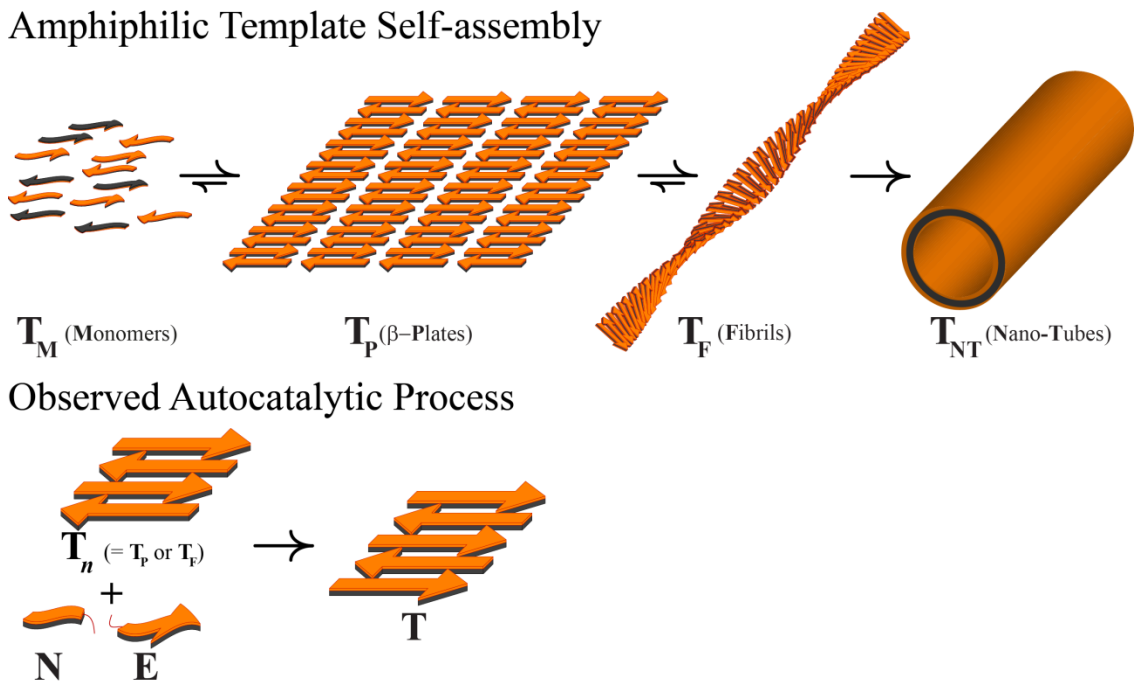

Scheme 1: Schematic representation of the two processes as described in this thesis: (top) – dynamic self-assembly of β-sheet forming template; (bottom) – β-sheet assisted self-replication process.

The last section (3.5, p. 573.5) in this chapter describes the investigation of a β-sheet assisted glutamic acid peptide ligation. We designed a new β-sheet based replication system, in which peptide **2** acted as a replicator, and found dynamic epimerization and isomerization of the precursors. These processes led to four isomer products in the ligation reaction. By characterizing the different isomers, we proposed a mechanism of regio- and stereo-selective β-sheet assisted glutamic acid ligation.

3.1 Design and Structural Characterizations of β-Sheet Forming Peptides

3.1.1 Peptide Design

Based on previous works[50-53, 93] the sequence of the β-sheet forming peptide P_{FE}-5[52] was chosen as our model template peptide. This peptide is comprised of an alternating sequence of glutamic acid and phenylalanine, with proline residues at both termini. In peptide **2** (Scheme 2) the C-terminal proline was replaced by the capping aromatic 4-acetamidobenzoate (ABA), in order to enhance UV absorption (Table 1). ABA has a high molar extinction coefficient of ~18000 $M^{-1}cm^{-1}$ at 270 nm. Peptide **2** was then modified to include an Ala-Cys dyad in the middle of the sequence, as the site for breaking the full sequence, to form the N- and C-termini fragments that required for native chemical ligation, resulting in the peptide **1** sequence (Scheme 2). Moreover, this ligation site in the middle position of the core sequence was chosen since effects of different amino acid substitutions in these positions on β-sheet formation were expected to be relatively low. As shown [50], a peptide constructed of only two Glu-Phe dyads formed a relatively stable β-sheet monolayer at the air/water interface. Peptide **1** can thus be formed by condensation of shorter electrophilic and nucleophilic peptides (**E1** and **N1** in Table 1) through native chemical ligation.

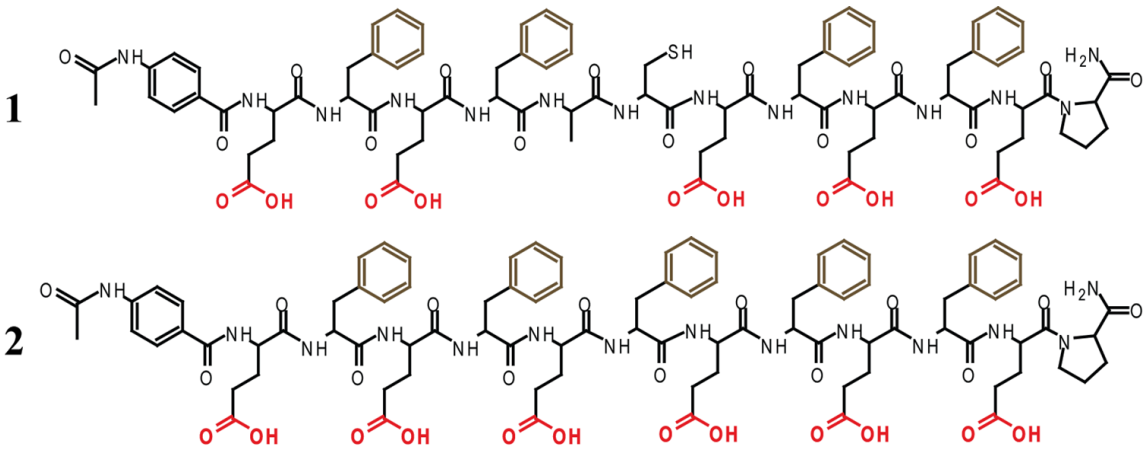

Scheme 2: Stick representation of peptide **1** (top) and peptide **2** (bottom).

Peptide	Sequence
P_{FE}-5[52]	Pro-Glu-Phe-Glu-Phe-Glu-Phe-Glu-Phe-Glu-Phe-Glu-Pro
2	ABA-Glu-Phe-Glu-Phe-Glu-Phe-Glu-Phe-Glu-Phe-Glu-Pro-$CONH_2$
1	ABA-Glu-Phe-Glu-Phe-Ala-Cys-Glu-Phe-Glu-Phe-Glu-Pro-$CONH_2$
E1	ABA-Glu-Phe-Glu-Phe-Ala-$COSR^*$
N1	Cys-Glu-Phe-Glu-Phe-Glu-Pro-$CONH_2$
1^{gg}	ABA-Glu-Phe-Gly-Phe-Ala-Cys-Glu-Phe-Gly-Phe-Glu-Pro-$CONH_2$
E^g	ABA-Glu-Phe-Gly-Phe-Ala-$COSR^*$
N^g	Cys-Glu-Phe-Gly-Phe-Glu-Pro-$CONH_2$
Sc	ABA-Lys-Phe-Val-Ala-Lys-Ala-Lys-Lys-Leu-Val-Gly-Phe-$CONH_2$
S	ABA-Ala-Ala-$CONH_2$

Table 1: The sequences of the peptides used in the present chapter. SR^* = S-(3-amino-3-oxopropyl) thioester

As a control for replication system **1** we designed the peptide **1^{gg}**, for which the sequence of peptide **1** was modified by changing two glutamic acid residues for glycine residues. **E1** and **N1** were also modified, resulting in sequences of **E^g** and **N^g**. Another control peptide, **Sc**, was designed. This peptide consisted of a portion of a 12 amino acid sequence of a peptide that folded into a α-helix, with ABA molecule at the N-terminus. In addition, peptide **S** was used as an internal standard for the replication experiments.

3.1.2 Peptide Synthesis – SPPS

Solid phase peptide synthesis (SPPS)[94] was used to prepare the peptides. Two major methods are used in the SPPS – Fmoc chemistry (base labile α-amino protecting group), and t-Boc chemistry (acid labile α-amino protecting group).

The electrophilic fragments, **E1** and **E^{g}**, were synthesized manually, using a modified procedure of t-Boc-chemistry in order to form the thioester group at the C-terminus of the peptide. In this procedure, TMP (3-triphenylmethylthiopropionic acid) is coupled to the resin, and from then on the next amino acids are coupled using the regular t-Boc-chemistry procedure. Following cleavage and deprotection, an alkyl thioester peptide is obtained (Scheme 3).

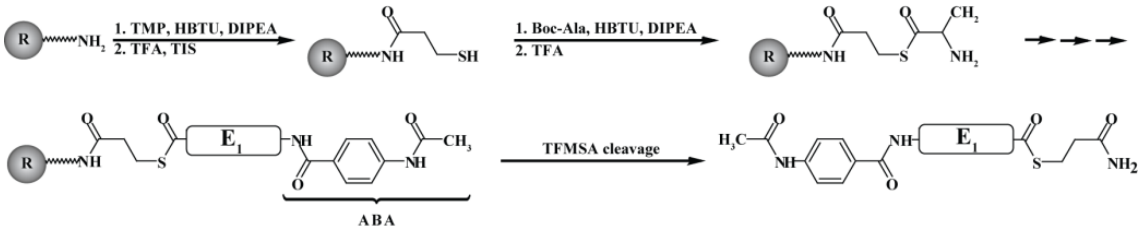

Scheme 3: General synthesis of the electrophiles via t-Boc chemistry.

All the other peptides were synthesized by the automatic peptide synthesizer or manually, using Fmoc SPPS, purified by preparative HPLC, and characterized by analytical HPLC and mass spectra. Figure 15 and Figure 16 show the HPLC analyses of the crude mixture of selected peptides obtained after cleavage and global deprotection (a), and HPLC (b) and MALDI-TOF (c) characterizations of the pure compound, obtained after purification with preparative HPLC.

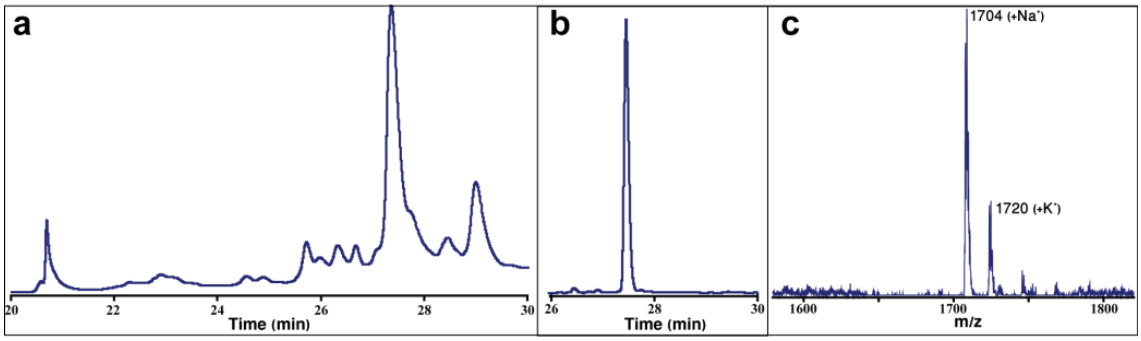

Figure 15: Characterization of peptide **1** obtained by Fmoc SPPS.

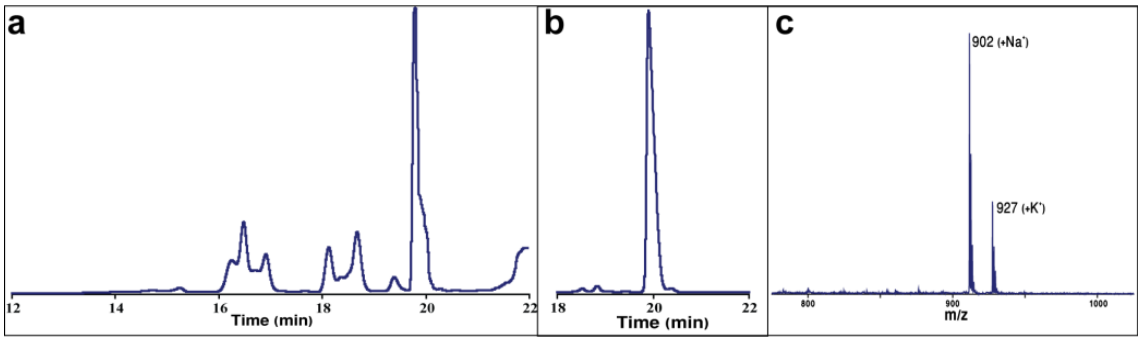

Figure 16: Characterization of the electrophilic fragment **E1** obtained by t-Boc SPPS.

3.1.3 Peptide Structural Characterization

3.1.3.1 Analysis of peptide self-assembly at the air/water interface

3.1.3.1.1 Langmuir-Blodgett films

The tendency of the amphiphilic peptides **1** and **2** to form stable β-sheet assemblies at the air/water interface was studied using Langmuir-Blodgett (LB) trough. A LB trough apparatus is used to compress monolayers of molecules on a surface of a given sub-phase, and measures surface phenomena due to this compression.[95]

Monolayers were prepared by spreading peptide solutions (approximately 0.1 mg/mL in trifluoroacetic acid/chloroform (1:9 v/v)), on deionized water. Langmuir surface-pressure versus molecular area (Π - *A*) isotherms of **1** and **2** suggested that both peptides form stable monolayers. The peptide chains in these monolayers are oriented with their long molecular axes parallel to the water surface, as suggested by the limiting area per molecule (Figure 17) found to be 250 $Å^2$ (**1**) and 240 $Å^2$ (**2**). The limiting molecular areas were determined from tangents drawn to the slope of each curve (dashed line in Figure 17), and give measure to the unit cell area which is the multiplication of molecular length by distance of spacing, i.e., hydrogen bonds. The control peptide $\mathbf{1}^{\mathbf{gg}}$ had high solubility in water and therefore it did not form a monolayer on LB trough.

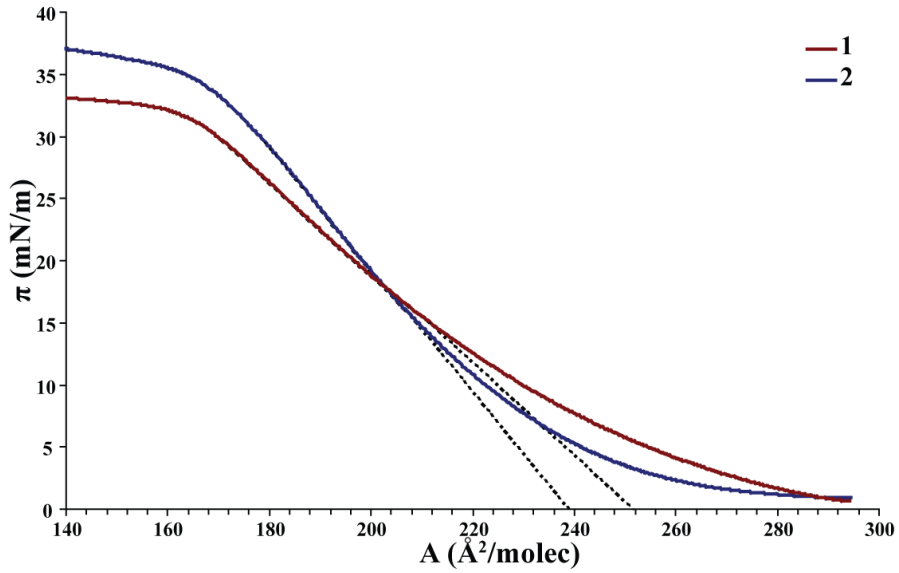

Figure 17: Surface pressure-area (π-A) isotherms of peptides **1** and **2** on deionized water at r.t.

3.1.3.1.2 Grazing-incidence X-ray diffraction

Grazing-incidence X-ray diffraction (GIXD) was used, in collaboration with Prof. Hanna Rapaport (Biotechnology Engineering department, BGU), in order to further investigate the molecular dimensions of the amphiphilic peptides. GIXD is a scattering geometry combining the Bragg condition with the conditions for X-ray total external reflection from crystal surfaces. This provides superior characteristics of GIXD as compared to the other diffraction schemes in the studies of thin surface layers, since the penetration depth of X-rays inside the slab is reduced by three orders of magnitude, typically from 1-10 μm to 1-10 nm (10-100 Å).

The peptide films were spread on deionized water at room temperature and diffraction measurements were performed at 5°C. GIXD experiments on films of **1** or **2** suggested assembly of the peptides into two-dimensional crystalline β-sheet monolayers. Diffraction patterns obtained in the expanded state of the monolayer showed Bragg peaks at q_{xy}=0.108 Å^{-1}, d=58.1 Å and at q_{xy}=1.315 Å^{-1}, d=4.8 Å for **1**. The GIXD pattern of **2** was similar with Bragg peaks at q_{xy}=0.121 Å^{-1}, d=51.9 Å and at q_{xy}=1.310 Å^{-1}, d = 4.8 Å (Figure 18a).

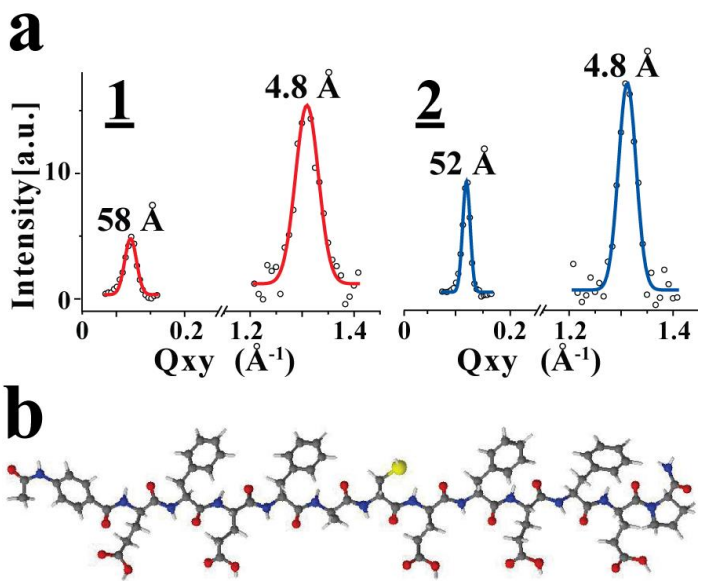

Figure 18: a) GIXD patterns showing Bragg peaks corresponding to hydrogen bonds and peptide length spacing. b) Molecular model of peptide **1** generated using force field CHARMM27.

The 4.8 Å spacing is characteristic of interstrand hydrogen bonds along β-sheet plates. The 58 Å and 52 Å spacing for **1** and **2**, respectively, are close to the estimated projected length of the β-sheet on the water interface, according to a molecular model (using force field CHARMM27) (Figure 18b and Figure 49a), with the first being slightly longer, probably due to minor alterations in the peptide conformation where Ala-Cys residues replace Glu-Phe.

3.1.3.2 Analysis of peptide self-assembly in aqueous solutions

3.1.3.2.1 Circular dichroism spectroscopy

The secondary structures of the amphiphilic peptides **1** and **2** in aqueous solutions were first examined by circular dichroism (CD) spectroscopy. CD spectroscopy can be used to elucidate the secondary structure of macromolecules, including proteins and peptides, by measuring differences in the absorption of left-handed polarized light versus right-handed polarized light that arises due to structural asymmetry. The absence of a regular structure results in zero CD intensity, while an ordered structure results in a spectrum which can contain both positive and negative signals. α-Helix, β-sheet, random coil and other structures give rise to a characteristic

shape and magnitude of CD spectrum. In the case of the β-sheet structure, there is a typical minimum adsorption around 216 nm.[96]

A sample of the desired peptide was dissolved in water or in 3-(N-morpholino) propanesulfonic acid (MOPS) buffer pH 7 followed by vigorous sonication prior to the measurement. The CD spectra of peptides **1** and **2** suggested the formation of β-sheet assemblies in buffered and non-buffered water solutions. The formation of β-sheet structures in water could be ascertained from a CD minimum at 216 nm, and a maximum at about 195 nm (Figure 19a). Another minimum was found in these conditions at around 201 nm and correlated with some random coil contribution, and the spectrum of **1** showed a broad minimum at 227 nm, which probably accounts for a small fraction of a helix.

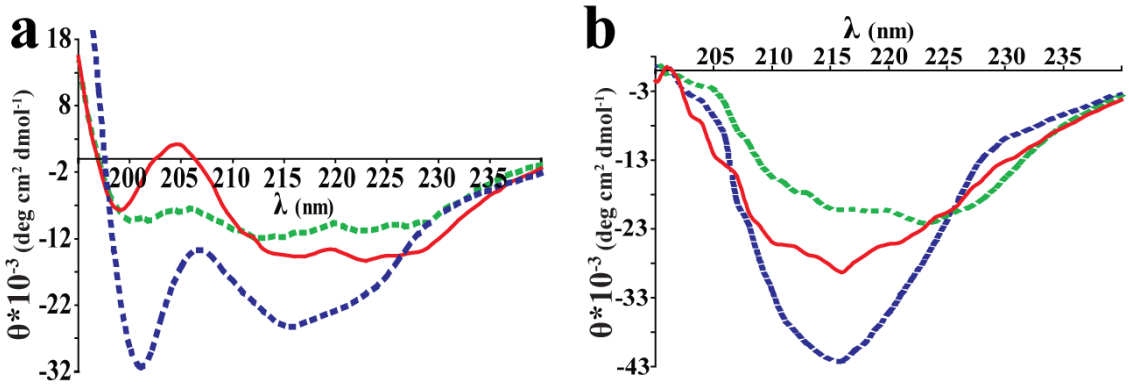

Figure 19: CD spectra obtained in a) water (pH of circa 5.5) and b) MOPS buffer (pH=7) of peptides **1** (red lines), **2** (blue lines) and **1**^{gg} (green lines).

At pH 7 (Figure 19b), the spectra of both peptides showed a clear minimum at 216 nm. The spectrum of **1** included additional "knees", of which the minima at about 206 and 225 nm can correlate with some α-helix contribution. In addition, the spectra of both peptides at the buffered solution, at the same concentration as in water solution, showed higher minima at 216 nm (Figure 19b), illustrating a better peptides solubility at pH=7. CD spectra of the modified peptide **1**^{gg} were also recorded. In both media, **1**^{gg} show no evidence of β-sheet formation, but rather some helical and random coil structures.

3.1.3.2.2 Thioflavin T fluorescence assays

Thioflavin T (ThT) is a benzothiazole dye (insert in Figure 20) that exhibits enhanced fluorescence upon binding to amyloid fibrils and is commonly used to diagnose amyloid fibrils, both *ex vivo* and *in vitro*. In aqueous solutions, ThT was found to exist as micelles at concentrations published to monitor fibrils by fluorescence assay (~10–20 µM).[97]

A sample of the desired peptide was dissolved in MOPS buffer pH 7, mixed with freshly prepared ThT solution, at a 1:1 molar ratio, and vigorously sonicated prior to the measurement. The ThT assay showed higher emission at the typical wavelength of 490 nm for peptide **2** than for **1** (Figure 20)**,** implying a higher amount of assembled fibrils of peptide **2** in comparison to peptide **1** at same concentration (see section 3.1.4, p. 33, for thorough discussion).

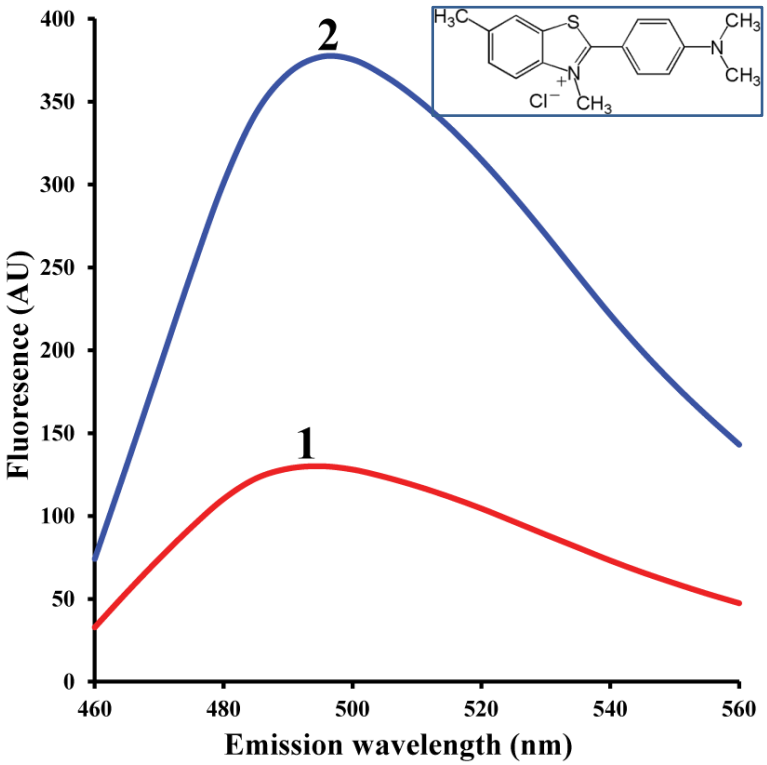

Figure 20: ThT fluorescence spectra of peptides **1** and **2** (120 µM; MOPS buffer pH 7; r.t.; Excitation wavelength 440 nm). Insert – the Thioflavin T molecule.

3.1.3.2.3 Dynamic light scattering

Additional characterization of peptide **1** in aqueous solutions was performed using dynamic light scattering (DLS). In these experiments we examined the distribution of **1** soluble assembles. The experiments were carried out in water and in buffered solution (ammonium bicarbonate pH=7) with various concentration of **1**.

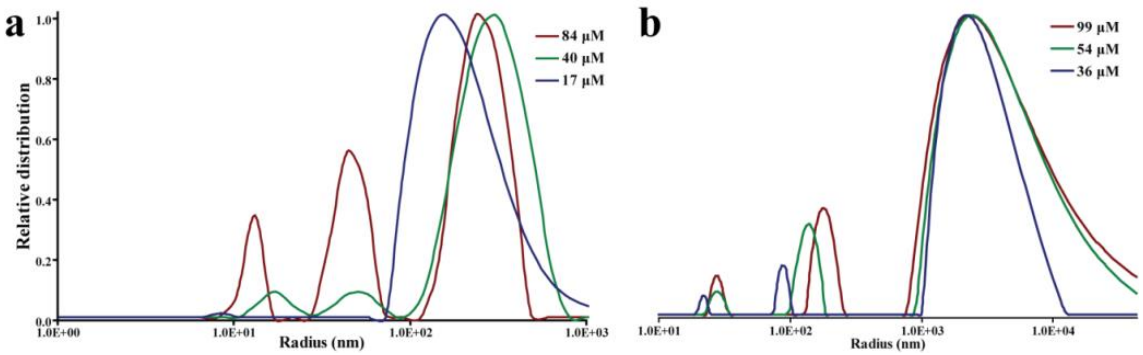

Figure 21: Intensity weighted size distribution of peptide **1**, obtained from dynamic light scattering experiments in a) water and b) buffered solutions pH 7 at various different concentrations.

Both experiments (Figure 21) showed that only one type of large assemblies is formed at low concentration, while an increasingly higher amount of two kinds of smaller assemblies are obtained as the concentration is elevated (see section 3.2.6, p. 40 for thorough discussion).

3.1.3.2.4 Cryo transmission electron microscopy

Imaging of peptides **1** and **2** assemblies in aqueous solutions was obtained by cryo transmission electron microscope (cryo-TEM; in collaboration with Prof. Oren Regev). Drops from water and buffered solutions of peptide **1** (100 µM) and from buffered solutions of peptide **2** (50 µM) were frozen by liquid ethane and deposited on a glow-discharged TEM grid. Long and entangled fibrils, about 20 nm in width, were observed in the samples obtained in water (Figure 22a). Cryo-TEM images in buffered solution (0.2 M MOPS buffer at pH 7), revealed well-organized 2D β-pleated sheets (Figure 22b and Figure 22c for peptide **1** and **2**, respectively), which were ~5 nm in width, corresponding well with the molecular length of **1** and **2** along the β-strand long axis. Images of longer equilibration time for solution of peptide **2** showed mainly fibrillar structures of different widths (Figure 22d).

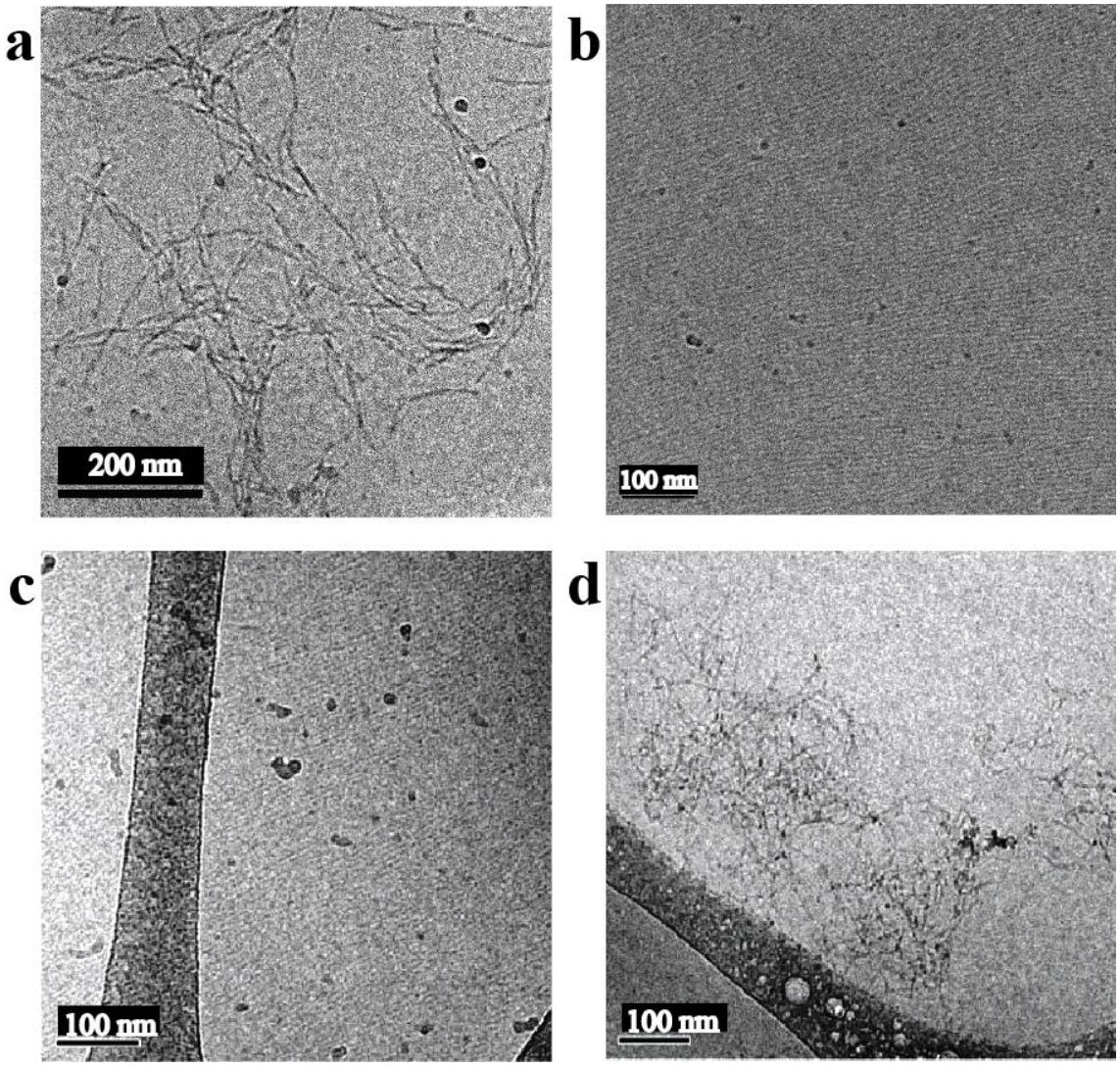

Figure 22: Cryo-TEM images of frozen 2D assemblies formed from 100 μM solution of **1** in a) water and b) 0.2 M MOPS buffer pH 7, 30 min and 15 min of equilibration respectively, and from 50 μM solutions of **2** in 0.2 M MOPS buffer pH 7, following c) 15 min and d) 30 min of equilibration.

3.1.3.2.5 Atomic force microscopy

Additional imaging of the supramolecular structures formed by peptides **1** and **2** was done using atomic force microscopy (AFM; in collaboration with Prof. Nurit Ashkenasy). In these experiments we characterized by AFM imaging adsorbed solutions of the peptides onto silicon oxide substrate.

AFM measurements revealed elongated and twisted fibrillar structures (Figure 23) with helicity pitches of 31±8 and 33±3 nm, for **1** and **2,** respectively. Furthermore, the formation of high aspect ratios and almost perfectly stretched fibril structures,

observed in the AFM measurements of **2** (Figure 23b), were qualitatively better organized than those observed for **1** (Figure 23a – see section 3.1.4, p. 33, for thorough discussion).

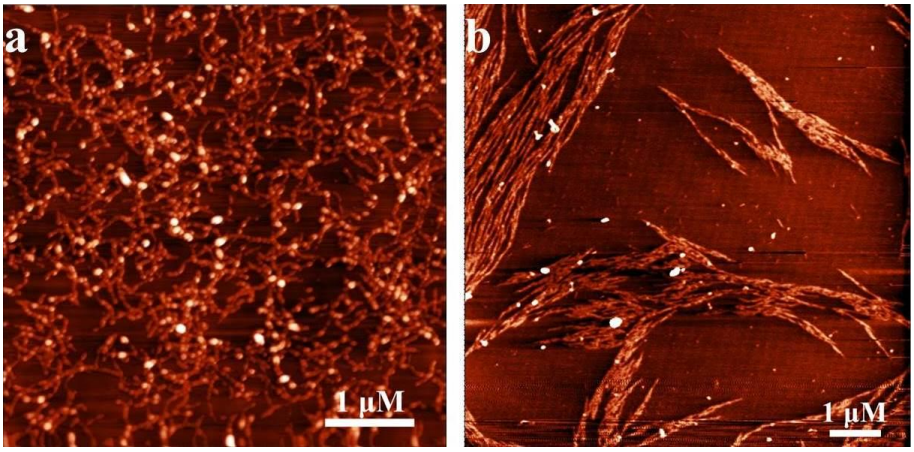

Figure 23: AFM topography images of **1** and **2** (a and b respectively, 100 μM). Fibrils were formed after 30 min of equilibration in water (z scale = 4 nm)

3.1.3.2.6 Molecular dynamic simulations study

The self-assembly of peptides **1** and **2** into fibrillar structures was also studied by molecular dynamic (MD) simulations (performed by Dr. Yifat Miler). [45] In order to construct the fibril models, we considered different bilayers made of 24 molecules, occupying the most likely monomer organizations. Since these peptides possess amphiphilic characteristic, we predicted the formation of a hydrophobic core, in which the hydrophilic residues are exposed to the solution. Arrows in Figure 24 show the four plausible arrangements of peptides **1** and **2** conformers obtained by MD simulation: Figure 24a presents two anti-parallel monolayers arranged in an anti-parallel orientation with respect to each other; in Figure 24b antiparallel monolayers are arranged in a parallel orientation; in Figure 24c parallel monolayers are arranged in a parallel orientation, and in Figure 24d parallel monolayers are arranged in an antiparallel orientation. As a control, we constructed the two respective parallel and antiparallel monolayer models (not shown). To study the relative stability of the above predicted conformers, each structure was explicitly solvated and minimized at physiological pH. MD simulations were then performed in the NPT ensemble at 310 K for 60 ns, using the NAMD program with the all-atom CHARMM27 force-field.

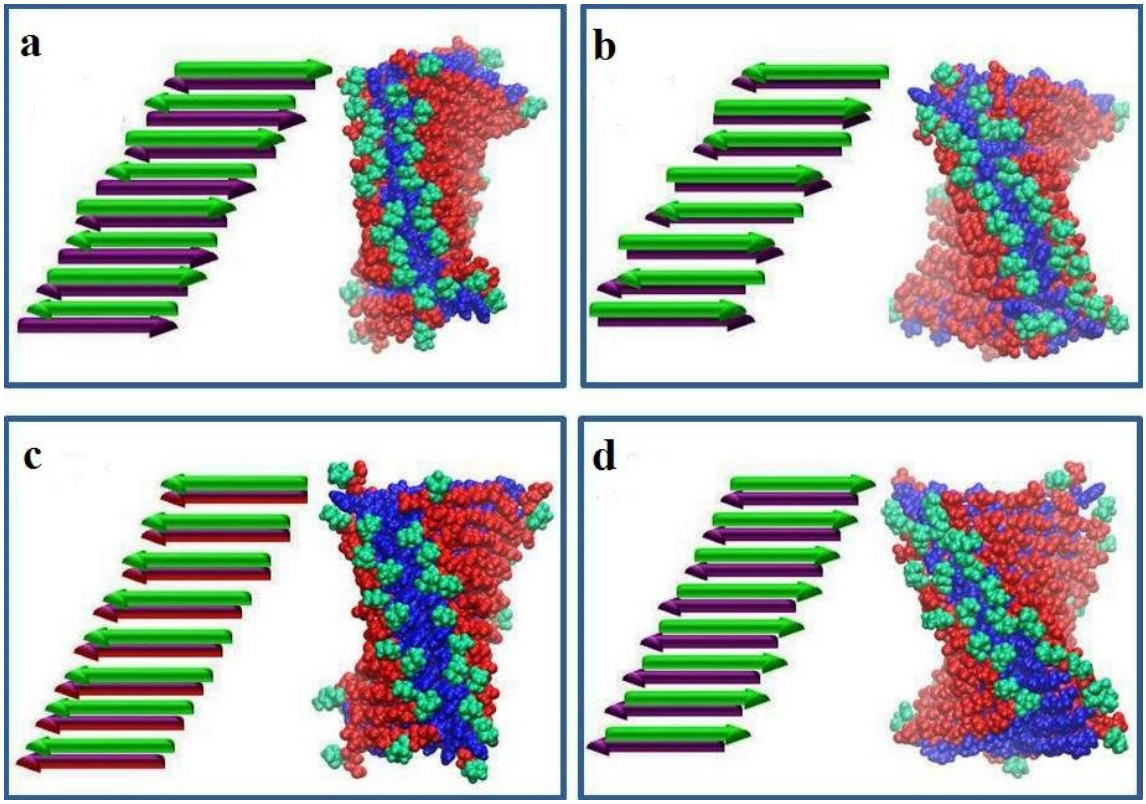

Figure 24: Schematic presentation of the four most likely fibril-like conformers formed by peptides **1** and **2** (arrows presentation) and the structures obtained after 60 ns MD simulation for each conformer of peptide **2**: a) anti-parallel monolayer – anti-parallel bilayer orientation; b) anti-parallel – parallel; c) parallel – parallel and d) parallel monolayer – anti-parallel bilayer. Color code: Pro (green), Glu (red), Phe (blue).

The simulation results illustrate that both peptides formed stable structures in water. Both peptides organized similarly in a single-leaflet monolayer, namely, anti-parallel β-sheet assemblies. However, while for peptide **2** only one preferable fibril bilayer conformation (an anti-parallel bilayer) was found, peptide **1** can form two relatively stable bilayer conformations, both parallel and anti-parallel. The helicity pitches of the fibrillar structures, as calculated from the simulations: 32.±10.1 nm for **2**, and 26.±5.8 and 29.6±5.2 nm for **1** were in good agreement with those measured by AFM (Figure 23). Additionally, the diameter of these simulated conformers was 3.9±0.3 nm, while from the AFM measurements (Figure 23) it was found to be 3.8±0.7 nm.

3.1.4 Conclusions

All the structural measurements obtained by the analytical tools and MD simulations thus suggested the formation of β-sheet based structures for the newly designed peptides **1** and **2** at the air/water interface and in solution, depending on the working conditions. In our opinion, the stretched fibril structure of **2** with superior β-sheet characteristics, as found by GIXD, and CD spectroscopy, may be due to self-assembly into only one type of fibrillar structure, as found from MD simulations. The less perfectly stretched fibrils and inferior β-sheets, observed for peptide **1**, may thus account for two heterogeneous structures, which compete during self-assembly. In our opinion, this fact led to lower ThT fluorescence of peptide **1**, compared to peptide **2** in the same concentration. The propensity to form soluble β-sheet based structures both in water and buffer solutions is an important characteristic of the present new system. As described later (section 3.3, p. 42), all the replication experiments are a function of different equilibration time of the β-sheet forming peptide, and then initiating ligation (and replication) by adding the precursors.

3.2 Analyzing the Self-assembly Pathway of Peptide 1.

Several analytical tools, CD, ThT assay and cryo-TEM, were employed in order to investigate the kinetics of the self-assembly process and to reveal the structural hierarchy. For all experiments in this section, vigorous sonication was employed in order to achieve homogeneous stock solutions of peptide **1**. Stock solutions of ca. 1 mM were prepared by weighing lyophilized peptides into Eppendorf tubes, and sonication (at 40 KHz) for 10 min, after which the peptide was diluted in 3-(N-morpholino) propanesulfonic acid (MOPS) buffer at pH = 7 to the desired concentration. The diluted solution was sonicated for additional 10 min (total 20 min of sonication), in order to achieve full disassembly of peptide **1** aggregates to monomers**.** All kinetic studies (CD, ThT assay and cryo-TEM) were initiated immediately after sonication. In the following sections, self-assembly or equilibration time referred as the time after sonication.

3.2.1 The Solubility of Peptide 1 in Neutral Aqueous Solution

In order to verify that peptide **1** did not precipitate during the experiment time period we performed a solubility experiment. In this experiment, three solutions of different concentrations (16.5, 40 and 95 μM) of **1** were centrifuged (~ 10,000 rpm) at different times after sonication, and right after the centrifugation the supernatant was injected to HPLC.

Very small changes in the peptide concentrations were observed over the time course of 3 hours (Figure 25), confirming the existence of perfectly soluble peptide under the studied conditions.

3.2.2 Time Dependent CD Spectroscopy of Peptide 1

Solutions of 25 and 60 μM peptide **1** were prepared in MOPS buffer pH 7 according to the procedure described above (p. 34). In these experiments, the β-sheet formation was followed, as indicated by CD absorbance at 216 nm over time.

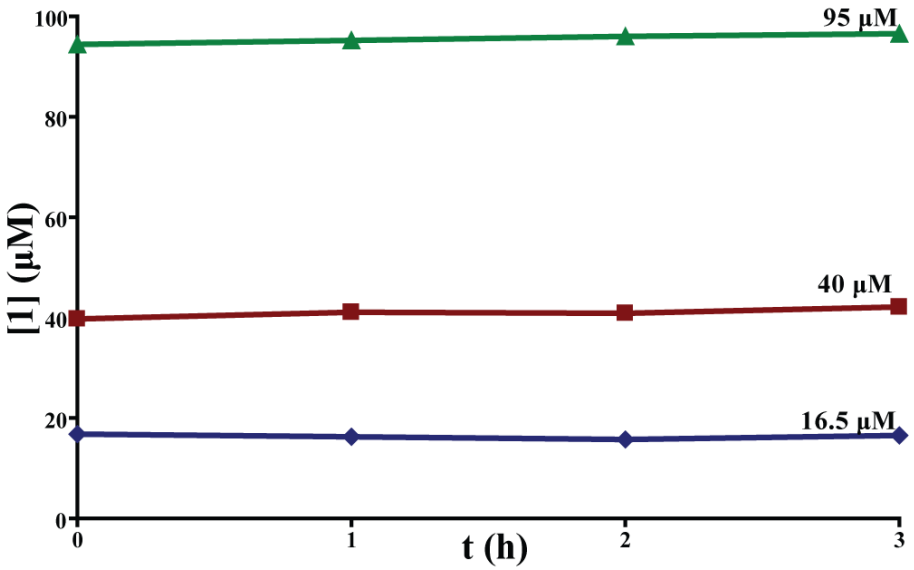

Figure 25: Precipitation experiments. Solutions of the designated concentrations of peptide **1,** in 0.2 M MOPS buffer at pH 7 and TCEP at r.t., were sonicated for 10 min, centrifuged at the indicated time points and the supernatants were immediately injected to HPLC for analysis.

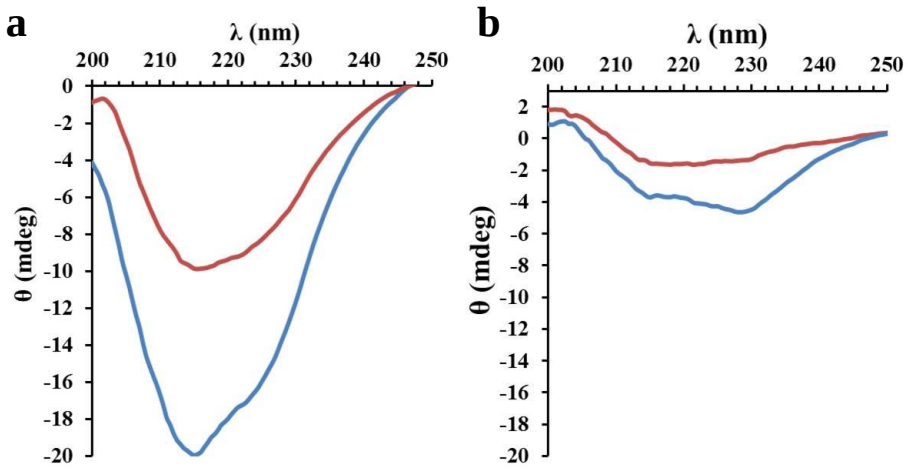

Figure 26: CD spectra obtained a) 1 min and b) 120 min after sonication (red – 25 µM; blue – 60 µM; MOPS buffer pH 7; r.t.).

CD measurements (Figure 26a and Figure 27) assessed after short time of equilibration (1 min) indicated the typical spectra of β-sheet structures, with the indicative minima at 216 nm (Figure 26a), followed by a decrease in signal. While the decrease in signal for 60 µM solution began after the first minute with fast transition after ~15 minutes, the signal for 25 µM solution remained the same for 30 min and followed a slower transition. CD spectra of both solutions after 2 hours, showed low

ellipticity at 216 nm and formation of new minima at 230 nm, which could be addressed to some helical structures (Figure 26b).

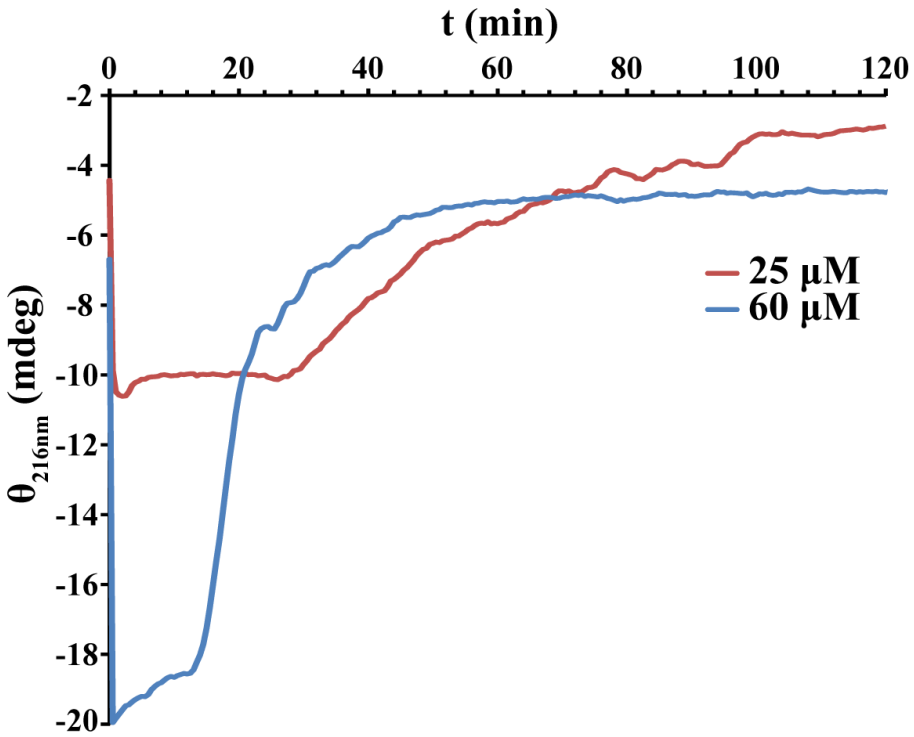

Figure 27: CD ellipticity at 216 nm as a function of self-assembly time for 25 and 60 µM solutions of **1** (MOPS buffer pH 7; r.t.)

The time dependent CD spectroscopy revealed a dynamic self-assembly process (Figure 27). During the time of inspection, the β-sheets that were formed, decomposed or transformed to other supramolecular structures.

3.2.3 Time Dependent ThT Fluorescence of Peptide 1

ThT fluorescence was employed in order to add information on the dynamic self-assembly process peptide **1** undergoes. Solutions of 27 and 60 µM peptide **1** and equimolar amounts of ThT were prepared in MOPS buffer pH 7 according to procedure described above (p. 34). In these experiments, the fluorescence of ThT at 490 nm was followed over time. The fluorescence increased at early stages and then started to decrease, after 20 and 90 min, for the 60 and 27 µM solutions, respectively (Figure 28).

This was similar to the profile we found in time-dependent CD spectroscopy experiments, namely an earlier transition for the more concentrated solution (60 μM), relative to the less-concentrated one (27 μM). This observation can be attributed to formation of a new phase, or alternatively to self-quenching between closely positioned ThT molecules bound to the fibrils.

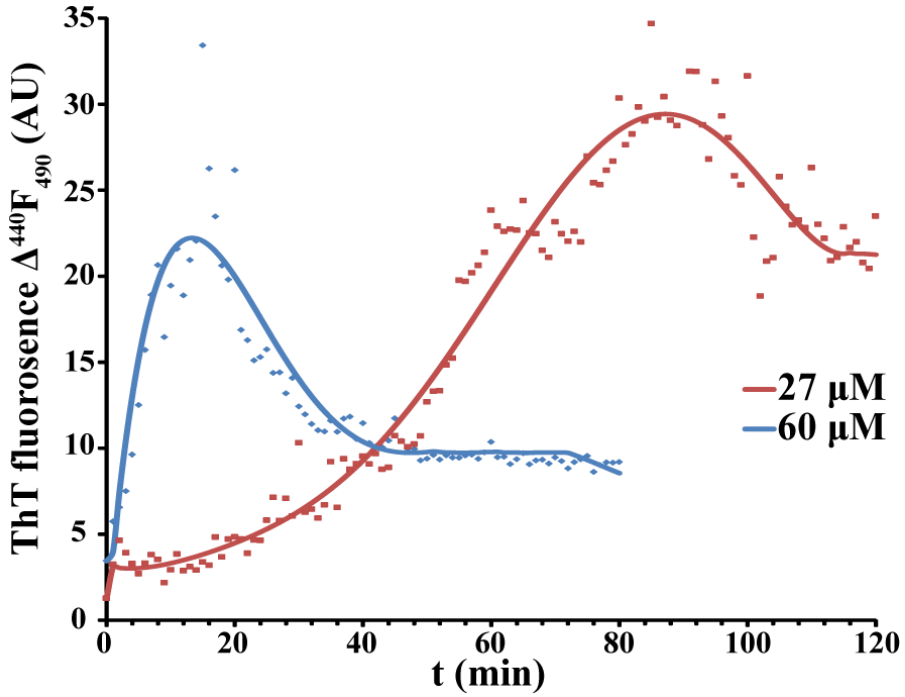

Figure 28: ThT fluorescence over time of 27 and 60 μM solutions of **1** at pH 7.

3.2.4 Kinetic Studies by Cryo-TEM

We further characterized the time-dependent formation of supramolecular structures of **1** in the course of several hours, by taking electron microscopy images of frozen samples (cryo-TEM), at various time points after vigorous sonication of 60 μM solutions in buffer at pH 7 (Figure 29).

Images taken immediately after the sonication showed no particular structures, but rather "islands" of amorphic powder (Figure 29a). After a short time of equilibration (~15 minutes), large β-plates assemblies were observed (Figure 29b, Figure 22b). These assemblies were made of elongated structures with measured inter-strand distances of ~5.5 nm, corresponding well with the previously found molecular length of **1** (p. 25).

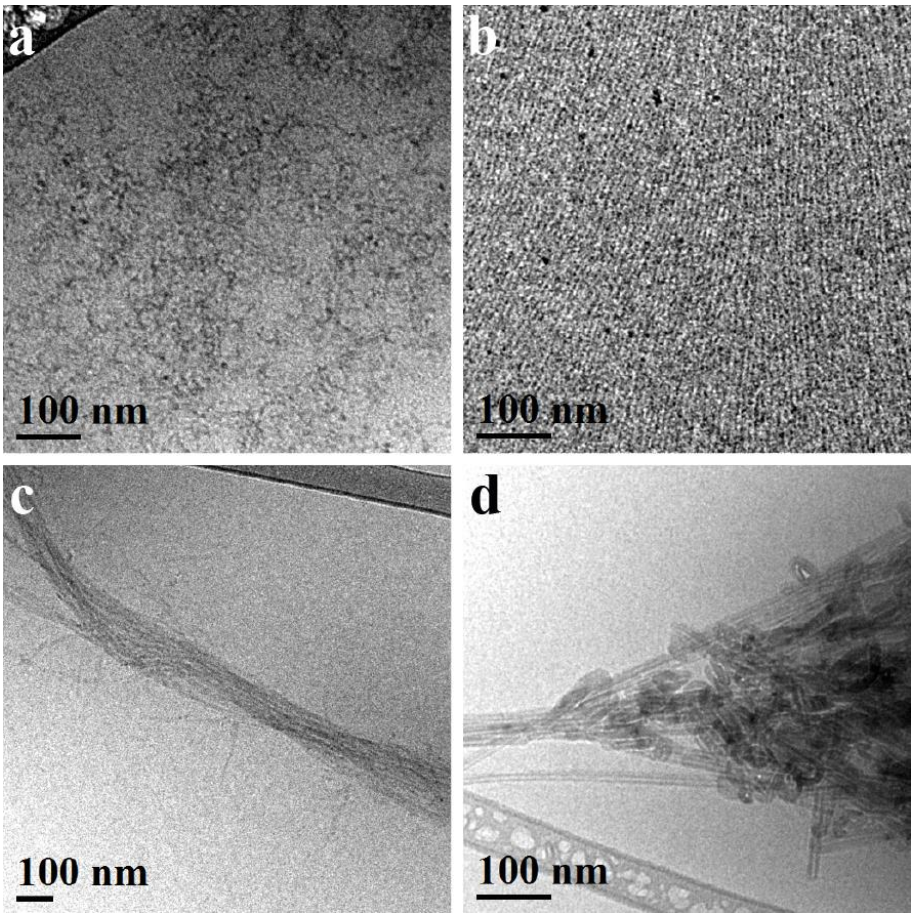

Figure 29: Cryo-TEM images of frozen two-dimensional structures formed from 60 μM solution of **1** (0.2 M MOPS buffer pH 7, CsOH used for positive staining) obtained a) immediately; b) 15 min; c) 60 min; d) 2 hours after sonication.

Images taken from samples equilibrated for longer times (30 – 60 minutes after sonication), predominantly showed fibrillar structures (Figure 29c), made of mono-fibrils and/or wider fibril bundles. Those structures were probably obtained by processes previously described [54, 55], in which the mono(proto)-fibrils align side by side to form wider fibrils, which in turn helically coil to form fibers of over 100 nm width. When the system is equilibrated for longer times (2 hours to overnight), we mainly observed the appearance of wide hollow tubular assemblies (Figure 29d), with 13 – 30 nm width.

3.2.5 Analysis of the Fibrillar Structures

Data presented in the previous section (3.2.4) suggested that the formation of fibril structures, was dominant over the time window relevant to the kinetic experiments of replication system (*vide infra* p. 42), usually done over 1-3 h. Therefore we decided to analyze these species in more detail (Figure 30).

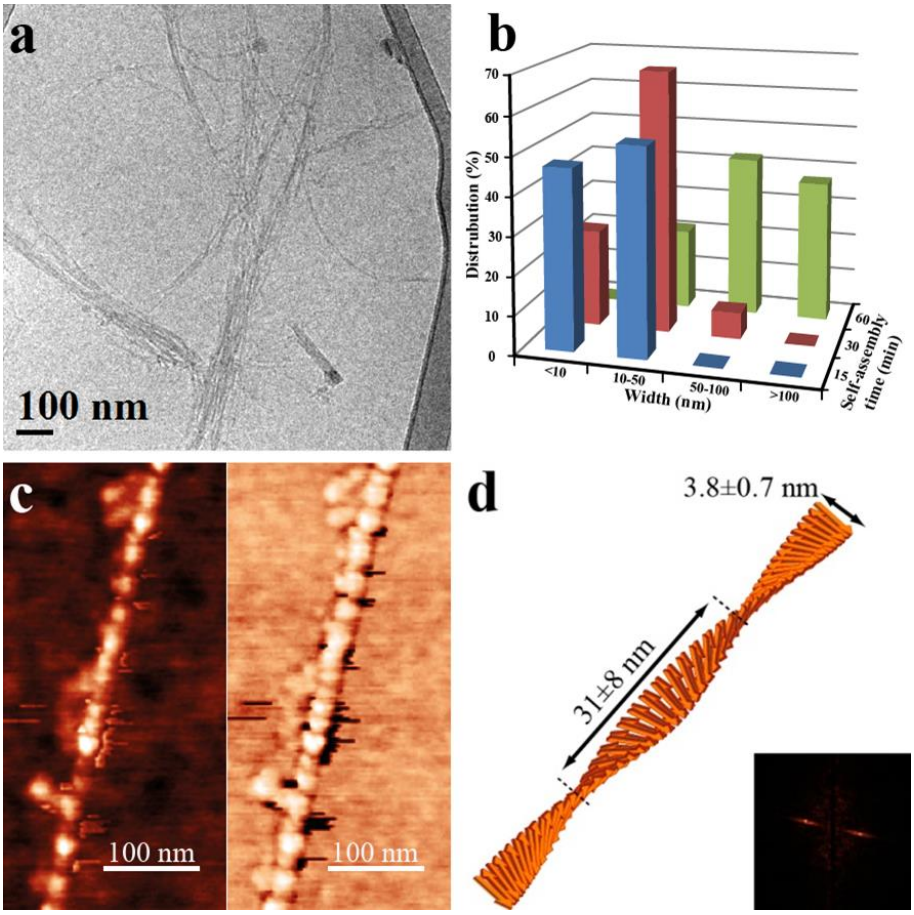

Figure 30: Detailed characterization of the fibril structures formed by peptide **1**. (a) Sample cryo-TEM image showing fibrillar structures of different sizes found after 60 min of equilibration. (b) Statistical analysis of fibrillar structure widths in cryo-TEM micrographs as a function of equilibration time. (c) AFM image, topography (left) and phase (right), of a mono-fibril formed in a 60 μM solution of **1** in buffer at pH 7. (d) Analysis of fiber dimensions as obtained from statistics on a large number of AFM measurements. Inset: Fourier transformed diffraction pattern evidencing the repetitive helical features in the fibrillar structure.

A reasonable assumption for the self-assembly pathway would be that mono-fibrils were first formed and then coiled around each other to form the wider bundles. Figure 30b presents width distribution of fibrillar structures as function of self-assembly

time, calculated from statistical analysis of multiple cryo-TEM images (25 images, at least 2 measurements per image; Figure 30a for example). This analysis was done to follow the process of fibril widening over time and revealed that while only narrow fibrils were formed after a short time of self-assembly, after one hour of equilibration or longer only wide fibers existed (Figure 29c, Figure 30a). Interestingly, the wide fibers were found to be even wider than the nano-tubes formed at these later stages, with width almost twice larger than the nanotubes diameter, a finding that was suggested to be explained via packing of the less ordered fibrils to form the nanotubes.[55]

To further analyze the fibril structure, mono-fibrils formed in 60 μM solutions were characterized at higher resolution using AFM (Figure 30c). We were able to reconfirm that the width of the mono-fibril correlates well with that of the length of the monomer, and also to extract the dimensions of the pitch (31 nm; Figure 23a, Figure 30d for example) obtained for coiling of the elongated structure. These values are in good agreement with those calculated from the MD simulations. [45]

3.2.6 Conclusions

Careful analysis of the self-assembly pathway of **1**, as found by different analytical tools, led us to suggest, that the first step in the self-assembly process was a rapid formation of β-pleated sheets, via formation of hydrogen-bond net, which gave high ellipticity in CD. As described in sections 1.1.4 and 1.2.3, this step is the nuclei formation of the fibrillar structures. Important to mention is that the cryo-TEM images of β-pleated sheets obtained in this study provided the first visualized evidence of nucleation step of fibrillar structures. The next step of the self-assembly process is partial decomposition of relatively wide β-plates. This decomposition is illustrated by the changes in ellipticity at 216 nm minima during the course of two hours, and corresponded to phase transitions between different β-sheet containing structures.[54, 98] As shown (Figure 27), the transition had occurred earlier for the more concentrated solution, ~15 and 30 minutes for 60 and 25 μM solutions, respectively. The β-plates rearranged to small fibrils for which the assembly is driven by dehydration of

hydrophobic domains (rich in phenylalanine residues) to form tail-to-tail bi-layers. These bi-layers are stabilized by exposed hydrophilic surfaces, illustrated by an increase in ThT fluorescence (Figure 28). The protofibrils in turn aggregated to well-packed fibrils, a process that is suggested to cause a decrease both in ellipticity and in ThT fluorescence. The decrease in ThT fluorescence might be explained by self-quenching due to close proximity of ThT molecules one to another in the fibrillar structure. In the final stage, in order to dehydrate the hydrophobic termini, the grown fibrils folded to form a helical/cylindrical ribbon – the nano-tubes. This resulted in low CD ellipticity, due to high symmetry of these structures, and formation of a new minimum at 230 nm. The formation of different supramolecular structures was illustrated also by DLS, in samples that had been analyzed at ~30 min of self-assembly (Figure 21, p. 29). The DLS samples (both aqueous and buffered) which showed existence of mainly one, relatively wide, specie in all examined concentrations, implied on the wide β-pleated sheets. Increase of peptide concentrations, resulted in formation of two smaller species, namely, bi-layer fibrils and well packed nano-tubes.

3.3 Kinetic Studies of Replication System 1

The chemo- and regio-selectivity in peptide fragment coupling is of paramount importance, especially when free peptides having reactive side chains are employed in aqueous solutions. Kent's Native Chemical Ligation (NCL)[87, 90] method in which the N-terminal peptide fragment is pre-activated as a thioester (electrophilic fragment E) and the C-terminal fragment is equipped with a free Cys residue at its N-terminus (nucleophilic fragment N) can be used for this purpose. Such a coupling strategy prevents the need for addition of external coupling reagents to the reaction mixture. In addition, the coupling reaction becomes highly chemo-selective in producing the desired amide bond at the intended coupling site (Scheme 4), because of the appropriate stability of the different thioester bonds in neutral aqueous solutions, as well as the greater nucleophilicity of the sulfhydryl functionality of the cysteine residue at neutral pH as compared to all other side chain moieties.

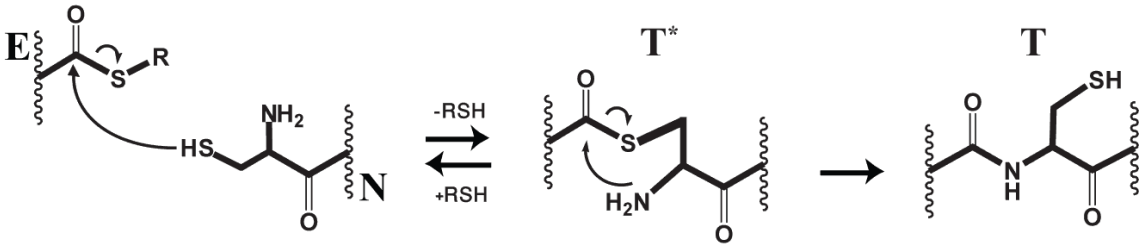

Scheme 4: Native Chemical Ligation.

NCL utilizes the rapid and specific reaction of an N-terminal Cys residue with a C-terminal thioester group to form a native *irreversible* amide bond. This reaction is mediated by thioester exchange and followed by a rapid S to N acyl shift (Scheme 4).

The structural characterizations of peptide **1**, suggested that solutions of relatively high concentration of **1** are not homogenous. Therefore, for the kinetic replication experiments, we designed a Teflon 30-well plate, where in each well the reaction was run for a different time using same peptide concentrations. The entire volume of each well was taken at the studied time points. In addition, the stock solution of peptide **1** was sonicated prior to addition of other components. The analysis of the replication experiments was done by analytical RP-HPLC. In these experiments we

followed the formation of **1** from its precursors (Scheme 5), at different time points (Figure 31). Each HPLC peak is marked with the eluted peptide. **S** is the ABA-labeled peptide that was used as a standard in all the experiments; the elution of **N1** could not be followed, because it does not contain ABA**.**

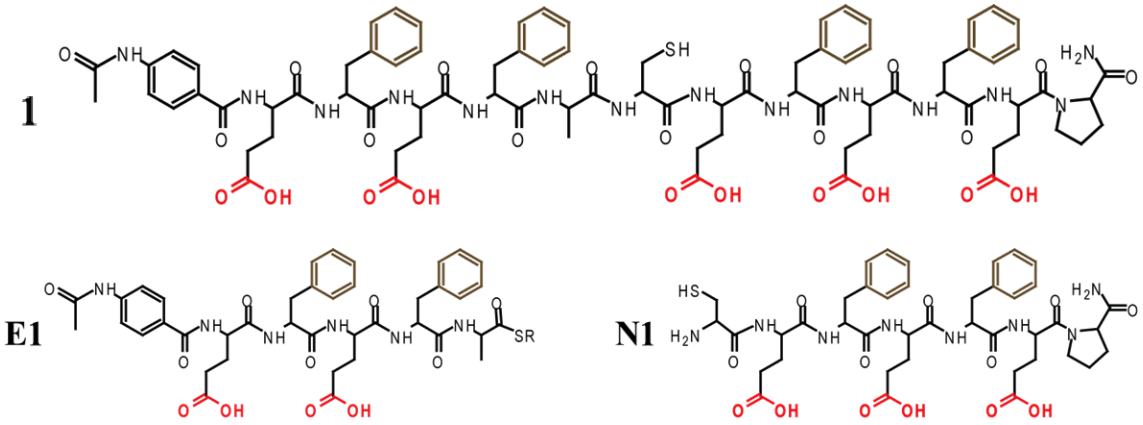

Scheme 5: Stick representation of replication system **1**.

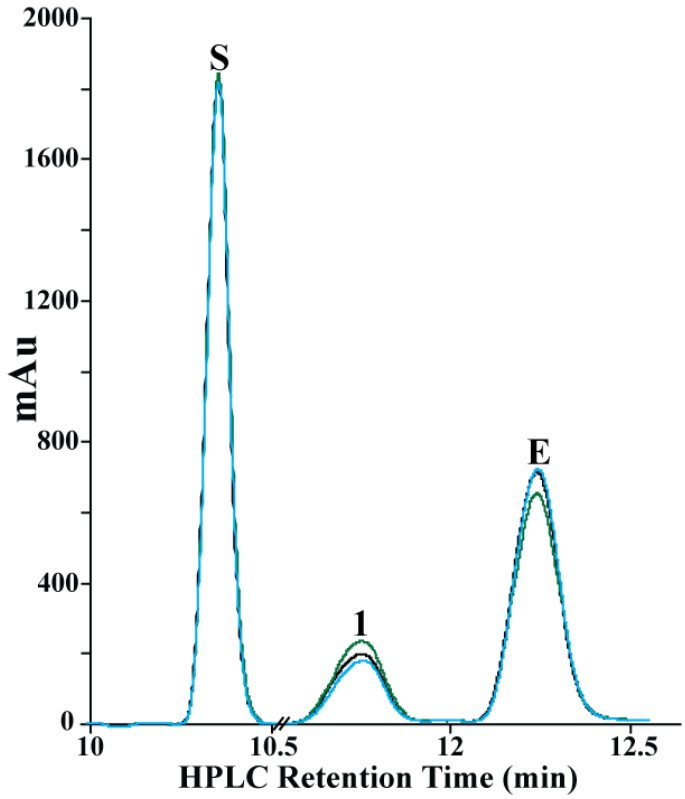

Figure 31: Representative set of HPLC chromatograms (at 270 nm). The chromatograms were obtained for reactions that proceeded for 15 (cyan), 30 (black) and 180 (green) minutes. Integration of the elution peaks of **1** corresponded to 56 (Δ**1** = 15), 63 (22) and 74 (33) μM, respectively (Δ**1** = $[\mathbf{1}]_t - [\mathbf{1}]_0$).

Figure 31 shows a representative set of HPLC chromatograms (detected at 270 nm) that was used to follow the kinetics of the ligation reaction between **E1** and **N1** (250 µM each; Scheme 5), seeded with 41 µM of **1** as a template for replication (full results of particular experiment are shown in Figure 34). All kinetic experiments were carried out in 0.2 M MOPS buffer at pH 7, with TCEP as reducing agent for disulfide bonds. 50% acetic acid was added at quenching point.

3.3.1 Kinetics of Template Free Reaction

In order to investigate the ligation reactions between the two short precursors, **E1** and **N1**, an equimolar solution of peptides was mixed with MOPS buffer at pH 7 and TCEP as reducing agent. In a control reaction, we followed the formation of the modified peptide $\mathbf{1}^{gg}$ from its precursors, $\mathbf{E}^{g}$ and $\mathbf{N}^{g}$ (Figure 32).

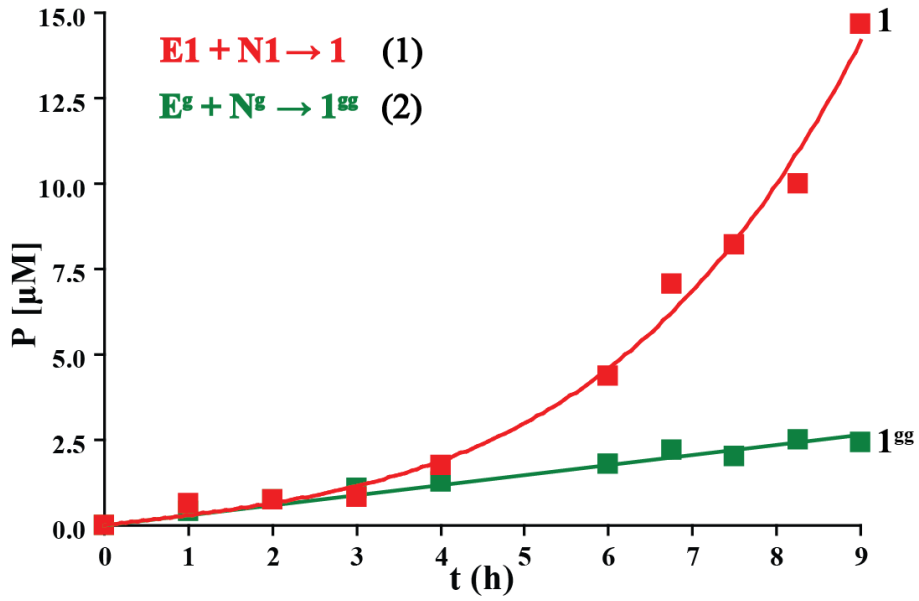

Figure 32: Production over time of **1** in the template free reactions between **E1** and **N1** (250 µM each) in 0.2 M MOPS buffer at pH 7 (TCEP; r.t.). The linear production over time of the control peptide, $\mathbf{1}^{gg}$, from its precursors $\mathbf{E}^{g}$ and $\mathbf{N}^{g}$ (250 µM each), that cannot form β-sheets is shown for comparison.

A signature of a template-assisted autocatalytic production of **1** was observed in this background reaction. After a lag phase of ~3 h during which **1** had formed slowly (Equation 1; inserted in Figure 32), the rate of formation increased significantly, allowed

us to suggest that only after reaching a certain critical concentration the assembly of peptide **1** became more pronounced, hence accelerated autocatalysis. The results of a control reaction showed that production of the modified peptide $\mathbf{1}^{gg}$ (Equation 2; Figure 32) proceeded linearly over the entire inspected nine hours.

3.3.2 Template Assisted Reactions

In order to further study the autocatalytic properties of **1** and the influence of self-assembly process on replication, we followed the rate of ligation of **E1** and **N1** in reactions that were initially seeded with different amounts of **1** and initiated at different time of equilibration, by the addition of the precursors.

3.3.2.1 Reactions that initiated without equilibration

In this set of experiments, the ligation reactions initiated immediately after vigorous sonication of samples with the desired concentration of **1** (Equation 3 in Figure 33). The aim of this experiment is to examine the ligation reaction when the replication process initiated simultaneously with the self-assembly process of peptide **1**.

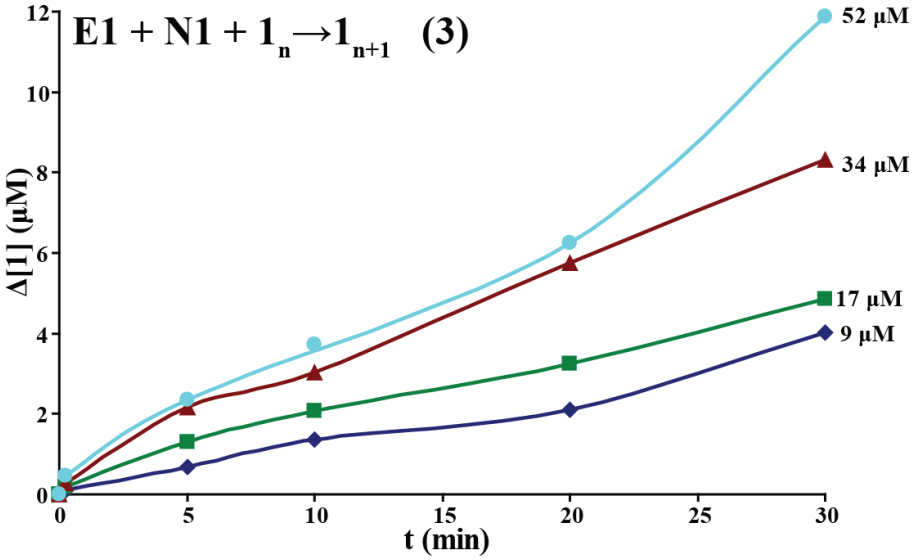

Figure 33: Production over time of **1** in template assisted reactions between **E1** (250 µM) and **N1** (1000 µM) that were initially seeded with different amounts of **1** as a template immediately after sonication (0.2 M MOPS pH 7; TCEP; r.t.). The amounts of initial seeded template are marked next to the curves ($\Delta[\mathbf{1}] = [\mathbf{1}]_t - [\mathbf{1}]_0$).

The results (Figure 33) showed an increase of the reaction rate (and final concentrations) with increase in initially seeded template concentrations, although the ligation reaction initiated from monomeric state of template peptide **1**. As found in kinetic experiments of the self-assembly process, during 30 min **1** folded to β-pleated sheets and fibrillar structures. This result illustrates the template effect of peptide **1** on replication process.

3.3.2.2 Reactions that initiated after 20 min of equilibration

Further investigation of the self-assembly process influence on the replication kinetics was done in experiments where the ligation reactions were initiated 20 minutes after sonication of samples with the desired concentration of peptide **1**.

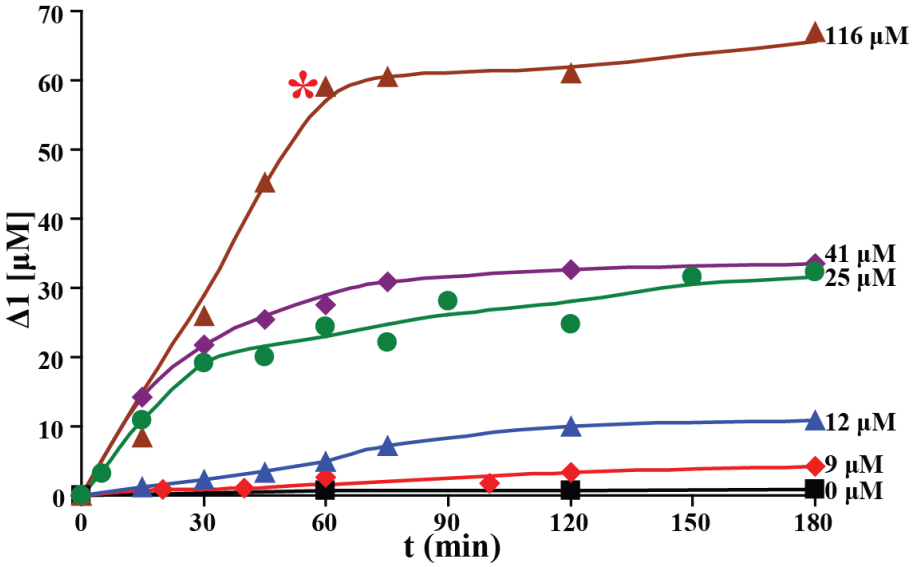

Figure 34: Production over time of **1** in template assisted reactions between **E1** and **N1** (250 μM each; 0.2 M MOPS pH 7; TCEP) that were initially seeded with the indicated amounts of **1** as a template (marked next to the curves); the production of **1** in a template-free reaction is shown in black for comparison ($\Delta\mathbf{1} = [\mathbf{1}]_t - [\mathbf{1}]_0$).

While less than 1 μM of **1** was formed after one hour of the template-free reaction, it was formed auto-catalytically and in proportion to the template seeding concentrations (Figure 34). The fastest reaction, seeded with 116 μM template, proceeded at a rate about 60-fold higher compared to the template-free reaction (red asterisk in Figure 34). With that, reactions that were initiated with relatively high initial template concentration (116 and 41 μM) proceeded at a decreased ligation rate after

some time (60 and 75 min, respectively) compared to the initial rate, regardless of sufficient amount of precursors, implying an inactive stage due to the self-assembly process.

3.3.2.3 Correlation between the two processes

In order to fully correlate between the self-assembly and the replication processes, another set of replication experiments were performed, where the initial seeded template concentrations were adjusted to concentrations of **1** used in the investigation of self-assembly kinetics (25 and 60 μM; Sections 3.2.2 and 3.2.3). We found three time points of equilibration interesting for investigation: 0, 20 and 60 min. At the beginning of the self-assembly process, namely, equilibration time of 0 min, peptide **1** is at monomeric state. Equilibration time of 20 min showed, for higher concentration (60 μM), the end of the fast phase transition in CD and decrease of ThT fluorescence, implying that the fibrillar structures were attained, as also suggested by cryo-TEM images. Results for solution of lower concentration (25 μM) showed high contents of β-pleated sheets and low content of fibrils at 20 min of equilibration. At 60 min of self-assembly, both low ellipticity and low ThT fluorescence (nano-tubes) were evident, for the higher concentration, while the solution of lower concentration commenced the formation of fibrils.

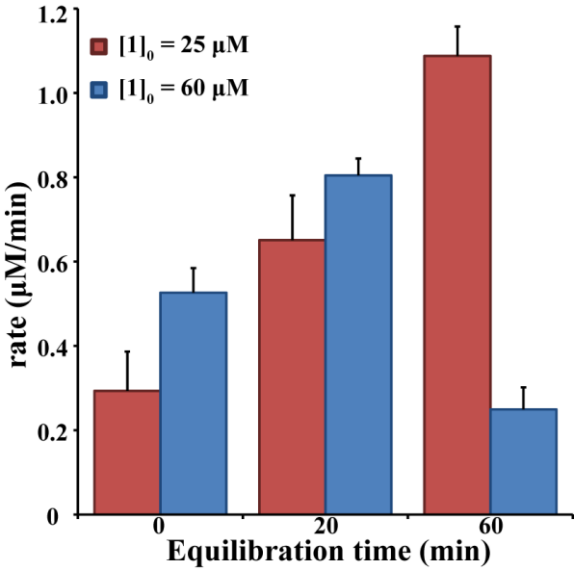

Figure 35: Investigation of replication system: Rate of formation of **1** in template seeded reactions as a function of self-assembly time. ([**E1**]$_0$ = [**N1**]$_0$ = 250 μM; 0.2 M MOPS pH 7; TCEP; r.t.) Data present an average±SD of 3 repetitive.

In the set of experiments presented in Figure 35 we initiated the ligation reaction at depicted time of equilibration by the addition of the precursors. The observed initial rates revealed that extending the equilibration time for up to 60 minutes for reactions seeded with 25 μM of **1** increased the rate of the reaction. The rate of reactions seeded with 60 μM of **1** was increased for reactions seeded after 20 minutes of equilibration, versus no equilibration, but then longer equilibration time (60 min) resulted in a decrease in rate.

3.3.2.4 Cross-catalysis reactions

Further investigation of the new replication system was done by cross-catalysis reaction experiments. In these experiments we tested the cross-catalysis of peptide **1** by several peptides with the same length as **1**. In these experiments we used the β-sheet forming peptide **2**, the modified peptide $\mathbf{1}^{gg}$, and peptide **Sc**, its sequence taken from a peptide which folds to α-helix and seeded them in solution with equimolar amounts of **E1** and **N1** (Figure 36; Equation 4).

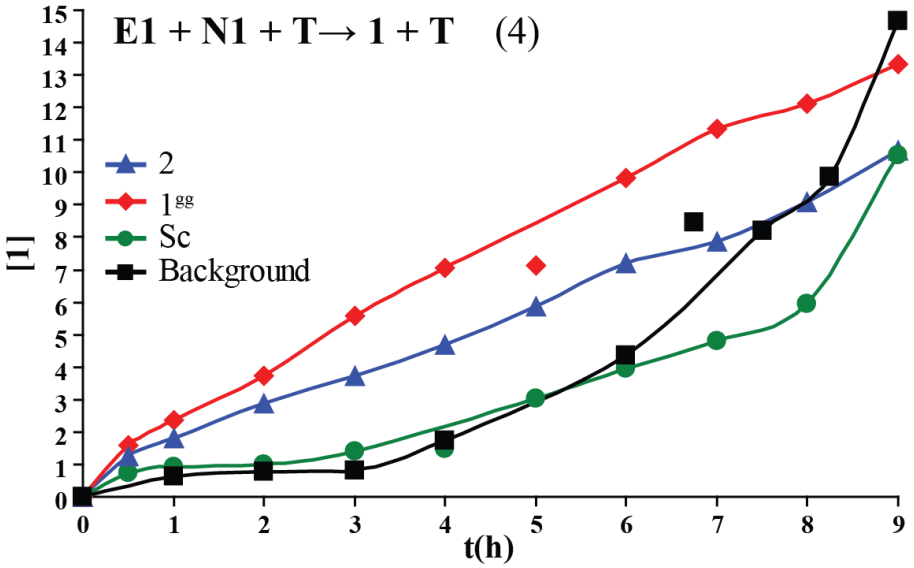

Figure 36: Cross-catalytic formation of peptide 1 by three other templates. Kinetic profiles are shown for reactions of **E1** and **N1** (250 μM each; 0.2 M MOPS; TCEP; r.t.), which were seeded with 100±10 μM of $\mathbf{1}^{gg}$ (red), **2** (cyan) or **Sc** (green). The formation over time of **1** in the template-free reaction is shown for comparison (black).

In comparison to data obtained in the presence of initially added template **1** (Figure 33 and Figure 34), the ligation reaction proceeded slowly when seeded with 100

μM of **1**^{gg} or with the 'scrambled' peptide, **Sc**. Furthermore, even seeding with peptide **2** enhanced the ligation only marginally, demonstrating the specificity of the system.

3.3.3 Reaction Order of Ligation

In order to understand the mechanism of the system, one needs to obtain additional physical information about each member of this new system. The replication system developed here is based on three peptides: two precursors **E1** and **N1** and the β-sheet forming peptide **1**. The partial order of the two reactants can be revealed by simple kinetic experiments. We thus performed an experiment (Figure 37), in which different concentrations of **E1** (35, 83, 112, 152 and 219 μM) reacted with relatively high concentration of **N1** (1 mM), in the presence of a low amount of template **1** (9 μM). By using an elevated concentration of one of the reactants and only a catalytic amount of the template, the reaction rate equation (Equation 5) is reduced to a pseudo-first-order rate equation (Equation 6).

$$\text{rate} = k \cdot [\text{E1}]^{\alpha} \cdot [\text{N1}]^{\beta} \cdot [1]^{p} \quad (5)$$

$$\text{rate} = k` \cdot [\text{E1}]^{\alpha} \quad (6)$$

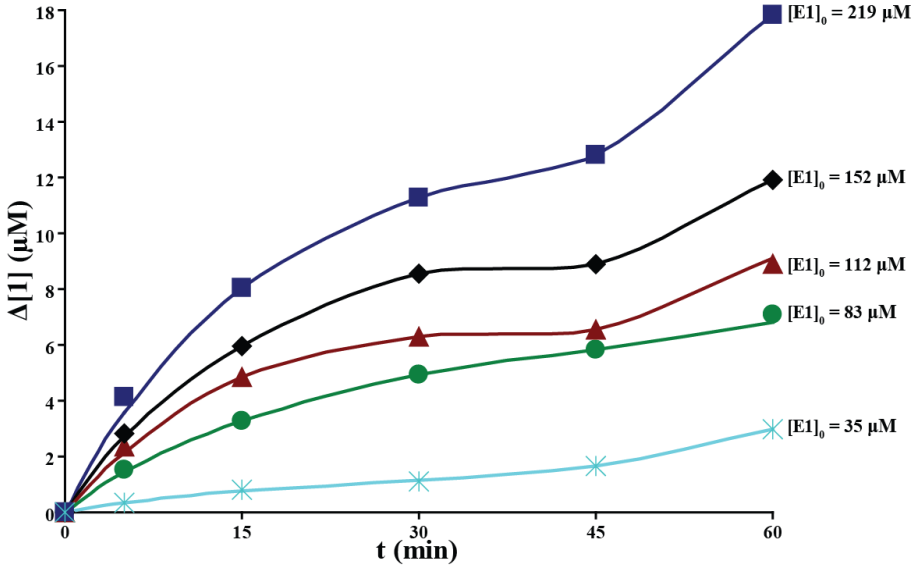

Figure 37: Production of **1** over time in the presence of various concentrations of **E1** (the initial concentrations of **E1** marked next to the curves). [**N1**]$_0$=1 mM; [**1**]$_0$ = 9 μM (0.2 M MOPS pH 7; TCEP; r.t.).

Presenting the experimental data in a log-log plot in which the x-axis is the initial **E1** concentration and y-axis is the initial reaction rate will result in a curve where the slope is the partial order of the reactant. The partial order of **E1** as obtained from the experiments presented in Figure 37 is practically equal to 1 (Figure 38). The reaction between the reactants is molecular, meaning that one molecule of **E1** reacts with one molecule of **N1**, thus, we assume that the partial order of **E1** equals to the partial order of **N1**: $\alpha=\beta=1$.

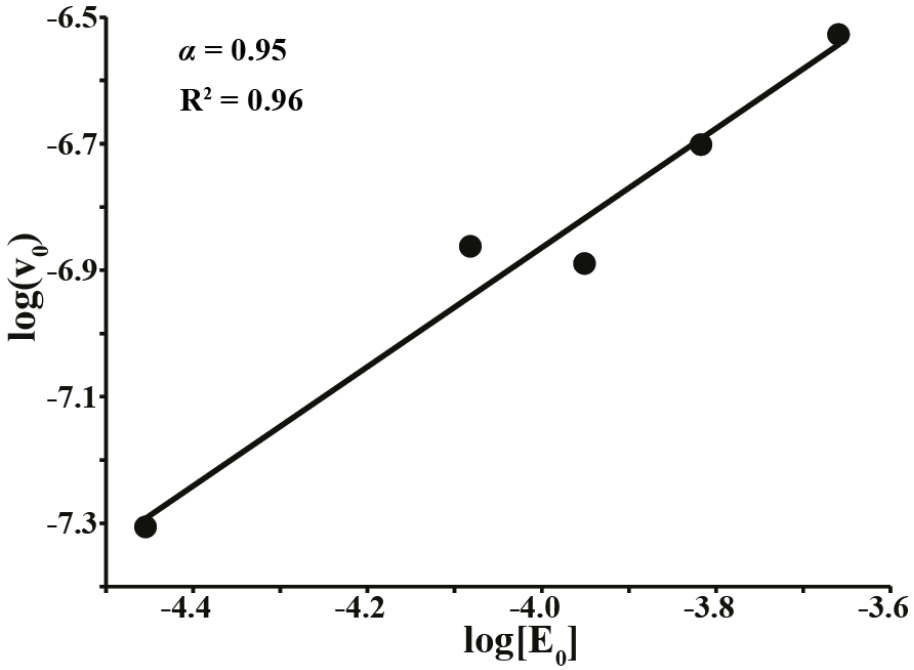

Figure 38: A logarithmic plot of the initial rates extracted from the reactions shown in Figure 37 as a function of the initial concentrations of **E1**. The initial rate (v_0) calculated from a slope at 30 min, in M/min units.

Next target was to find the catalytic order of **1** (*p* in Equation 6). While analysis of the logarithmic plot of the initial rates versus the initial concentrations of the seeded template, derived from the kinetic data of experiments that initiated immediately after sonication (Figure 33), gave catalytic order of p=0.9 (Figure 39), the catalytic order found for experiments that initiated after 20 min of template equilibration is p=1.2 (Figure 40). These values reflect an efficient process, in which after each step of ligation a new catalytic site is formed with the same catalytic properties as the old one.

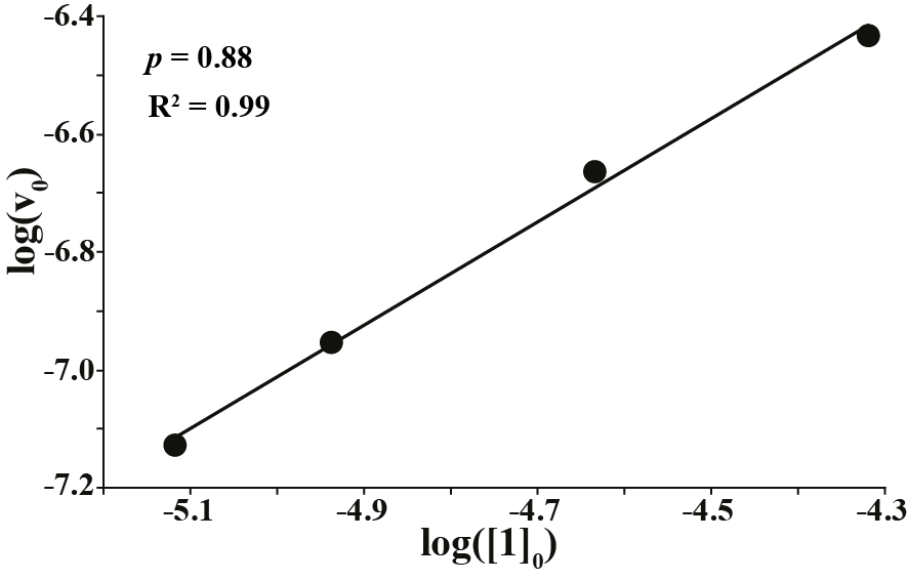

Figure 39: Logarithmic plot of the initial rates extracted from the data shown in Figure 33 as a function of the initial seeded template concentration.

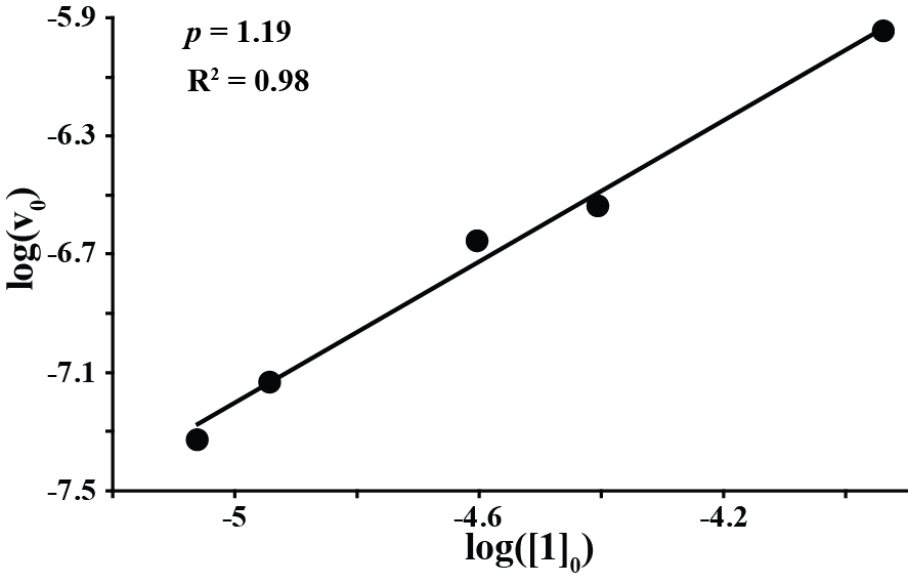

Figure 40: Logarithmic plot of the initial rates extracted from the data shown in Figure 34 as a function of the initial seeded template concentration.

The nonlinearity of the catalysis, characterized by p>1 resulted for experiments that initiated after 20 min of template equilibration, suggested that the kinetic rate of ligation was proportional not only to monomer concentration but also to the number of

aggregates, so the rate increased with increase of aggregates amount that formed in the reaction mixture.

3.3.4 Conclusions

The investigation of the replication reaction, namely, ligation of **E1** and **N1**, clearly illustrated the self-replication properties of peptide **1**. Furthermore, the autocatalysis is specific in that mutants of peptide **1** that could not form β-sheets did not replicate. The ligation reaction was influenced not only by the increased amount of initially seeded template but also by the difference between the supramolecular structures formed by peptide **1**. When the ligation reaction initiated at the monomeric state of the template molecule **1**, followed by fast self-assembly to β-pleated sheets, the catalytic order was found to be somehow close to exponential growth. On the other hand, reactions that initiated after some equilibration of the template solution, showed increase of the catalytic order, suggesting that the fibrillar structures formed were more efficient in the catalysis of the ligation reaction. This can be explained by the relatively high amount of free edges available for binding the precursors in the fibrillar structures, as found from the cryo-TEM imaging. Reactions that initiated after relatively long time of equilibration proceeded in a low ligation rate, due probably to transition of the template into a non-catalytically active phase containing the nanotubes. In addition, the results of cross-catalysis experiments suggested that the enhanced rates of ligation in mixtures that were seeded with **1** were not just due to a "crowding effect", obtained from the peptide presence, but rather a result of molecular recognition. In contrast to previously reported self-replication systems (section 1.2.2, p. 11), the template directed synthesis shown in this research achieved by rather oligomeric structures. Monomers of template molecule **1** self-assembled to supramolecular structures, where the free edges act as recognition surface to facilitate formation of a new monomer.

3.4 Replication System Full Mechanism

This section summarizes the experimental results presented in previous sections (3.2 and 3.3) by proposing full system mechanism and kinetic model.

3.4.1 Two Parallel Processes

In order to account for all the obtained data, the replication system mechanism should include the replication reaction itself, as well as the dynamic self-organization of the template peptide to β-sheet structures. Taken together the self-assembly and replication kinetic data, allowed us to conclude that molecule **1** can serve as an active template for a certain amount of time after its solubilization. Peptide **1** acts as a template, when certain species, predominately β-plates and fibrils, exist in the mixture. Scheme 6 thus describes the two-level mechanism that is suggested to reflect the supramolecular catalysis, in which catalytic species of **1** are formed during self-assembly (*top*), and serve as templates and catalysts for ligation of the precursors to form new **1** molecules (*bottom*). A full description of the two processes is presented in pages 40 and 52. This description served us for suggesting a kinetic model that can be used to describe the observed reaction progress.

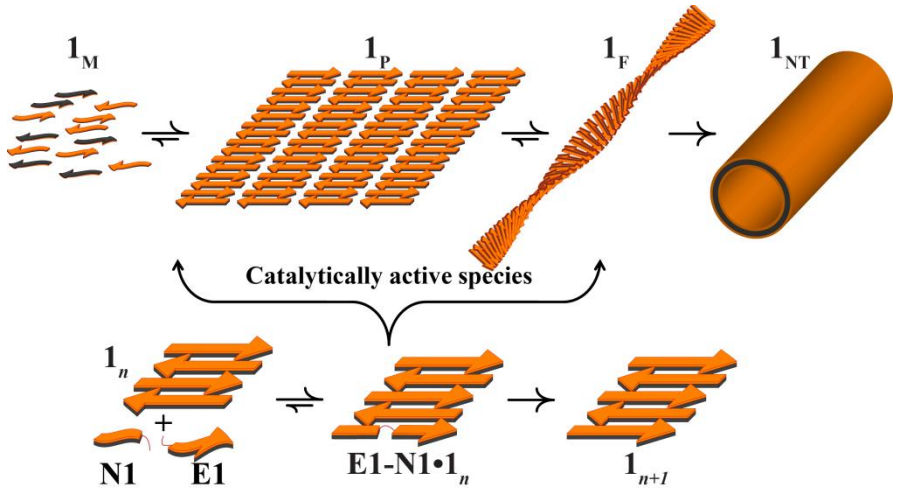

Scheme 6: Schematic representation of the two processes that take place in parallel: *top* – dynamic self-assembly of monomers ($\mathbf{1_M}$) to anti-parallel β-pleated sheets ($\mathbf{1_P}$), fibers ($\mathbf{1_F}$), and finally nanotubes ($\mathbf{1_{NT}}$); *bottom* – autocatalytic reaction in which the β-sheet structure (generally depicted as $\mathbf{1_n}$) serves as template for registered association of **E1** and **N1**, which then react to form a new copy of **1** and the larger aggregate ($\mathbf{1_{n+1}}$), available to serve again as a template.

3.4.2 Kinetic Model

Scheme 7 presents the kinetic model we used to describe the processes shown in Scheme 6, simplified in that only one type of transient species, the mono-fibril F, is considered as a catalyst for the replication.

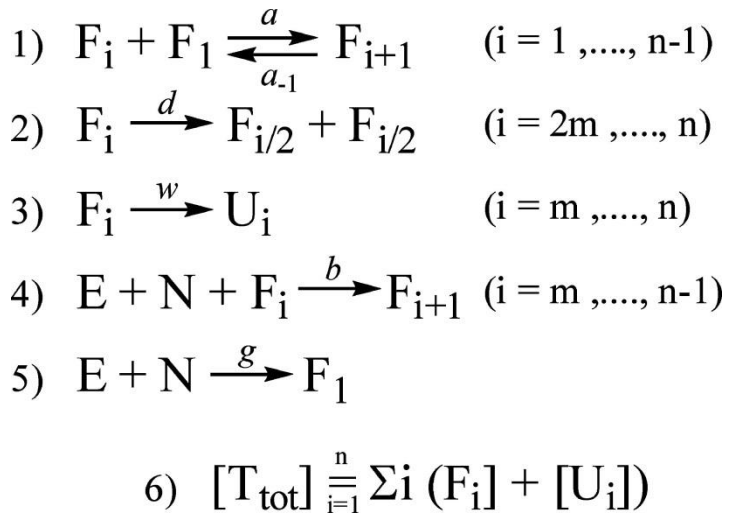

Scheme 7: A kinetic model used to describe the processes shown in this research.

The first three reactions (Equations 1-3 in Scheme 7) refer to the self-assembly of the peptides into fibril and nanotube structures, and the two other reactions (Equations 4-5 in Scheme 7) account for the peptide self-replication. The growth of a fibrillar structure is given in Equation 1 (Scheme 7), describing the reversible association of F_i, a fibril of length i, together with a monomeric peptide F_1, into F_{i+1}, a fibril of length *i+1*. Equation 2 describes the dissociation of a relatively long fibril F_i into two shorter fibrils $F_{i/2}$, and Equation 3 describes the irreversible transformation of a fibril F_i into a corresponding nanotube U_i. The replication process is then described as a ligation reaction of E and N aided by a fibril template F_i (Equation 4), accompanied by a slow background template-free ligation (Equation 5). According to our analysis using the simulation (Figure 41), this is the minimal mechanism required to describe the overall self-assembly driven replication of peptide **1**. Note that only fibrils with minimal 'seeds' of length *m* are considered as species of relatively long half-lives, capable of acting as catalytic templates or capable of transforming into nanotubes (Equations 3-4), and only fibrils longer than *2m* are considered to be capable of dissociation (Equation

2). Interestingly, the mechanism of Equation 2, which describes the decomposition of the fibril, is necessary in order to summarize the transitions among the various forms of catalytic templates in Scheme 6, namely $\mathbf{1_P}$ and $\mathbf{1_F}$ of various sizes.

3.4.3 Simulation of Kinetic Model

Based on this kinetic model (Scheme 7), with help from Dr. N. Wagner, we ran a simulation in Matlab™ in the following manner. At first, the system is seeded only with monomeric strands, and thus only the self-assembly reactions (Equations 1-3 in Scheme 7) are implemented, allowing the system to form the different aggregates. Then, at a pre-set time of template equilibration, the fragments E and N are seeded, and all reactions (Equations 1-5 in Scheme 7) are implemented in parallel. At every time step, after the initial template equilibration time, the various concentrations are computed. The total concentration of template ($[T_{tot}]$) is the sum over all strands of the fibrils F_i and the nanotubes U_i (Equation 6 in Scheme 7). The system was simulated many times using: (i) experimentally relevant initial concentrations of E and N (250 μM each) and F (0-100 μM); (ii) values for m and n of 10 and 100, respectively; (iii) typical values for the rate constants a, a_{-1}, d, w, b and g of 10^4, 10^{-2}, 10^{-2}, 10^{-2}, 10^6 and 10^{-3}, respectively.[99]

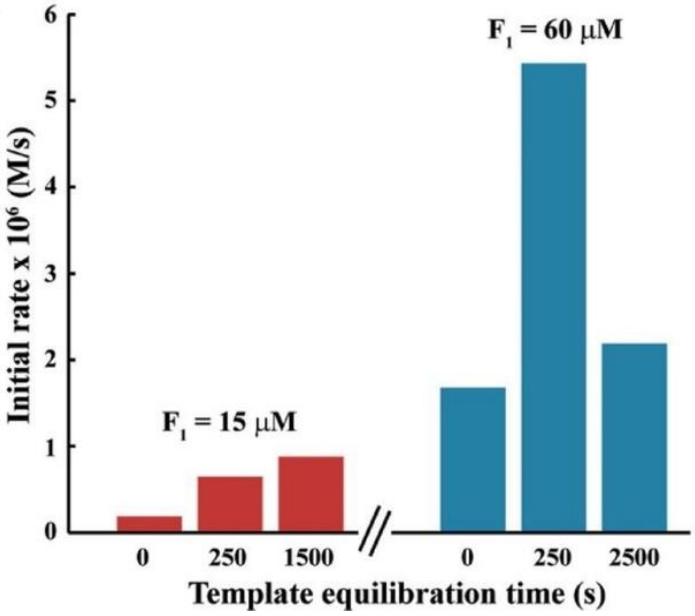

Figure 41: Rate of formation of F_1 in simulated template seeded reactions as a function of the self-assembly time.

Figure 41 shows a snapshot of the product concentrations at a specific time, 400 sec, for the two initial concentrations of F_1, (15 and 60 μM) with each showing three separate values for different template equilibrium times. As expected, the higher initial concentration of F_1 yielded higher product formation. Similarly, higher values for the template equilibrium time generally yielded higher concentrations, since the longer times allowed further aggregation into catalytically active templates. An exception took place for F_1 = 60 μM after template equilibrium time of 2500 sec. In this case, the longer aggregation time allowed significant formation of catalytically inactive nanotubes, yielding a lower concentration than the corresponding case after template equilibrium time of 250 sec. This is consistent with our experimental results (Figure 35).

3.4.4 Conclusions

The proposed mechanism of β-sheet replication summarizes the experimental results of kinetic studies both of self-assembly and self-replication processes. The mechanism designates the two processes that take place in parallel, the dynamic self-assembly of the monomeric template molecules to supramolecular β-sheet rich structures, and their role in replication process through autocatalytic reactions. Together with the full mechanism we proposed a kinetic model, using relatively basic chemical equations. The kinetic model was simulated and showed high correlation with the experimental results.

3.5 Regio and Stereo-selective Ligation by β-Sheet Peptides

This section describes the study conducted on a newly designed replication system, in which the possibility that peptide **2** (Scheme 8) may act as a template molecule for cysteine-free ligation reactions, namely, ligation through glutamic acid residue. Preliminary results of this replication system, as well as a study of self-assembly process that peptide **2** undergoes, was demonstrated by our former student Elina Shtelman as a part of her M.Sc. thesis.[100] For this replication system, we designed a new electrophilic (**E2**) and nucleophilic (**N2**) fragments, which possess a thioester on the C-terminal Glu residue and the free N-terminal Phe, respectively.

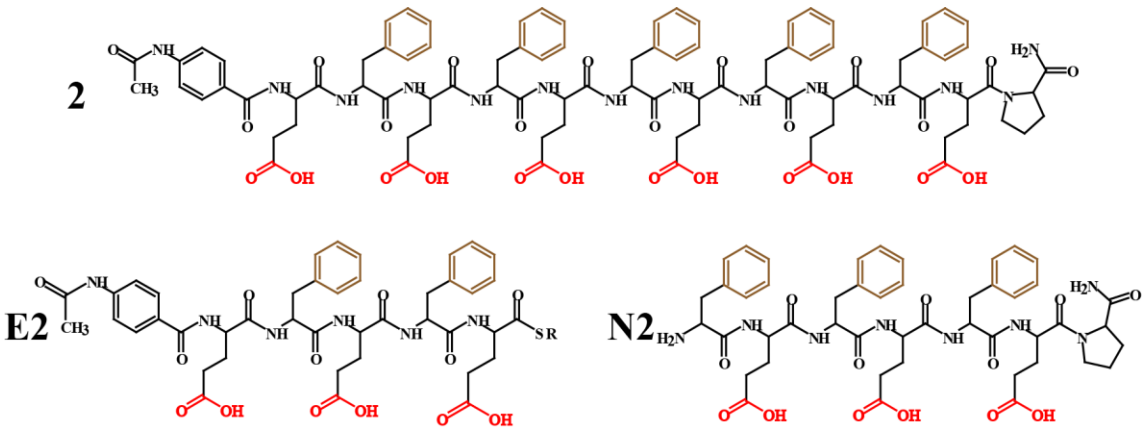

Scheme 8: Stick representation of replication system **2**.

Using previously described research, [101] we envisioned that the thioester on an α-acid of C-terminal Glu will form a glutaric anhydride, by nucleophilic attack of the γ-carboxylate on α-carbonyl (Scheme 9). As a result of anhydride formation in neutral aqueous solutions, two phenomena may take place: first, free thiol migration will cause an opening of the glutaric anhydride ring, either on α- or γ-carbonyls, resulting in two structural isomers; second, the anhydride, which is strong electron withdrawing group, will elevate the acidity of C_α proton resulting in epimerization of L to D configuration. Thus **E2** may exist in four isomers which differ in the location of the C-terminal thioester (Ctt): (1) **E-α-L**, the "native" electrophilic fragment where the Ctt is on the α-carbonyl of L-Glu; (2) **E-γ-L**, where the Ctt is on the γ-carbonyl of L-Glu; (3) **E-α-D**,

where the Ctt is on the α-carbonyl of D-Glu; and (4) **E-γ-D**, where the Ctt is on the γ-carbonyl of D-Glu (Table 2). The ligation reactions with **N2** should yield four products: **2-α-L**, the "native" product (**2;** Scheme 8); the structural isomer **2-γ-L**, which buries two CH_2 groups in the backbone; and their two respective epimers **2-α-D** and **2-γ-D** (Table 2).

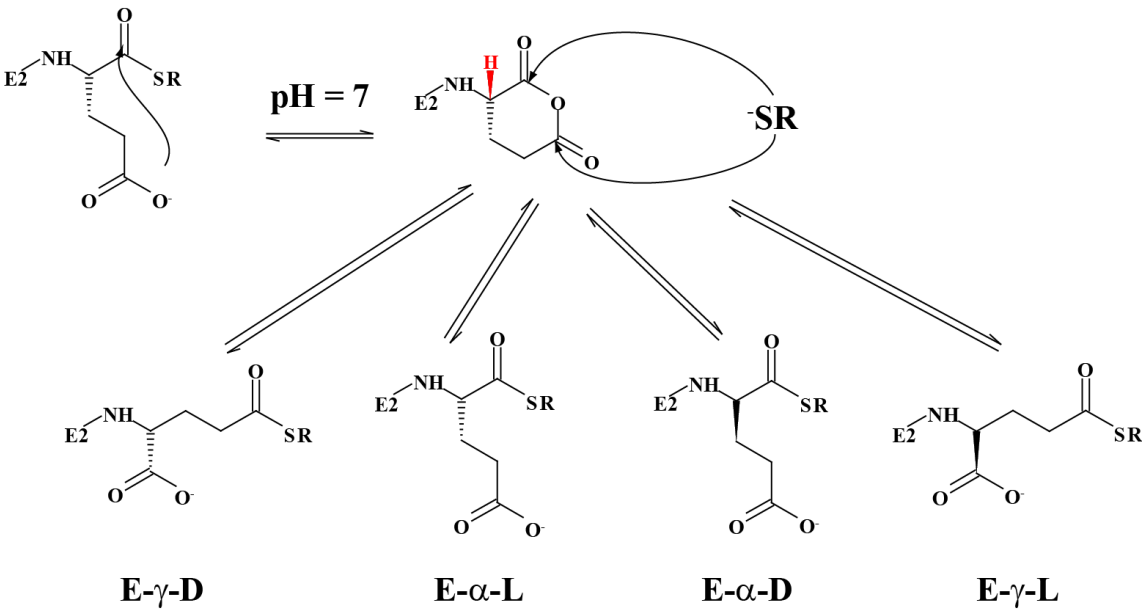

Scheme 9: Proposed mechanism for formation of structural and diastereo isomers by C-terminal glutamic acid.

Peptide	Sequence
2-α-L (2)	ABA-Glu-Phe-Glu-Phe-(L)Glu$^{\alpha}$-Phe-Glu-Phe-Glu-Phe-Glu-Pro-$CONH_2$
2-γ-L	ABA-Glu-Phe-Glu-Phe-(L)Glu$^{\gamma}$-Phe-Glu-Phe-Glu-Phe-Glu-Pro-$CONH_2$
2-α-D	ABA-Glu-Phe-Glu-Phe-(D)Glu$^{\alpha}$-Phe-Glu-Phe-Glu-Phe-Glu-Pro-$CONH_2$
2-γ-D	ABA-Glu-Phe-Glu-Phe-(D)Glu$^{\gamma}$-Phe-Glu-Phe-Glu-Phe-Glu-Pro-$CONH_2$
E-α-L (E2)	ABA-Glu-Phe-Gly-Phe-(L)Glu$^{\alpha}$-$COSR^*$
E-γ-L	ABA-Glu-Phe-Gly-Phe-(L)Glu$^{\gamma}$-$COSR^*$
E-α-D	ABA-Glu-Phe-Gly-Phe-(D)Glu$^{\alpha}$-$COSR^*$
E-γ-D	ABA-Glu-Phe-Gly-Phe-(D)Glu$^{\gamma}$-$COSR^*$
N2	Phe-Glu-Phe-Gly-Phe-Glu-Pro-$CONH_2$
S	ABA-Ala-Ala-$CONH_2$

Table 2: The sequences of the peptides used in the present chapter. SR^* = S-(2-sulfoethyl) thioester.

All peptides (Table 2) were synthesized manually or by an automated synthesizer in our lab. The purity and identity of all peptides was verified by RP-HPLC, MALDI-TOF and LCMS (see experimental details in Chapter 5).

3.5.1 Stability of the Electrophiles

In order to examine the proposed equilibria between the four electrophiles and to examine their hydrolysis rate, we conducted an experiment where each of the electrophiles allowed equilibrating at neutral aqueous solution, and samples of the solutions were analyzed at different time points by HPLC (Figure 42).

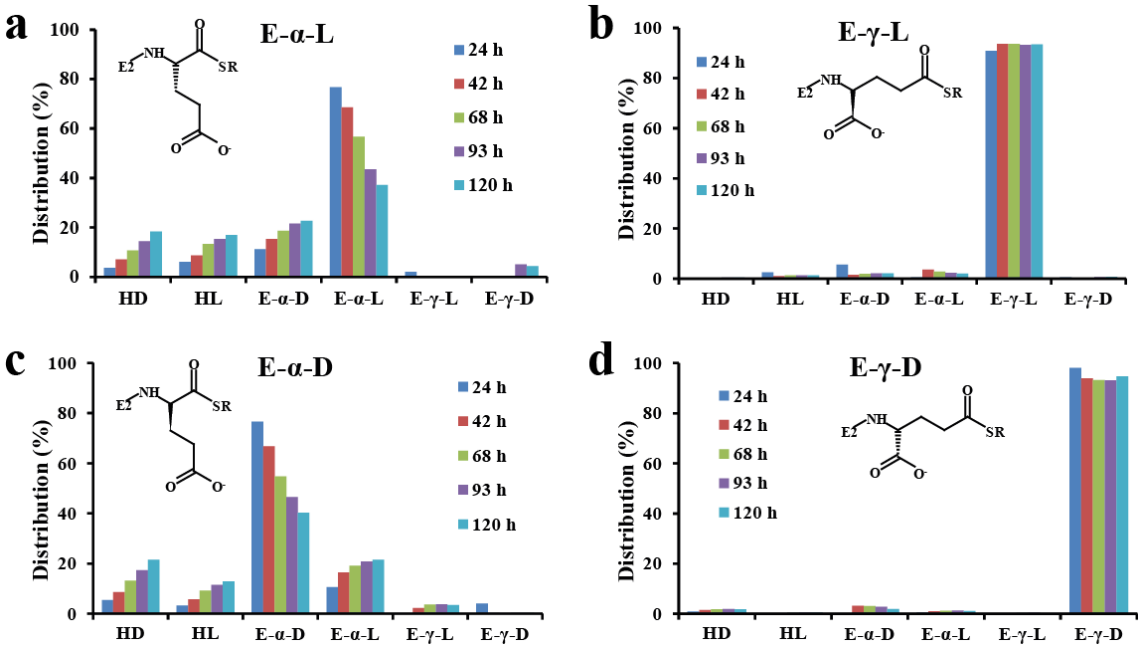

Figure 42: Distribution of products in stability experiments of a) **E-α-L**, b) **E-γ-L**, c) **E-α-D** and d) **E-γ-D**. **HL** and **HD** are hydrolyzed form of electrophiles L and D, respectively (; $[E]_0$ = 65-80μM; 0.2 M MOPS pH 7; r.t.).

The results showed that both α epimers, **E-α-L** and **E-α-D,** underwent epimerization to form one another. Approximately 20% of epimerization took place after 120 h with ~40% total hydrolysis (depicted as **HD** and **HL**). Structural isomerization was also found to low extent. With that, both γ epimers, **E-γ-L** and **E-γ-D**,

were found to be relatively stable both to epimerization, isomerization (<5% after 120h) and hydrolysis (~2% after 120h), probably due to steric effects as a result of elongation of the peptide backbone by two CH_2 groups.

3.5.2 Kinetic Studies of Replication System 2

The study presented here and the study described in section 1.2.4 showed that mechanical stress had high impact on self-assembly process of β-sheet forming peptides. Mechanical forces acted as a selection pressure in the competition between replicators and determined the outcome of a covalent synthesis.[92] In addition, E. Shtelman showed that the self-assembly process of peptide **2** was almost twice as fast as that found for peptide **1**.[100] Peptide **2** achieved the nano-tubular structures, which were found to be less effective catalytic species than the transient fibrillar structures, in shorter time of self-assembly for peptide concentration of 60 μM, compared to peptide **1**. Taking this into account, as well as the fact that the ligation reaction without a cysteine residue, but only with the primary amine of Phe, (pKa ~9.4), is expected to be slow, gives a narrow time window for efficient catalysis. In order to overcome these difficulties, we decided to employ "shaking" during the ligation reaction. Using this methodology, we expected to increase the diffusion of the precursors and thus the ligation kinetics, and also to break the large supramolecular structures formed during the reaction, in order to expose more catalytic sites. In the following experiments we used orbital shaking of the reaction mixture at 500-600 rpm during the time of inspection.

3.5.2.1 Template free reactions

Investigation of template free reactions was performed first in reactions between equimolar amounts of each of the electrophiles and the nucleophilic peptide (600 μM each) for 160 h. Figure 43 shows representative HPLC chromatogram separation of the four isomers of **2,** found at 100 hours of the experiment presented in Figure 45. Figure 44 shows product distribution of template free reactions performed with each of the electrophiles at 160 h. Sodium 2-mercaptoethanesulfonate (MESNA) was added to reaction mixture, in order to investigate the influence of additional nucleophile on product distribution and reactions rate.

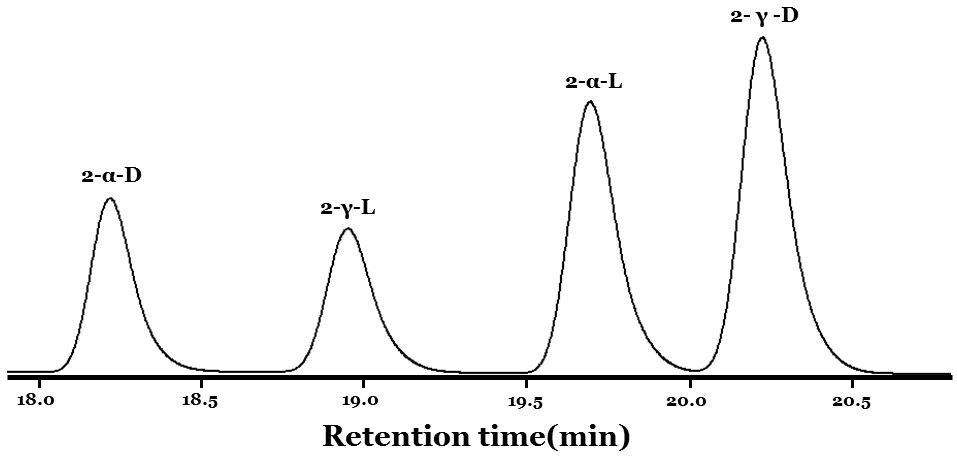

Figure 43: Representative HPLC chromatogram (270 nm) of the four products of peptide **2**.

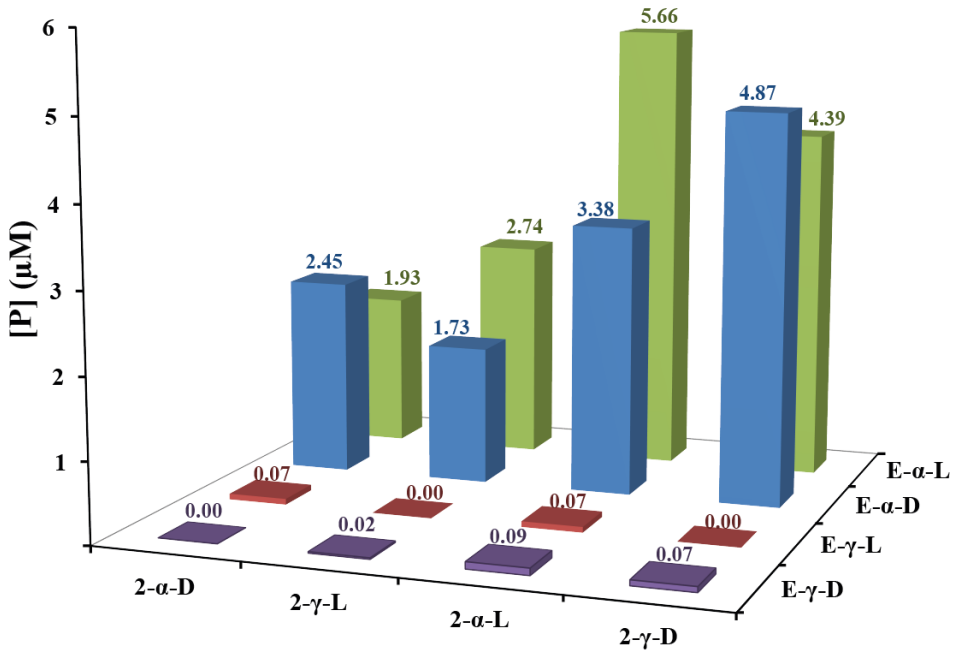

Figure 44: Template free reactions with 4 electrophiles. $[\mathbf{E}]_0=[\mathbf{N2}]_0=[\text{MESNA}]_0$=600±10 μM; 0.2 M MOPS pH 7; Shaking (500-600 rpm); r.t.

The results (Figure 44) ilustrate that under the presented experimental conditions, the reactions performed with both γ electrophiles (**E-γ-L** and **E-γ-D**) proceeded with relatively low final product concentration, $[P]_{Total}$<2 μM. On the other hand, the reactions performed with α electrophiles (**E-α-L** and **E-α-D**) proceeded with relatively high final product concentration, $[P]_{Total}$=15 μM for reaction initiated with **E-**

α-L, and $[P]_{Total}$=12.5 µM for the reaction initiated with **E-α-D**. In the reactions, initiated with **E-α-L**, the formation of **2-α-L** proceeded at the highest final concentration (and highest rate), compared with the formation of the other 3 isomers. Most interesting, the reactions initiated with **E-α-D** gave rise to the product **2-γ-D**, although a very low concentration of **E-γ-D** was found in the experiment mixture, during the time of inspection. These results imply that the formation of **2-γ-D** increased due to self-replication process, similar to that expected for formation of 2-**α-L**.

The results shown in Figure 42 and Figure 44, suggested that only α electrophiles (**E-α-L** and **E-α-D**) were active for the ligation reaction. Further investigation, of template free reactions, was performed using racemic mixtures of **E-α-L** and **E-α-D** (300 µM each = 600 µM total) with **N2** (600 µM). In these experiments we sought to examine the product distribution from a racemic mixture of the reactants, and reach additional understanding of the ligation mechanism.

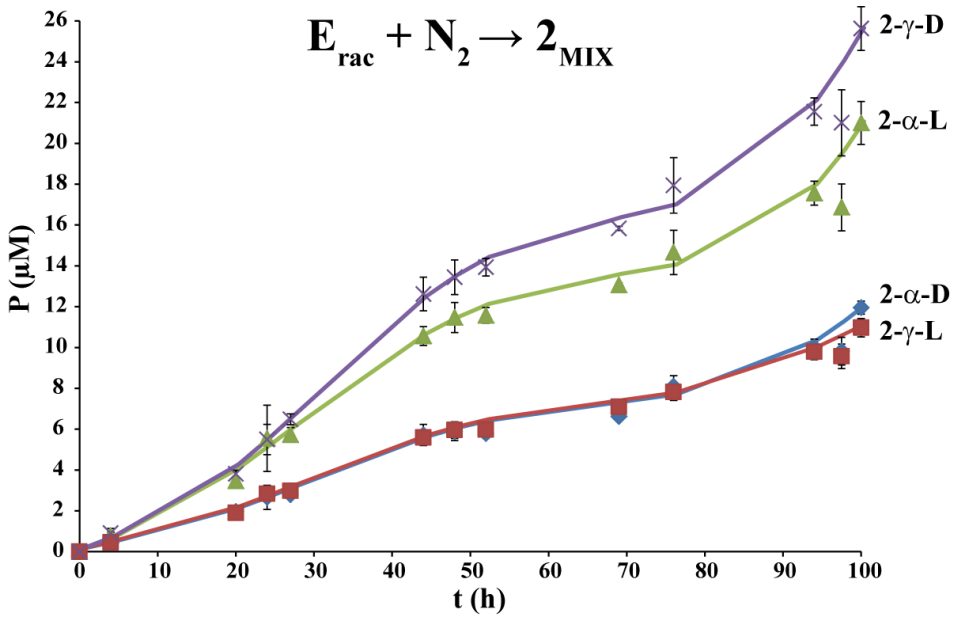

Figure 45: Template free reaction with racemic mixture of electrophiles. $[E\text{-}\alpha\text{-}L]_0$=$[E\text{-}\alpha\text{-}D]_0$=300±10 µM; $[N2]_0$=600±10 µM; 0.2M MOPS pH 7; Shaking (500-600 rpm); r.t. Data present an average±SD of 3 repetitive experiments.

The results (Figure 45) show that the reactions to form **2-α-D** and **2-γ-L** proceeded at a somewhat low rate (and low final concentrations), compared with the rate in reactions to form **2-α-L** and **2-γ-D**. The rates of formation of **2-α-L** and **2-γ-D**

increased after 4 h of inspection, again suggesting that only after reaching a certain critical concentration, the assembly of peptide **2-α-L** and, probably, **2-γ-D** became more pronounced hence accelerated auto-catalysis. In addition, although the reactions to form **2-α-L** and **2-γ-D** advanced at an almost similar rate in the first 24 hours, the rate of formation of **2-γ-D** increased even higher than for **2-α-L**, despite the fact that at all time points the concentration of the reactant **E-α-L** was found to be at least two orders of magnitude higher than the concentration of **E-γ-D**. Also notable that only 20% of electrophiles hydrolyzed in these experiment conditions after 100 h.

3.5.2.2 Template assisted reaction

In another set of experiments using [**E-α-L**]$_0$=[**N2**]$_0$=250 µM, 0.2 M MOPS pH 7, without shaking, we followed the formation of ligation products, in reactions where the ligation mixtures were seeded with 10 or 20 µM of **2-α-L**. The reactions were initiated immediately after vigorous sonication of the template samples. Figure 46 presents product distribution at 48 h in the template seeded reactions normalized to the template free reaction (BG) that were performed as a control to these experiments.

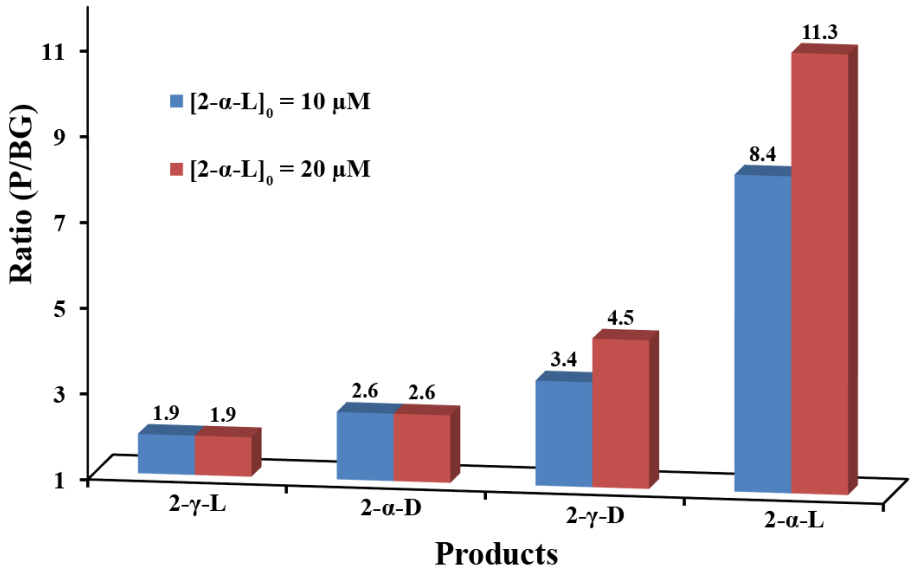

Figure 46: Products in template assisted reactions normalized to template-free reaction (BG) at 48 h. [**E-α-L**]$_0$=[**N2**]$_0$=250 µM, 0.2 M MOPS pH 7, without shaking.

The results of the current experiment showed that the formation of **2-α-L** and **2-γ-D** increased with increase in initially seeded template concentrations. The concentrations of the two other isomers were not influenced by the increase in initial seeded template concentration. Thus, these results illustrate the regio- and stereo-selectivity of β-sheet assisted ligation. It is shown that even the smaller amount of the initial seeded native template increased its own concentration by auto-catalytic process by almost one order of magnitude. In addition, the concentration of **2-γ-D** augmented following the increase of the initial seeded template, probably due to cross-catalytic reaction.

3.5.3 Investigation of the β-sheet assisted glutamic ligation mechanism

One question arising from the experiments shown in this section is: Why (and how) the reaction leading to formation of **2-γ-D** is catalyzed? In order to address this question we characterized and compared the secondary structure of all the four isomers of peptide **2**, utilizing CD spectroscopy, AFM topology analysis and minimization of peptides monomers using CHARMM27 force field methods.

3.5.3.1 CD spectroscopy

CD spectroscopy was employed to investigate the secondary structures of the new isomers of peptides **2** (Figure 47). CD spectra of peptides **2-α-D** and **2-γ-L** showed relatively low minima at 225 and 213 nm, respectively, which can be accounted for different structures (β-hairpin, partial helix)[96], rather than anti-parallel β-sheet. The CD spectrum measured for peptide **2-α-L** showed a minimum at 216 nm, similar to previously measured (Figure 19b). In addition, the CD spectrum measured for peptide **2-γ-D** also showed a minimum at 216 nm, although lower than for **2-α-L**, suggesting self-assembly of this peptide to anti-parallel β-sheet structure.

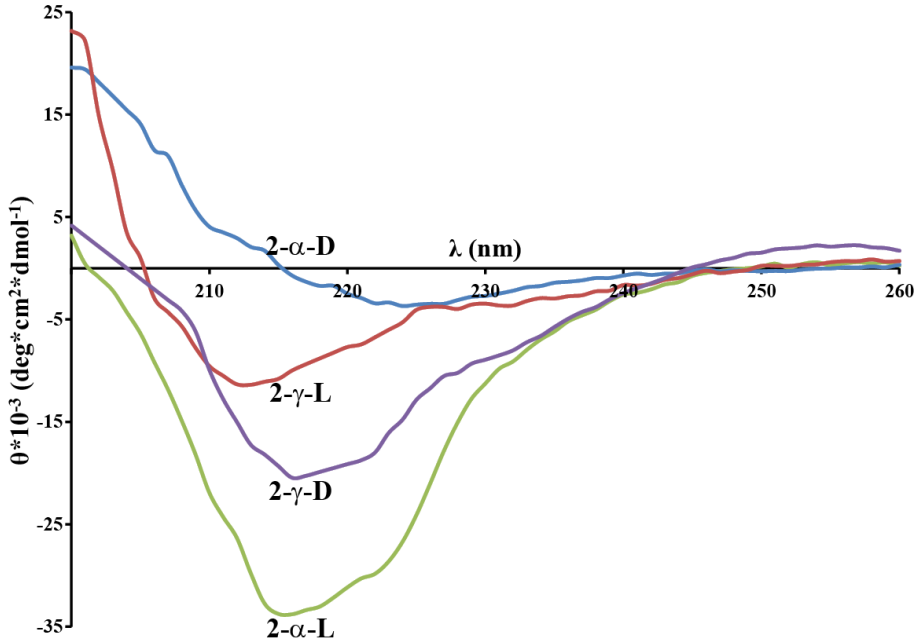

Figure 47: CD spectra of 50±2 μM of the four isomers of peptides **2** in MOPS buffer pH 7, taken immediately after sonication, as described in p. 34.

3.5.3.2 AFM topology

The result from CD spectroscopy, which showed that **2-γ-D** can self-assemble to β-sheet secondary structure, led us to suggest that the relatively fast formation of this isomer in template free reactions is due to folding to fibrillar structures. We decided to image samples of **2-γ-D** using AFM and to compare the obtained morphology to that presented for **2-α-L**. AFM image of peptide **2-γ-D** (Figure 48) showed an elongated and branched fibrillar net with fibrils of different widths, from mono fibrils (~5 nm width), up to coiled wide fibers (>100 nm width). This image resembled the images obtained for peptide **1** (Figure 23a).

3.5.3.3 Minimization analysis of peptides' monomers

Additional information on peptide folding was achieved by minimization of peptides monomers, using CHARMM27 force field (Figure 49). The minimized form of **2-α-L** (Figure 49a) monomer was found to be a starched β-strand where the 5 phenylalanine residues point in opposite direction to the 6 glutamic acids' side-chains, forming aromatic hydrophobic and charged hydrophilic planes, similar to that found in MD simulations.[45] For **2-α-D** (Figure 49b) and **2-γ-L** (Figure 49c) monomers,

minimization brought the γ and α side chains acids of the middle Glu residues, respectively, to the hydrophobic plane, a phenomenon that can disrupt the alternating nature of the β-strand, and preclude the formation of stable anti-parallel β-sheet secondary structure. Interestingly, the double inversion of the middle Glu in **2-γ-D** (Figure 49d), both via chirality change and isomerization, placed the α-acid side chain back in the plane of the acids, restoring the alternating amphiphilic characteristic of the β-strand, thus promoting the formation of anti-parallel β-sheet structure.

These results clarify previously obtained results from replication experiments and structural characterizations by CD spectroscopy and AFM topology of peptide **2-γ-D**. Due to disruption of the alternating nature in the β-strands of **2-α-D** and **2-γ-L**, these peptides did not fold to β-sheet secondary structure, and thus the reactions to form these two isomers proceeded at the same relatively low rate. Despite the additional two CH_2 groups in the backbone of **2-γ-D**, this peptide exhibits alternating arrangement of the aromatic and charged side chains. This phenomenon, in our opinion, stabilized the β-sheet secondary structure and thus folding to the fibrillar supramolecular structures, which are previously found to be catalytically active in ligation reaction.

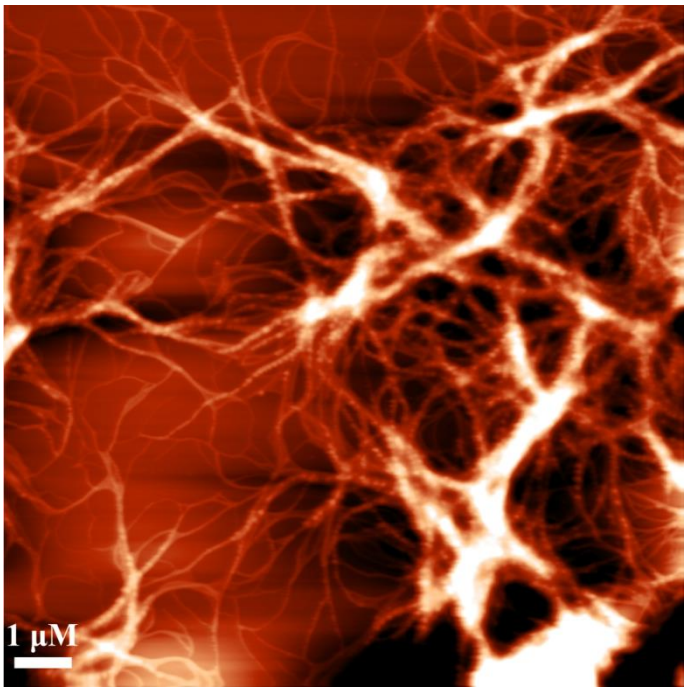

Figure 48: AFM topography image of **2-γ-D** fibrils (100 µM), formed after 30 min of equilibration in MOPS buffer pH 7.

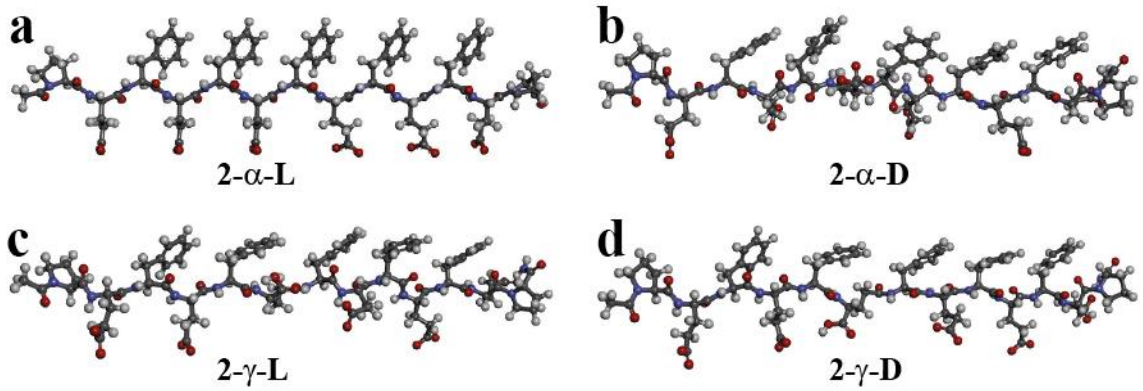

Figure 49: Balls and sticks representation of the four isomers of peptides **2**, as found after minimization by CHARMM27 force field.

3.5.4 Conclusions

Scheme 10 summarizes our proposed mechanism of β-sheet assisted glutamic acid peptide ligation.

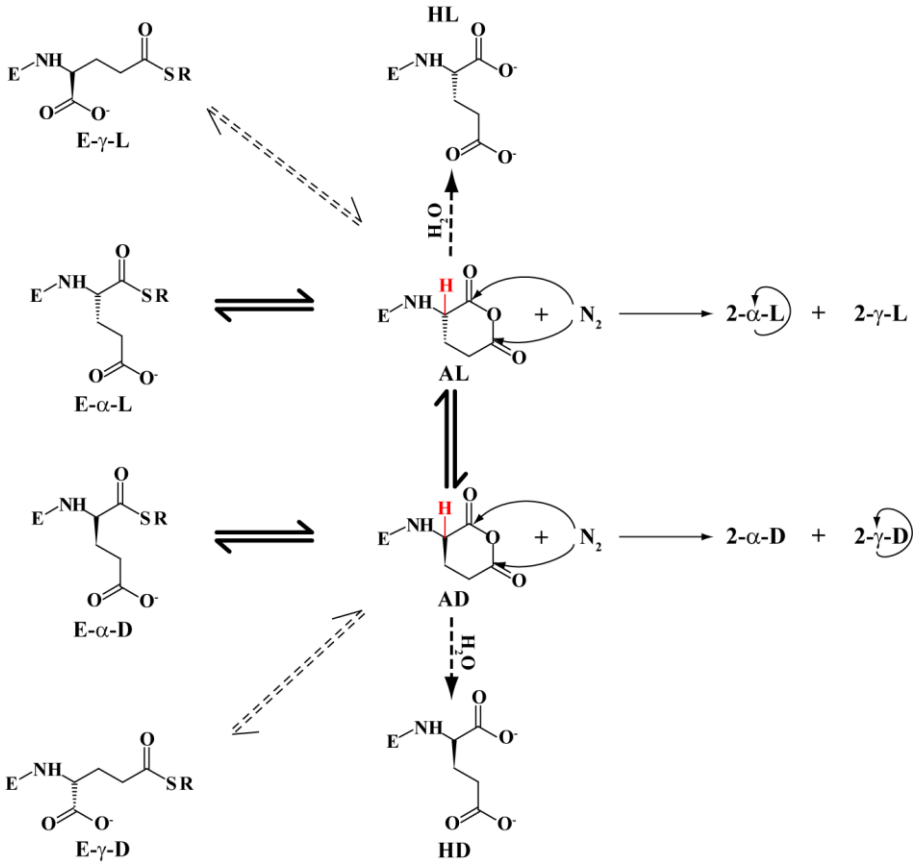

Scheme 10: Proposed network mechanism of β-sheet assisted glutamic acid ligation described above and in p. 58.

E-α-L and **E-α-D** maintain fast equilibrium to the glutaric anhydrides **AL** and **AD**, respectively, by nucleophilic attack of γ-carboxyl on α-carbonyl. The anhydrides in turn, maintain fast equilibrium between each other, by the change of the acidic α-proton. The equilibriums between **E-γ-L** and **E-γ-D** with the respective anhydrides are relatively slow, probably due to the steric constrains. Based on the results from experiment presented in Figure 44, we believe that the anhydrides and not the electrophiles react with the nucleophilic fragment (**N2**). In turn, **N2** can attack the anhydrides through α- or γ-carbonyl to form **2-α-L** and **2-γ-L**, when reacts with **AL**. When **N2** reacts with **AD**, **2-α-D** and **2-γ-D** were formed. Another evidence for these processes is illustrated in reactions where additional thiols were added to the reaction mixtures (3.5.2.1, Figure 44). The thiols shifted the equilibrium from the anhydrides back to the electrophiles, resulting in lower final concentrations of the products, compared with experiments performed without thiols (Figure 45). Since both **2-α-L** and **2-γ-D** folded to β-sheet secondary structure, they promoted auto-catalysis. The high branching and "disorder" of the fibrillar structures formed by **2-γ-D** (Figure 48), may explain the relatively high rates of ligation (and elevated final concentration) compared to **2-α-L**, which forms much ordered and aligned fibrils (Figure 23b). It is suggested that the disordered fibrillar structures formed a higher amount of available catalytic sites compared to high organized fibrils.

4 Summary and Conclusions

The study described herein allows expanding the repertoire of families of replicating molecules. For the first time efficient replication was achieved using short peptides, possessing only alternating aromatic and charged amino acids. Pre-organization of the reactants (**E** and **N** fragment peptides) on the template β-sheet nanostructure occurred at first based on the self-complementarily recognition, which promoted the condensation of the fragment peptides, and then the template β-sheet organizes the newly-generated peptide (chemically identical copy of the template) on the template in association with the promotion of (re)folding to β-sheet. These steps resulted in self-amplification of the β-sheet nanostructure. In contrast to the self-replicating systems employing coiled-coil peptides, and also ordinary enzymatic catalysis, it is suggested that the β-sheet based structures did not require the dissociation of the reacted substrates to maintain the template effect and the catalytic activity. From the molecular structure of the β-sheet forming peptides, and well-supported by our results, it is suggested that the monomeric form of the template peptides cannot serve as a template for the ligation of the electrophilic and the nucleophilic fragments. Thus, the assembly of the template peptides into β-sheet nanostructures is crucial for their function as catalysts of ligation process. This aspect provides a unique example for probing the reactivity of transient nanostructures formed by self-assembly processes through weak bonds, and showed how a careful synchronization between the kinetics of the self-assembly process and the desired activity (template directed synthesis in our case) improved the function significantly. In addition, we managed to probe cysteine free ligation, namely, ligation of glutamic acid residues with a primary amine from phenylalanine, and showed regio- and stereo-selectivity of ligation performed from a racemic mixture of reactants.

Recent works on kinetic mechanism of prion propagation [102-104] illustrated the pathological cascade that leads from soluble protein to insoluble aggregates, composed of fibrillar structures. Our proposed mechanism of β-sheet replication resembled that of the prions. Both systems undergo conversion of soluble proteins (PrP^c in prions; **E** and **N** in our systems) to monomeric units with high tendency to β-sheet

self-assembly, which in turn act as a nucleus for self-replication. However, some differences should be pointed out. While in the prions the synthesis is in equilibrium ($PrP^{c} \leftrightarrows PrP^{Sc}$), via partially unfolded protein (a relatively stable intermediate) [105], the synthesis of the β-sheet forming peptides in our system is non-reversible, due to the formation of an amide bond. The major difference between both systems is in the reaction decay. In the prions, the decay is a result of dilution by various biochemical processes. These processes result in the conversion of catalytically active aggregates to soluble proteins. However, the decay in catalysis of our system is suggested to take place due to conversion of the β-sheet aggregates to highly stable supramolecular structures, *i.e.*, the nano-tubes.

A recent review paper summarized the catalytic abilities of peptide β-sheets in water.[24] By pointing out the β-sheet properties, and specifically, its efficiency in hydrolyzing oligo-ribonucleotides and preventing amino acid racemization, it was suggested that such systems may have played a role in the origin of life. This view is also discussed in recent reports that showed how short peptides can be formed under prebiotic conditions.[106, 107] In addition, the origin of molecular chirality also probed in peptide chain elongation experiments, showing that significant homo-chiral amplification of peptides is obtained via the formation of β-sheets.[38, 39] Our results provide new aspects to these hypotheses, and offer a tunable platform for studying the effect of various structural features and amino acid contents on the replication process.

A list of publications resulting from this work is presented on page 80.

5 Materials and Methods

All chemicals and reagents were purchased from Aldrich, D-Chem or Merck and were used without further purification. Amino acids, resins and coupling reagents were purchased from Novabiochem. DMF was purchased in biotech grade. Unless described differently, all reactions were carried out at room temperature. Analytical HPLC was performed on a Thermo Finnigan Surveyor using a reverse phase C18 column at a flow rate of 1.5 mL/min. Preparative HPLC was performed on a Thermo Spectra Physics instrument using a C18 reverse phase preparative column at a flow rate of 20 mL/min. Mass spectrometry analysis was performed either by MALDI-TOF (reflex IV Bruker Daltonics) or LCMS (LC-MS Thermo Surveyor 355).

5.1 Peptide Synthesis

Peptide synthesis performed with the two commonly used SPPS- Fmoc- and t-Boc, based methods. The synthesis is described in Scheme 11.

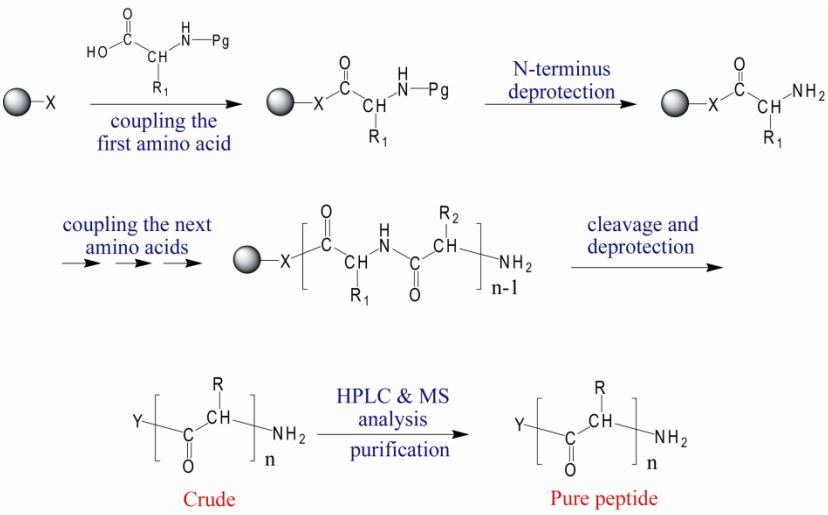

Scheme 11: Solid phase peptide synthesis (SPPS).

5.1.1 Fmoc Method

Peptides **1, 1^{gg}**, **Sc**, **S, N1**, and **N^{g}**, **2-α-L, 2-γ-L, 2-α-D** and **2-γ-D** were synthesized manually (at 0.1 mmol scale) or automatically (at 0.07 mmol scale) using a

fourfold excess of Fmoc-amino acids relative to the Fmoc-Rink amide MBHA resin (0.74 mmol/g). Deprotection was performed using 25% piperidine/DMF twice, for 8 min each time. Coupling was performed using 1:1:5 amino acid/HBTU/DIPEA in DMF, for 45 min to 2 hours. DMF top washes were performed between the deprotection and coupling steps. After the desired sequence was synthesized, the resin was washed with diethyl ether and dried under high vacuum for at least 4 hours. A mixture of TFA containing the appropriate scavengers (10 ml/mg resin) was added to the resin and stirred for 2 hours, to cleave the peptide off the resin and the side chain global deprotection. The resin was removed by filtration under reduced pressure and the TFA was evaporated out of the peptide mixture. 8-10 times volume of cold ether was added to precipitate the crude peptide. The peptide was then isolated from the ether by centrifuge and purified by RP-HPLC.

Peptides **E-α-L, E-γ-L, E-α-D** and **E-γ-D** were synthesized manually (at 0.1 mmol scale) or automatically (at 0.07 mmol scale) using Dbz resin. After regular Fmoc synthesis of desired sequence, the resin washed with DMF and DCM. 4-nitrophenyl chloroformate (0.5 mmol) was added under N_2 and left for 1 h. After wash with DCM, 0.5 M DIPEA in DMF was added for 30 min. Global cleavage of the peptides was performed as described above. The peptides were purified by RP-HPLC prior to exchange of the Nbz group by small thiol. The lyophilized peptide-Nbz (2 mM) and Sodium 2-mercaptoethanesulfonate (MESNA; 10 eq) were dissolved in a screw-tap tube containing degassed buffer (0.2 M phosphate buffer, 6 M guanidine hydrochloride, 0.02 M TCEP, pH 7). The reaction was monitored by RP-HPLC, and after its completion (~1-1.5 h) the reaction mixture acidified with 0.1% TFA, lyophilized and purified by RP-HPLC.

5.1.2 t-Boc Method

Peptides **E** and $\mathbf{E^g}$ were synthesized manually at a 0.1 mmol scale with MBHA resin using a fourfold excess of Boc-amino acids relative to the resin. TMP was first coupled to the resin (3 eq. relative to the resin) using HBTU (3 eq.) and DIPEA (20eq.)

overnight, and then the resin was treated with a mixture of TFA and TIS (95:5) solution for 5 min and then for an additional 10 min to remove the trityl group.

Coupling was performed using 1:1:5 amino acid/HBTU/DIPEA in DMF, for 20-45 min. 4-acetamidobenzoic acid was coupled to the N-terminus of the electrophilic peptide using the same procedure. Deprotection was performed using TFA solution twice. DCM and DMF top washes were performed between the deprotection and coupling steps. After the desired sequence was synthesized, the resin washed with diethyl ether and dried under high vacuum for at least 4 hours. A mixture of TFMSA and TFA containing the appropriate scavengers (10 ml/mg resin) was added to the resin and stirred for 2 hours to cleave the peptide off the resin and the side chain global deprotection. The resin was removed by filtration under reduced pressure. 8-10 times volume of cold ether was added to precipitate the crude peptide. The peptide was then isolated from the ether by centrifugation and purified by HPLC.

5.1.3 Purification and Analysis

All the peptides, except electrophilic, were purified by preparative HPLC using a C18 reverse phase column (AXIA packed NX-C18 Phenomenex Gemini), with a step gradient of solvent A (0.1 M NH_4HCO_3 in water; pH 8) and B (acetonitrile). The identity and purity of the peptides were analyzed by analytical HPLC (with the same solvent system for elution, on NX-C18 Phenomenex Gemini column), MALDI-TOF MS (reflex IV Bruker Daltonics, α-Cyano-4-hydroxycinnamic acid was used as the ionization matrix) and LCMS (LC-MS Thermo Surveyor 355).

The electrophilic peptides were purified by preparative HPLC using C18 reverse phase column (Dionex 1100) with a step gradient of solvent A (99% water, 1% acetonitrile (ACN), 0.1% TFA) and B (90% ACN, 10% water, 0.07% TFA). The identity and purity of the peptides were analyzed by analytical HPLC (with the same solvent system for elution), MALDI-TOF MS (α-Cyano-4-hydroxycinnamic acid was used as ionization matrix) and LCMS.

Only peptides of 95% purity or higher were used for further structure and function analysis.

5.2 Structural Characterizations

5.2.1 Sonication of Peptides Samples

Stock solution of ca. 0.75 mM were prepared by weighing lyophilized peptides into Eppendorf tubes, dissolved in Millipore water/ACN (50/50%) and then was sonicated (at 40 KHz) for 10 min, after which the peptide was diluted in 3-(N-morpholino)propanesulfonic acid (MOPS) buffer at pH 7 to desired concentration (10-120 μM). The exact final concentration of each peptide solution was determined from its UV absorbance at 270 nm, based on the known absorbance of 4-acetamidobenzoat (ABA). The diluted solution was sonicated for additional 10 min, in order to achieve full aggregates disassembly of peptides to monomers (total 20 min of sonication)**.** All structural characterizations (CD, AFM, cryo-TEM and ThT assay), and kinetic replication experiments were initiated at various time after.

5.2.2 CD Analysis

Solution with desired peptide concentration was sonicated according to the above procedure (5.2.1). The measurements were carried out on a Jasco-815 CD spectropolarimeter, at 25 ^{o}C, by using a quartz cell with 1.0 mm path length and 4 second averaging times. CD spectra were obtained as the average of three scans and collecting data at 1 nm intervals from 260 to 200 nm. The CD signals resulting from buffer alone were subtracted from the spectrum of each peptide solution. Data was converted to ellipticity (θ in deg*cm^{2}*dmol^{-1}) according to the equation: $[\theta] = \Psi / (1000\ nlc)$, where Ψ is the CD signal in degrees, n is the number of peptide bonds, l is the path length in centimeters, and c is the concentration in decimoles per cm^{3}.

5.2.3 ThT Assays

A ThT stock solution (1.0 mM) was prepared by dissolving 1.6 mg ThT in 5 ml Millipore water. This stock solution was filtered through a 0.2 μm filter, than diluted 10× in a 0.02 M MOPS buffer before use. Solution with desired peptide concentration was sonicated according to the above procedure (5.2.1) and added to ThT solution prior the measurements (total volume of 100 μL). The fluorescence spectra were recorded on a Varian Cary Eclipse fluorescence spectrometer, 96-microwellplate reader. The excitation wavelength was 440 nm (slit width 5.0 nm) and the emission wavelength was 490 nm (slit width 5 nm). The fluorescence intensity of the ThT solution without any addition was subtracted from the fluorescence intensities of the samples to correct the samples for the background intensity.

5.2.4 Cryo-TEM Imaging

Samples for direct imaging of the aqueous dispersions using cryo-transmission electron microscopy (cryo-TEM) were prepared as follows. In the controlled environment box of a vitrification robot (Vitrobot), a drop of the solution was deposited on a glow-discharged TEM grid (300-mesh Cu Lacey substrate; Ted Pella, Ltd.). The excess liquid was automatically blotted with a filter paper, and the specimen was rapidly plunged into liquid ethane and transferred to liquid nitrogen where it was kept until used. The samples were examined below -175 ºC using an FEI Tecnai 12 G^2 TWIN TEM operated at 120 kV in low-dose mode and with a few micrometers under focus to increase phase contrast. The images were recorded with a Gatan charge-coupled device camera (model 794) and analyzed by Digital Micrograph software, Version 3.1.

5.2.5 AFM Imaging

Silicon substrates with native oxide layer were cleaned using freshly prepared Piranha solution (solution of 3:7 30% H_2O_2 and concentrated H_2SO_4) for 30 min followed by three times immersion in Millipore water for 10 min. The peptide solution

(60 μM of **1** in buffer pH 7) was put on the surface (maximum 10 μL, 10 seconds), followed by drying under nitrogen flow.

Atomic force microscopy (AFM) (Solver-Pro, NTMDT, Ru) topography and phase images were acquired using noncontact tips (NSG03 NT-MDT, Ru (5.1 N m^{-1}, 150 kHz, and 1.74 N m^{-1}, 90 kHz, respectively)) in the N. Ashkenasy lab.

5.2.6 Surface-Pressure Measurements

Monolayers were prepared by spreading peptide solutions in trifluoroacetic acid/chloroform (1:9 v/v) at a concentration of approximately 0.1 mg/mL, on deionized water. Films were allowed to equilibrate for 10 minutes before compression. Surface pressure-area isotherms of the monolayer films were measured using a KSV minitrough (in the H. Rapaport lab on a KSV Instruments LTD, Helsinki, Finland). The nominal area per molecule, A, is calculated from the area available on the Langmuir trough divided by the number of molecules spread.

5.2.7 GIXD Experiments

GIXD experiments were performed, by H. Rapaport and her coworkers, with the liquid surface diffractometer at the undulator BW1 beam line at the HASYLAB synchrotron source (Hamburg, Germany). The peptide films were spread at room temperature and diffraction measurements were performed at 5°C. A monochromatic X-ray beam was adjusted to strike the liquid surface at an incident angle ($a \approx 0.85ac$ where ac is the critical angle for total external reflection) which maximizes surface sensitivity. The dimensions of the footprint of the incoming X-ray beam on the liquid surface were approximately 2 by 50 mm. GIXD signals were obtained from two-dimensional crystallites randomly oriented about the water surface normal. The scattered intensity was collected by means of a position-sensitive detector (PSD) which intercepts photons over the range $0.0 \leq q_z \leq 1.3$ Å-1, q_z being the out of plane component of the scattering vector. Measurements were performed by scanning the horizontal component, $q_{xy} \approx$

$4\pi\sin\theta_{xy} / \lambda$, of the scattering vector, where $2\theta_{xy}$ is the angle between the incident and diffracted beam projected onto the horizontal plane. The diffraction data are represented in two ways: (1) The GIXD pattern $I(q_{xy})$, obtained by integrating over the whole q_z window of the PSD, shows Bragg peaks; (2) Bragg rod intensity profiles are the scattered intensities $I(q_z)$ recorded in channels along the PSD but integrated across the qxy range of each Bragg peak. The q_{xy} positions of the Bragg peaks yield the lattice spacing $d = 2\pi / q_{xy}$, which may be indexed by the two Miller indices h, k to yield the unit cell. The full width at half maximum ($FWHM(q_{xy})$) of the Bragg peaks yields the lateral 2D crystalline coherence length $L_{xy} \approx 0.9(2\pi) / FWHM(q_{xy})$. The width of the Bragg rod profile along q_z gives a first estimate of the thickness of the crystalline film: $L_z \approx 0.9(2\pi) / FWHM(q_z)$. The diffraction data are represented either as the measured intensities or after correction for the Lorenz-polarization and active area (LPA) factors. Bragg peak intensities for the proposed models can be roughly evaluated using the CERIUS2 computational package (Accelrys, Paris).

5.2.8 Dynamic Light Scattering

Samples were prepared by weighing lyophilized peptides in cylindrical glass ampoules (length ca. 8 cm; diameter ca. 0.8 cm) of high quality optical glass and dissolving in Millipore water to yield the desired concentrations. The concentration of each β-peptide solution was determined from the UV absorbance at 270 nm. Solutions were filtered (0.2 μm) or centrifuged to remove aggregates when necessary. Each sample was then placed in a vat filled with toluene as the index matching fluid. During the course of the measurements, the vat temperature was kept at room temperature. The light source was an argon ion laser (Spectra Physics, λ=514.5 nm) and photons scattered by the sample were collected by a photomultiplier tube mounted on the goniometer arm at 90^o to the direction of the incident radiation. The photoelectron count-time autocorrelation function was measured with a BI 2030AT (Brookhaven Instruments) digital correlator and analyzed using the constrained regularization algorithm, CONTIN. Applying the Stokes-Einstein equation to the translational diffusion coefficients provides an intensity-weighted distribution of the hydrodynamic sizes.

5.3 Kinetic Replication Experiments

Experiments were initiated by preparing aqueous mixtures containing **S, N**, tris(2-carboxyethyl)phosphine hydrochloride (TCEP; 2 mM) as reducing agent, the desired amounts of template and 0.2 M 3-(N-morpholino) propanesulfonic acid (MOPS) buffer at pH 7. The reaction solution was sonicated according to procedure above (5.2.1). The experiments were carried out in a thirty-well Teflon plate; here each well was used to run the reaction for different time. The reaction was initiated at different time points by adding **E** (equimolar amount to **N**) to the wells up to total volume of 50 μL. The entire volume of each well was removed at the studied time points, immediately quenched with 50% acetic acid in water, and stored frozen until analyzed by RP-HPLC, using gradient of solvents A and B at pH 8 (see peptide synthesis section above). The concentration of each compound, reactants or templates, was calculated by comparison with the HPLC peak of an ABA-labeled peptide **S** with known concentration. All experiments were repeated at least three times and showed the same results.

5.3.1 Template Free Reactions

Experiments were initiated by preparing aqueous mixtures containing **S** (50 μM)**, N** (250 μM of **N1** or $\mathbf{N^g}$; 250 or 600 μM of **N2**), TCEP (in experiments performed with **N1** or $\mathbf{N^g}$) and 0.2 M MOPS buffer at pH 7. The reaction solution was sonicated according to procedure above (5.2.1). Immediately after sonication the mixtures were divided to 10 wells on Teflon plate (for 10 time points), where each contained aqueous solution of **E** (250 μM of **E1** or $\mathbf{E^g}$; 250 or 600 μM of **E2**). The reaction solutions were quenched and analyzed according to procedure above.

5.3.2 Template Assisted Reactions

Experiments were initiated by preparing aqueous mixtures containing **S** (50 μM)**, N** (250 μM of **N1** or $\mathbf{N^g}$; 250 or 600 μM of **N2**), TCEP (in experiments performed with **N1** or $\mathbf{N^g}$), the desired amounts of template and 0.2 M MOPS buffer at pH 7. The

reaction solution was sonicated according to procedure above (5.2.1). Immediately after sonication the mixtures were divided to wells on Teflon plate according to number of desired time points. Aqueous solution of **E** (250 μM of **E1** or $\mathbf{E^g}$; 250 or 600 μM of **E2**) was added to each well after designed time of equilibration. The reaction solutions were quenched and analyzed according to procedure above.

6 Publications

- **Rubinov, B.**, Wagner, N., Rapaport, H., and Ashkenasy, G., "*Self-Replicating Amphiphilic β-Sheet Peptides"* Angewandte Chemie International Edition 2009, **48**: p. 6683-6686.
- Wagner, N., **Rubinov**, **B.,** and Ashkenasy, G., "*β-Sheet-Induced Chirogenesis in Polymerization of Oligopeptides*" ChemPhysChem 2011, **12**: p. 2771-2780.
- Bourbo, V., Matmor, M., Shtelman, E., **Rubinov, B.,** Ashkenasy, N. and Ashkenasy, G., "*Self-Assembly and Self-Replication of Short Amphiphilic β-Sheet Peptides*" Origins of Life and Evolution of Biospheres 2011, **41**: p. 563-567.
- **Rubinov, B.,** Matmor, M., Wagner, N., Regev, O., Ashkenasy N., and Ashkenasy, G., "*Transient Fibril Structures Facilitating non-Enzymatic Self-Replication*" ACS Nano 2012, **6**: p. 7893-7901. – *Highlighted in* Nature Nanotechnology 2012, **7**: p. 549.
- Raz, Y., **Rubinov, B.,** Matmor, M., Rapaport, H., Ashkenasy, G., and Miller, Y., "*Effects of Mutations in de novo Designed Synthetic Amphiphilic β-Sheet Peptides on Self-Assembly of Fibrils*", Chemical Communications, 2013, **49**: p. 6561-6563.
- Ivnitski, D., Amit, M., **Rubinov, B.,** Cohen-Luria, R., Ashkenasy, N., and Ashkenasy, G., "*Introducing charge transfer functionality into prebiotically relevant β-sheet peptide fibrils*", Chemical Communications, 2014, **50**: p. 6733-6736.
- **Rubinov, B.**, Nanda, J., Ivnitski, D., Shepelevski, E., Wagner, N., and Ashkenasy, G., "*Regio- and Sterio-Selective β-Sheet Peptide Replicator"*, in preparation.

7 References

1. Cavalli, S., F. Albericio, and A. Kros, *Amphiphilic peptides and their cross-disciplinary role as building blocks for nanoscience.* Chemical Society Reviews, 2010. **39**: p. 241-263.
2. Matson, J.B. and S.I. Stupp, *Self-assembling peptide scaffolds for regenerative medicine.* Chemical Communications, 2012. **48**: p. 26-33.
3. Zhang, S.G., D.M. Marini, W. Hwang, and S. Santoso, *Design of nanostructured biological materials through self-assembly of peptides and proteins.* Current Opinion in Chemical Biology, 2002. **6**: p. 865-871.
4. Zhang, S.G., *Fabrication of novel biomaterials through molecular self-assembly.* Nature Biotechnology, 2003. **21**: p. 1171-1178.
5. Loo, Y., S.G. Zhang, and C.A.E. Hauser, *From short peptides to nanofibers to macromolecular assemblies in biomedicine.* Biotechnology Advances, 2012. **30**: p. 593-603.
6. Aida, T., E.W. Meijer, and S.I. Stupp, *Functional supramolecular polymers.* Science, 2012. **335**: p. 813-817.
7. Mehta, A.K., K. Lu, W.S. Childers, Y. Liang, S.N. Dublin, J.J. Dong, J.P. Snyder, S.V. Pingali, P. Thiyagarajan, and D.G. Lynn, *Facial symmetry in protein self-assembly.* Journal of the American Chemical Society, 2008. **130**: p. 9829-9835.
8. Scanlon, S. and A. Aggeli, *Self-assembling peptide nanotubes.* Nano Today, 2008. **3**: p. 22-30.
9. Reches, M. and E. Gazit, *Casting metal nanowires within discrete self-assembled peptide nanotubes.* Science, 2003. **300**: p. 625-627.
10. Yuran, S., Y. Razvag, and M. Reches, *Coassembly of aromatic dipeptides into biomolecular necklaces.* ACS Nano, 2012. **6**: p. 9559-9566.
11. Roy, S., N. Javid, P. Frederix, D.A. Lamprou, A.J. Urquhart, N.T. Hunt, P.J. Halling, and R.V. Ulijn, *Dramatic specific-ion effect in supramolecular hydrogels.* Chemistry- A European Journal, 2012. **18**: p. 11723-11731.
12. Adamcik, J., V. Castelletto, S. Bolisetty, I.W. Hamley, and R. Mezzenga, *Direct observation of time-resolved polymorphic states in the self-assembly of end-capped heptapeptides.* Angewandte Chemie International Edition, 2011. **50**: p. 5495-5498.

13. Li, J.W., J.M.A. Carnall, M.C.A. Stuart, and S. Otto, *Hydrogel formation upon photoinduced covalent capture of macrocycle stacks from dynamic combinatorial libraries*. Angewandte Chemie International Edition, 2011. **50**: p. 8384-8386.
14. Faramarzi, V., F. Niess, E. Moulin, M. Maaloum, J.F. Dayen, J.B. Beaufrand, S. Zanettini, B. Doudin, and N. Giuseppone, *Light-triggered self-construction of supramolecular organic nanowires as metallic interconnects.* Nature Chemistry, 2012. **4**: p. 485-490.
15. Schulman, R., B. Yurke, and E. Winfree, *Robust self-replication of combinatorial information via crystal growth and scission.* Proceedings of the National Academy of Sciences of the United States of America, 2012. **109**: p. 6405-6410.
16. Orgel, L.E. and R. Lohrmann, *Prebiotic chemistry and nucleic acid replication.* Accounts of Chemical Research, 1974. **7**: p. 368-377.
17. Brack, A. and L.E. Orgel, *β structures of alternating polypeptides and their possible prebiotic significance.* Nature, 1975. **256**: p. 383-387.
18. Pauling, L. and R.B. Corey, *Configuration of polypeptide chains.* Nature, 1951. **168**: p. 550-551.
19. Pauling, L., R.B. Corey, and H.R. Branson, *The structure of proteins; two hydrogen-bonded helical configurations of the polypeptide chain.* Proceedings of the National Academy of Sciences of the United States of America, 1951. **37**: p. 205-211.
20. Astbury, W.T. and A. Street, *X-ray studies of the structures of hair, wool and related fibres. I. General*, in Philosophical Transactions of the Royal Society of London. 1932, The Royal Society. p. 75-101.
21. Nowick, J.S., E.M. Smith, and M. Pairish, *Artificial β-sheets.* Chemical Society Reviews, 1996. **25**: p. 401-415.
22. Miller, S.L., *A production of amino acids under possible primitive earth conditions.* Science, 1953. **117**: p. 528-529.
23. Miller, S.L. and L.E. Orgel, *The origins of life on the earth*. 1974: Prentice Hall.
24. Brack, A., *From interstellar amino acids to prebiotic catalytic peptides: A review.* Chemistry & Biodiversity, 2007. **4**: p. 665-679.
25. Rode, B.M., *Peptide and the origin of life.* Peptides, 1999. **20**: p. 773-786.
26. Orgel, L.E., *Prebiotic chemistry and the origin of the RNA world.* Critical Reviews in Biochemistry and Molecular Biology, 2004. **39**: p. 99-123.
27. Orgel, L.E., *Evolution of the genetic apparatus.* Journal of Molecular Biology, 1968. **38**: p. 381-393.

28. Orgel, L.E., *Evolution of the genetic apparatus: A review.* Cold Spring Harbor Symposia on Quantitative Biology, 1987. **52**: p. 9-16.
29. Ikehara, K., *Possible steps to the emergence of life: The GADV -protein world hypothesis.* Chemical Record, 2005. **5**: p. 107-118.
30. Woolfson, A., *Life without genes*. 2000: HarperCollins.
31. Maury, C.P.J., *Self-propagating β-sheet polypeptide structures as prebiotic informational molecular entities: the amyloid world.* Origins of Life and Evolution of Biospheres, 2009. **39**: p. 141-150.
32. Brack, A. and G. Spach, *β-structures of polypeptides with L- and D-residues.* Journal of Molecular Evolution, 1979. **13**: p. 35-46.
33. Spach, G. and A. Brack, *β-structures of polypeptides with L- and D-residues.* Journal of Molecular Evolution, 1979. **13**: p. 47-56.
34. Brack, A. and G. Spach, *β-structures of polypeptides with L- and D-residues.* Journal of Molecular Evolution, 1980. **15**: p. 231-238.
35. Blocher, M., T. Hitz, and P.L. Luisi, *Stereoselectivity in the oligomerization of racemic tryptophan N-carboxyanhydride (NCA-Trp) as determined by isotope labeling and mass spectrometry.* Helvetica Chimica Acta, 2001. **84**: p. 842-848.
36. Hitz, T., M. Blocher, P. Walde, and P.L. Luisi, *Stereoselectivity aspects in the condensation of racemic NCA-amino acids in the presence and absence of liposomes.* Macromolecules, 2001. **34**: p. 2443-2449.
37. Zepik, H., E. Shavit, M. Tang, T.R. Jensen, K. Kjaer, G. Bolbach, L. Leiserowitz, I. Weissbuch, and M. Lahav, *Chiral amplification of oligopeptides in two-dimensional crystalline self-assemblies on water.* Science, 2002. **295**: p. 1266-1269.
38. Rubinstein, I., R. Eliash, G. Bolbach, I. Weissbuch, and M. Lahav, *Racemic β sheets in biochirogenesis.* Angewandte Chemie International Edition, 2007. **46**: p. 3710-3713.
39. Illos, R.A., F.R. Bisogno, G. Clodic, G. Bolbach, I. Weissbuch, and M. Lahav, *Oligopeptides and copeptides of homochiral sequence, via β-sheets, from mixtures of racemic alpha-amino acids, in a one-pot reaction in water; relevance to biochirogenesis.* Journal of the American Chemical Society, 2008. **130**: p. 8651-8659.
40. Rubinstein, I., G. Clodic, G. Bolbach, I. Weissbuch, and M. Lahav, *Racemic beta-sheets as templates for the generation of homochiral (isotactic) peptides from aqueous solutions of (RS)-valine or -leucine N-carboxy- anhydrides: relevance to biochirogenesis.* Chemistry- A European Journal, 2008. **14**: p. 10999-1009.

41. Weissbuch, I., R.A. Illos, G. Bolbach, and M. Lahav, *Racemic β-sheets as templates of relevance to the origin of homochirality of peptides: lessons from crystal chemistry.* Accounts of Chemical Research, 2009. **42**: p. 1128-1140.

42. Nery, J.G., G. Bolbach, I. Weissbuch, and M. Lahav, *Homochiral oligopeptides generated by induced "mirror symmetry breaking" lattice-controlled polymerizations in racemic crystals of phenylalanine N-carboxyanhydride.* Chemistry- A European Journal, 2005. **11**: p. 3039-3048.

43. Eliash, R., J.G. Nery, I. Rubinstein, G. Clodic, G. Bolbach, I. Weissbuch, and M. Lahav, *Homochiral oligopeptides via a lattice-controlled polymerisation in racemic crystals of valine N-carboxyanhydride suspended in aqueous solutions.* Chemistry- A European Journal, 2007. **13**: p. 10140-10151.

44. Wagner, N., B. Rubinov, and G. Ashkenasy, *β-Sheet-induced chirogenesis in polymerization of oligopeptides.* ChemPhysChem, 2011. **12**: p. 2771-2780.

45. Raz, Y., B. Rubinov, M. Matmor, H. Rapaport, G. Ashkenasy, and Y. Miller, *Effects of mutations in de novo designed synthetic amphiphilic β-sheet peptides on self-assembly of fibrils.* Chemical Communications, 2013. **49**: p. 6561-6563.

46. Yokoi, H., T. Kinoshita, and S.G. Zhang, *Dynamic reassembly of peptide RADA16 nanofiber scaffold.* Proceedings of the National Academy of Sciences of the United States of America, 2005. **102**: p. 8414-8419.

47. Zhao, X.B., F. Pan, H. Xu, M. Yaseen, H.H. Shan, C.A.E. Hauser, S.G. Zhang, and J.R. Lu, *Molecular self-assembly and applications of designer peptide amphiphiles.* Chemical Society Reviews, 2010. **39**: p. 3480-3498.

48. Zhang, S., H. Yokoi, F. Gelain, and A. Horii, *Designer self-assembling peptide nanofiber scaffolds*, in Nanotechnology for Biology and Medicine: At the Building Block Level, G.A. Silva and V. Parpura, Editors. 2012, Springer. p. 123-147.

49. Cui, H., M.J. Webber, and S.I. Stupp, *Self-assembly of peptide amphiphiles: From molecules to nanostructures to biomaterials.* Peptide Science, 2010. **94**: p. 1-18.

50. Rapaport, H., K. Kjaer, T.R. Jensen, L. Leiserowitz, and D.A. Tirrell, *Two-dimensional order in β-sheet peptide monolayers.* Journal of the American Chemical Society, 2000. **122**: p. 12523-12529.

51. Sneer, R., M.J. Weygand, K. Kjaer, D.A. Tirrell, and H. Rapaport, *Parallel β-sheet assemblies at interfaces.* ChemPhysChem, 2004. **5**: p. 747-750.

52. Isenberg, H., K. Kjaer, and H. Rapaport, *Elasticity of crystalline β-sheet monolayers.* Journal of the American Chemical Society, 2006. **128**: p. 12468-12472.

53. Rapaport, H., *Ordered peptide assemblies at interfaces.* Supramolecular Chemistry, 2006. **18**: p. 445-454.
54. Aggeli, A., I.A. Nyrkova, M. Bell, R. Harding, L. Carrick, T.C.B. McLeish, A.N. Semenov, and N. Boden, *Hierarchical self-assembly of chiral rod-like molecules as a model for peptide β-sheet tapes, ribbons, fibrils, and fibers.* Proceedings of the National Academy of Sciences of the United States of America, 2001. **98**: p. 11857-11862.
55. Mihara, H., S. Matsumura, and T. Takahashi, *Construction and control of self-assembly of amyloid and fibrous peptides.* Bulletin of the Chemical Society of Japan, 2005. **78**: p. 572-590.
56. Hamley, I.W., *Peptide fibrillization.* Angewandte Chemie International Edition, 2007. **46**: p. 8128-8147.
57. Whitesides, G., J. Mathias, and C. Seto, *Molecular self-assembly and nanochemistry: a chemical strategy for the synthesis of nanostructures.* Science, 1991. **254**: p. 1312-1319.
58. Whitesides, G.M. and B. Grzybowski, *Self-assembly at all scales.* Science, 2002. **295**: p. 2418-2421.
59. Service, R.F., *Molecules get wired.* Science, 2001. **294**: p. 2442-2443.
60. von Kiedrowski, G., *A self-replicating hexadeoxynucleotide.* Angewandte Chemie International Edition, 1986. **25**: p. 932-935.
61. von Kiedrowski, G., B. Wlotzka, and J. Helbing, *Sequence dependence of template-directed syntheses of hexadeoxynucleotide derivatives with 3'–5' pyrophosphate linkage.* Angewandte Chemie International Edition, 1989. **28**: p. 1235-1237.
62. Zielinski, W.S. and L.E. Orgel, *Autocatalytic synthesis of a tetranucleotide analogue.* Nature, 1987. **327**: p. 346-7.
63. Dadon, Z., N. Wagner, and G. Ashkenasy, *The road to non-enzymatic molecular networks.* Angewandte Chemie International Edition, 2008. **47**: p. 6128-6136.
64. Kim, D.-E. and G.F. Joyce, *Cross-catalytic replication of an RNA ligase ribozyme.* Chemistry & Biology, 2004. **11**: p. 1505-1512.
65. Lincoln, T.A. and G.F. Joyce, *Self-sustained replication of an RNA enzyme.* Science, 2009. **323**: p. 1229-1232.
66. Severin, K., D.H. Lee, J.A. Martinez, and M.R. Ghadiri, *Peptide self-replication via template-directed ligation.* Chemistry- A European Journal, 1997. **3**: p. 1017-1024.
67. Yao, S., I. Ghosh, R. Zutshi, and J. Chmielewski, *A pH-modulated, self-replicating peptide.* Journal of the American Chemical Society, 1997. **119**: p. 10559-10560.

68. Lee, D.H., J.R. Granja, J.A. Martinez, K. Severin, and M.R. Ghadiri, *A self-replicating peptide.* Nature, 1996. **382**: p. 525-528.

69. Yao, S., I. Ghosh, R. Zutshi, and J. Chmielewski, *A self-replicating peptide under ionic control.* Angewandte Chemie International Edition, 1998. **37**: p. 478-481.

70. Ashkenasy, G., R. Jagasia, M. Yadav, and M.R. Ghadiri, *Design of a directed molecular network.* Proceedings of the National Academy of Sciences of the United States of America, 2004. **101**: p. 10872-10877.

71. Wintner, E.A. and J. Rebek, *Autocatalysis and the generation of self-replicating systems.* Acta Chemica Scandinavica, 1996. **50**: p. 469-485.

72. Wang, B. and I. O. Sutherland, *Self-replication in a Diels-Alder reaction.* Chemical Communications, 19971495-1496.

73. Kassianidis, E. and D. Philp, *Reciprocal template effects in a simple synthetic system.* Chemical Communications, 20064072-4074.

74. Harrison, R.S., P.C. Sharpe, Y. Singh, and D.P. Fairlie, *Amyloid peptides and proteins in review,* in Reviews of Physiology, Biochemistry and Pharmacology, S.G. Amara, E. Bamberg, B. Fleischmann, T. Gudermann, S.C. Hebert, R. Jahn, W.J. Lederer, R. Lill, A. Miyajima, S. Offermanns, and R. Zechner, Editors. 2007, Springer Berlin Heidelberg. p. 1-77.

75. McLaurin, J., D. Yang, C.M. Yip, and P.E. Fraser, *Review: Modulating factors in amyloid-β fibril formation.* Journal of Structural Biology, 2000. **130**: p. 259-270.

76. Bekris, L.M., C.E. Yu, T.D. Bird, and D.W. Tsuang, *Genetics of Alzheimer disease.* Journal of Geriatric Psychiatry and Neurology, 2010. **23**: p. 213-227.

77. Jan, A., D.M. Hartley, and H.A. Lashuel, *Preparation and characterization of toxic Aβ aggregates for structural and functional studies in Alzheimer's disease research.* Nature Protocols, 2010. **5**: p. 1186-1209.

78. Kodali, R., A.D. Williams, S. Chemuru, and R. Wetzel, *Aβ(1-40) forms five distinct amyloid structures whose β-sheet contents and fibril stabilities are correlated.* Journal of Molecular Biology, 2010. **401**: p. 503-517.

79. Luhrs, T., C. Ritter, M. Adrian, D. Riek-Loher, B. Bohrmann, H. Dobeli, D. Schubert, and R. Riek, *3D structure of Alzheimer's amyloid-β(1-42) fibrils.* Proceedings of the National Academy of Sciences of the United States of America, 2005. **102**: p. 17342-13747.

80. Sawaya, M.R., S. Sambashivan, R. Nelson, M.I. Ivanova, S.A. Sievers, M.I. Apostol, M.J. Thompson, M. Balbirnie, J.J. Wiltzius, H.T. McFarlane, A.O. Madsen, C. Riekel,

and D. Eisenberg, *Atomic structures of amyloid cross-β spines reveal varied steric zippers.* Nature, 2007. **447**: p. 453-457.

81. van der Wel, P.C.A., J.R. Lewandowski, and R.G. Griffin, *Solid-state NMR study of amyloid nanocrystals and fibrils formed by the peptide GNNQQNY from yeast prion protein Sup35p.* Journal of the American Chemical Society, 2007. **129**: p. 5117-5130.
82. Lansbury, P.T., *A Reductionist View of Alzheimer's Disease.* Accounts of Chemical Research, 1996. **29**: p. 317-321.
83. Teplow, D.B., *Structural and kinetic features of amyloid beta-protein fibrillogenesis.* Amyloid, 1998. **5**: p. 121-142.
84. Thirumalai, D., D.K. Klimov, and R.I. Dima, *Emerging ideas on the molecular basis of protein and peptide aggregation.* Current Opinion in Structural Biology, 2003. **13**: p. 146-159.
85. Miller, Y., B. Ma, and R. Nussinov, *The unique Alzheimer's β-amyloid triangular fibril has a cavity along the fibril axis under physiological conditions.* Journal of the American Chemical Society, 2011. **133**: p. 2742-2748.
86. Carny, O. and E. Gazit, *A model for the role of short self-assembled peptides in the very early stages of the origin of life.* FASEB Journal, 2005. **19**: p. 1051-1055.
87. Dawson, P.E., T.W. Muir, I. Clark-Lewis, and S.B. Kent, *Synthesis of proteins by native chemical ligation.* Science, 1994. **266**: p. 776-779.
88. Takahashi, Y. and H. Mihara, *Construction of a chemically and conformationally self-replicating system of amyloid-like fibrils.* Bioorganic & Medicinal Chemistry, 2004. **12**: p. 693-699.
89. Rubinov, B., N. Wagner, M. Matmor, O. Regev, N. Ashkenasy, and G. Ashkenasy, *Transient fibril structures facilitating nonenzymatic self-replication.* ACS Nano, 2012. **6**: p. 7893-7901.
90. Rubinov, B., N. Wagner, H. Rapaport, and G. Ashkenasy, *Self-replicating amphiphilic β-sheet peptides.* Angewandte Chemie International Edition, 2009. **48**: p. 6683-6686.
91. Bourbo, V., M. Matmor, E. Shtelman, B. Rubinov, N. Ashkenasy, and G. Ashkenasy, *Self-assembly and self-replication of short amphiphilic β-sheet peptides.* Origins of Life and Evolution of Biospheres, 2011. **41**: p. 563-567.
92. Carnall, J.M.A., C.A. Waudby, A.M. Belenguer, M.C.A. Stuart, J.J.-P. Peyralans, and S. Otto, *Mechanosensitive self-replication driven by self-organization.* Science, 2010. **327**: p. 1502-1506.

93. Degrado, W.F. and J.D. Lear, *Induction of peptide conformation at apolar water interfaces. 1. A study with model peptides of defined hydrophobic periodicity.* Journal of the American Chemical Society, 1985. **107**: p. 7684-7689.

94. Merrifield, R.B., *Solid phase peptide synthesis. I. The synthesis of a tetrapeptide.* Journal of the American Chemical Society, 1963. **85**: p. 2149-2154.

95. Chechel, O.V. and E.N. Nikolaev, *Devices for Production of Langmuir-Blodgett-Films - Review.* Instruments and Experimental Techniques, 1991. **34**: p. 750-762.

96. Kelly, S.M., T.J. Jess, and N.C. Price, *How to study proteins by circular dichroism.* Biochimica Et Biophysica Acta-Proteins and Proteomics, 2005. **1751**: p. 119-139.

97. Picken, M. and G. Herrera, *Thioflavin T stain: An easier and more sensitive method for amyloid detection*, in Amyloid and Related Disorders, P.F.M.M. Picken Md, M.D.P.D.A. Dogan, and M.D.G.A. Herrera, Editors. 2012, Humana Press. p. 187-189.

98. Pashuck, E.T. and S.I. Stupp, *Direct observation of morphological tranformation from twisted ribbons into helical ribbons.* Journal of the American Chemical Society, 2010. **132**: p. 8819-8821.

99. Wagner, N. and G. Ashkenasy, *Systems chemistry: logic gates, arithmetic units, and network motifs in small networks.* Chemistry- A European Journal, 2009. **15**: p. 1765-1775.

100. Shtelman-Shepelevski, E., *Self-assembly and self-replication of short amphiphilic β–sheet peptides ligated through glutamic acid*, in *Chemistry*. 2013, Ben-Gurion University of the Negev.

101. Villain, M., H. Gaertner, and P. Botti, *Native chemical ligation with aspartic and glutamic acids as C-terminal residues: Scope and limitations.* European Journal of Organic Chemistry, 2003. **2003**: p. 3267-3272.

102. Sindi, S.S. and T.R. Serio, *Prion dynamics and the quest for the genetic determinant in protein-only inheritance.* Current Opinion in Microbiology, 2009. **12**: p. 623-630.

103. Aguzzi, A. and A.M. Calella, *Prions: protein aggregation and infectious diseases.* Physiological Reviews, 2009. **89**: p. 1105-1152.

104. Morris, A.M., M.A. Watzky, and R.G. Finke, *Protein aggregation kinetics, mechanism, and curve-fitting: A review of the literature.* Biochimica Et Biophysica Acta-Proteins and Proteomics, 2009. **1794**: p. 375-397.

105. Cohen, F., K. Pan, Z. Huang, M. Baldwin, R. Fletterick, and S. Prusiner, *Structural clues to prion replication.* Science, 1994. **264**: p. 530-531.

106. Leman, L., L. Orgel, and M.R. Ghadiri, *Carbonyl sulfide-mediated prebiotic formation of peptides*. Science, 2004. **306**: p. 283-286.

107. Danger, G., L. Boiteau, H. Cottet, and R. Pascal, *The peptide formation mediated by cyanate revisited. N-carboxyanhydrides as accessible intermediates in the decomposition of N-carbamoylamino acids*. Journal of the American Chemical Society, 2006. **128**: p. 7412-7413.

העבודה נעשתה בהדרכת

פרופ׳ גונן אשכנזי

במחלקה לכימיה

בפקולטה למדעי הטבע

הצהרת תלמיד המחקר עם הגשת עבודת הדוקטור לשיפוט

אני החתום מטה מצהיר/ה בזאת: (אנא סמן):

√ חיברתי את חיבורי בעצמי, להוציא עזרת ההדרכה שקיבלתי מאת מנחה/ים.

√ החומר המדעי הנכלל בעבודה זו הינו פרי מחקרי מתקופת היותי תלמיד/ת מחקר.

___ בעבודה נכלל חומר מחקרי שהוא פרי שיתוף עם אחרים, למעט עזרה טכנית הנהוגה בעבודה ניסיונית. לפי כך מצורפת בזאת הצהרה על תרומתי ותרומת שותפי למחקר, שאושרה על ידם ומוגשת בהסכמתם.

תאריך _____ שם התלמיד/ה בוריס רובינוב חתימה _____.

תקציר

פפטידים וחלבונים משתנים, בתנאים שונים, ממבנים על-מולקולריים מסיסים (עשירים בסלילי-α; α-helix) למבנים סיביים לא מסיסים (עשירים ביריעות-β; β-sheet) הידועים בתור רובד עמילואידי ונחשבים כאחראים למגוון מחלות מערכתיות וניוון עצבים, הנקראות "עמילואידוזיס", כגון, אלצהיימר, פרקינסון ועוד. תהליכי ההתארגנות העצמית של הפפטידים נחקרו רבות בעשור האחרון, והושם דגש מיוחד על רצפים אמפיפיליים. פפטידים אלו מורכבים מרצפים של חומצות אמינו בלבד, הידרופוביות והידרופיליות, לסירוגין (איור 1), ובכך יוצרים שני משטחים שונים, האחד הידרופובי והשני הידרופילי. בתמיסות מימיות, המשטחים ההידרופוביים ממסכים עצמם ממים, עובדה שמהווה את הכוח המניע להתארגנות העצמית של הפפטידים, בדומה לתופעת קיפול ספונטני של חלבונים בטבע. תהליך ההתארגנות העצמית מבוסס על דיפוזיה ספונטנית ואינטראקציות בין-מולקולריות ספציפיות של קשרים לא קוולנטים, הכוללים קשרים אלקטרוסטטיים, הידרופוביים, ואן דר ולס, קשרי מימן וקשרי-π ארומטיים. למרות שאינטראקציות אלו הינן חלשות, עם ריבוי הקשרים ניתן לקבל מבנים על-מולקולריים מאוד יציבים.

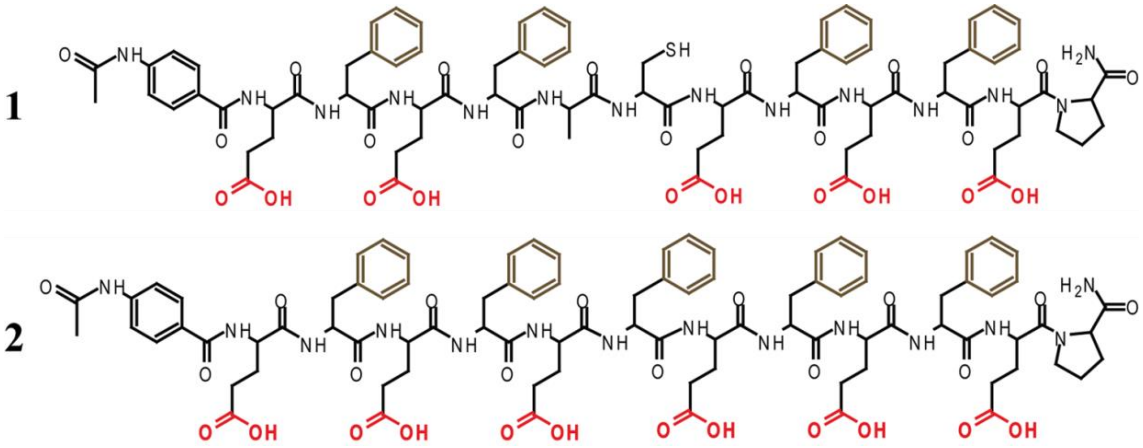

איור 1: תצוגה סכמתית של הפפטידים אמפיפיליים המוצגים בתזה זו, המורכבים מרצפים של פניל אלנינים (Phe) ארומטיים הידרופוביים וחומצות גלוטמיות (Glu) הידרופיליות טעונות, לסירוגין.

במהלך שני העשורים האחרונים בוצע מחקר מקיף בנושא שכפול מולקולארי שלא באמצעות אנזימים. המחקר התמקד בעיקר בסינתזה של פפטידים בעלי יכולת שכפול שיוצרים מבנה שניוני של סלילי-α ומתארגנים למבנה שלישוני של coiled-coil. עם זאת, החוקרים הניחו שפפטידים קצרים עם רצף פשוט יותר יכולים גם הם לשמש כתבניות לשכפול עצמי, בתנאי שיתארגנו למבנים יציבים. בתזה זו אני מתאר מחקר שנעשה על פפטידים פשוטים, דמוי הפפטידים אמפיפיליים בעלי רצף -$(Phe\text{-}Glu)_n$-, שיוצרים צברים חד-ממדיים של יריעות-β במים, ואשר חלקם מאיצים תגובת קשירה בין מקטעי פפטידים קצרים יותר ובכך מזרזים את שכפולם העצמי. אני אתאר תחילה את התכנון והאפיון המבני של הפפטידים החדשים שיוצרים מבני יריעות-β. לאחר

מכן, אני אציג את המחקר שנערך בכדי לקבוע את התהליך ההתארגנות הדינמית של פפטידים אלו. בעזרת תגובת Native Chemical Ligation, הצלחתי לבחון אילו מהמבנים העל-מולקולריים מזרזים את תהליך השכפול העצמי, ובכך מגבירים את קצב תגובת הקשירה (ligation reaction). לבסוף, על-ידי שילוב של תוצאות ניסיוניות המתארות את שני התהליכים המקבילים, כלומר, תהליך ההתארגנות העצמית ותהליך השכפול העצמי, הצענו מנגנון מלא של המערכת, כולל דגם קינטי. בנוסף, אני מתאר מחקר של תגובת קישור המתרחשת ללא החומצה האמינית ציסטאין (Cys), בין חומצה משופעלת בקצה ה-C ולבין ואמין ראשוני של חומצה אמינית בקצה ה-N, תגובה המדמה יצירת קשר פפטידי בטבע.

מחקרים קודמים הראו שלפפטידים בעלי רצפים מתחלפים של חומצה אמינית הידרופובית וחומצה אמינית הידרופילית, לסירוגין, יש נטייה גבוהה להתקפל למבנה שניוני יציב של יריעות-β. בנוסף, מספר חוקרים קידמו את ההשערה שלפפטידים אלו תפקיד חשוב בראשית החיים, בזירוז תהליכים שונים, וביניהם, תהליך שכפול של מולקולות ביולוגיות שונות. בכדי לחקור טענה זו, תכננו וסינטזנו פפטידים יחסית פשוטים (**1** ו- **2** באיור 1), על מנת לבחון את יכולתם לזרז תהליך שכפול עצמי. על-ידי שימוש במגוון גדול של כלים אנליטיים, הן באזורי הממשק מים/אוויר והן בתמיסות מימיות, איפיינתי את המבנים העל-מולקולרים שפפטידים אלו יוצרים. השוואה של המבנים שהתקבלו מפפטיד **1** לאלו שהתקבלו מפפטיד **2**, הראתה שהמבנים המתקבלים מפפטיד **2** מאורגנים יותר, איכותית וכמותית.

מספר קבוצות מחקר הציעו מנגנון להתארגנות עצמית של פפטידים אמפיפילים היוצרים מבני יריעות-β, וכמו כן הראו היררכיה מבנית של המבנים העל-מולקולריים שנוצרים מפפטידים אלו. בתיזה זו אני מתאר את המחקר שביצענו בכדי לקבוע את ההיררכיה המבנית המתקבלת עבור פפטיד **1**, כלומר, את תהליך ההתארגנות הדינמי בו המונומרים מתארגנים למשטחי יריעות-β על-ידי יצירת רשת של קשרי מימן. משטחים אלו מתארגנים מחדש למבנים סיביים על-ידי הוצאת מולקולות מים מן האתרים ההידרופוביים, ויוצרים מבנים ננו-טובולריים בשלב האחרון (איור 2).

בהמשך אני מתאר את תוצאות ניסויי מערכת השכפול עבורה תכננו מקטע אלקטרופילי (E) ומקטע נוקלאופילי (N) שמגיבים דרך Native Chemical Ligation ונותנים את פפטיד **1**. עקבתי אחר תגובות רקע (ללא תוספת של הדגם-אב, **1**, הטמפלייט – template free) ואחר תגובות בהן תערובות התגובה הכילו ריכוזים שונים של **1**, בכדי לבחון את תכונות זירוז הייצור העצמי (זי"ע – auto-catalysis) של **1**. הצלחתי להראות הגברה של פי-60 בקצב התגובות בהן תערובת התגובה הכילה כמות התחלתית של הדגם-אב, לעומת תגובת רקע. כמו כן, חקרתי את השפעת המבנים העל-מולקולרים, הנוצרים מפפטיד **1**, על קצב תגובת הקישור. תגובות אלו הראו יעילות גבוהה יותר של המבנים הסיביים בזירוז תגובת הקישור, לעומת מבנים אחרים. מסדרת ניסויים זו הגענו למסקנה, שקצב תגובת הקישור תלוי גם בריכוז הדגם-אב וגם במבנה העל מולקולרי שנוצר על-ידי **1**. הצענו

מנגנון מלא למערכת, הכולל את שני התהליכים במקביל, ההתארגנות עצמית והשכפול עצמי (איור 2), ודגם קינטי, לו ביצענו סימולציה בכדי לאשש את התוצאות הניסוייות.

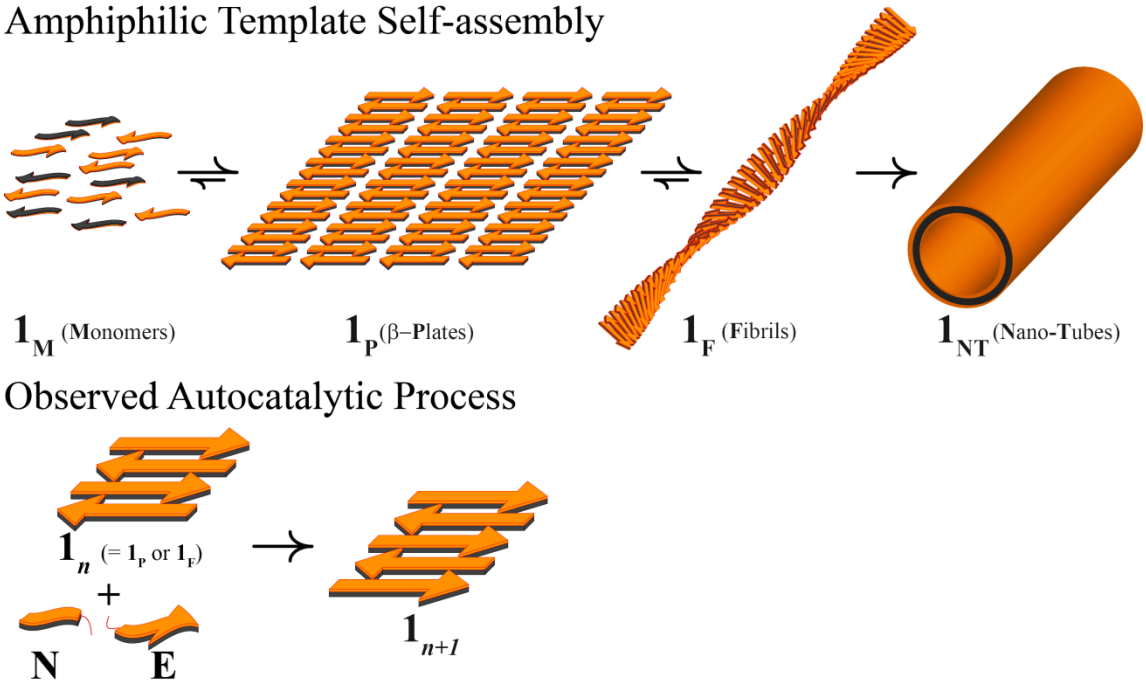

איור 2: תאור סכימטי של שני התהליכים המתרחשים במקביל במהלך תהליך השכפול: (עליון) התארגנות דינמית של מונומרים (1_M) למשטחי יריעות-β אנטי-פרללים (1_P), סיבים (1_F; Fibers), וננו-טיובים (1_{NT}). (תחתון) תגובת זירוז הייצור העצמי בה מבנה של יריעות-β (מוצג כ 1_n) משמש כדגם אב (template) לקישור מבוקר של המקטעים E ו N, אשר מגיבים ויוצרים עותק חדש של 1, כך ששולי התלכיד הגדול יותר (1_{n+1}) זמין לתפקד שוב כדגם-אב.

בחלק האחרון של תזה זו, מוצגת מערכת שכפול נוספת, בה פפטיד **2** מתפקד כזרז לייצור עצמי. בעזרת מערכת זו רצינו לדמות תהליך הקורה בטבע, כלומר, תהליך סינתזה ללא אנזימים של קשר פפטידי, מחומצה משופעלת ומאמין ראשוני. לצורך כך, תכננו מקטע אלקטרופילי חדש, בו החומצה הגלוטמית בקצה ה-C הוכנה עם תיו-אסטר, ומקטע נוקלאופילי חדש - עם אמין חופשי של פניל אלנין בקצה ה-N. ניסויים לבחינת היציבות של האלקטרופיל החדש הראו אפימריזציה (epimerization) ואיזומריזציה (isomerization) דינמית של החומצה הגלוטמית המשופעלת, כך שבתגובה עם המקטע הנוקלאופילי מתקבלים 4 תוצרים. תגובת קישור הפפטידים דרך החומצה הגלוטמית, בעזרת מבני יריעות-β, התקבלה ביעילות, באופן ייחודי, מרחבית ומקומית (regio- and stereo-selective), למרות שהנוקלאופיל לא הכיל ציסטאין.

המחקר המוצג מאפשר הרחבה של מגוון משפחות המולקולות בעלות יכולת שכפול. חשוב להדגיש שהשכפול של יריעות-β מושג בעזרת פפטידים קצרים המורכבים מרצפים של שתי חומצות אמינו, ארומאטית וטעונה, לסירוגין. כמו כן, המערכת מדגימה מנגנון רב-שלבי, בו פפטידים קצרים מתארגנים עצמית לתבנית מוגדרת, שהופכת בעצמה למשכפל יעיל. כמו כן, קישור הפפטידים על

בסיס היריעות-β הינו תהליך ספציפי, מרחבית ומקומית, עובדה שיכולה לרמז על תפקיד אפשרי של פפטידים בעלי מבנה של יריעות-β בראשית הופעת ה-homo chirality.

מילות מפתח:

פפטידים אמפיפיליים, יריעות-β, התארגנות עצמית, מבנים על-מולקולריים, תגובת קישור, זירוז הייצור העצמי, ראשית החיים.

מערכת שכפול עצמי פשוטה המבוססת על פפטידים אמפיפיליים

מחקר לשם מילוי חלקי של הדרישות לקבלת תואר "דוקטור לפילוסופיה"

מאת

בוריס רובינוב

הוגש לסינאט אוניברסיטת בן גוריון בנגב

אישור המנחה _____.

אישור דיקן בית הספר ללימודי מחקר מתקדמים ע"ש קרייטמן _____.

שבט תשע"ד **ינואר 2014**

באר-שבע

מערכת שכפול עצמי פשוטה המבוססת על פפטידים אמפיפיליים

מחקר לשם מילוי חלקי של הדרישות לקבלת תואר "דוקטור לפילוסופיה

מאת

בוריס רובינוב

הוגש לסינאט אוניברסיטת בן גוריון בנגב

שבט תשע"ד **ינואר 2014**

באר-שבע